Pontifícia Universidade Católica
do Rio de Janeiro

Marlon Medeiros Correia

Mode-locked fiber lasers for optical time-domain reflectometry and sensing

Tese de Doutorado

Thesis presented to the Programa de Pós–graduação em Engenharia Elétrica of PUC-Rio in partial fulfillment of the requirements for the degree of Doutor em Engenharia Elétrica.

Advisor: Prof. Jean Pierre von der Weid

Rio de Janeiro
March 2023

Pontifícia Universidade Católica
do Rio de Janeiro

Marlon Medeiros Correia

Mode-locked fiber lasers for optical time-domain reflectometry and sensing

Thesis presented to the Programa de Pós–graduação em Engenharia Elétrica of PUC-Rio in partial fulfillment of the requirements for the degree of Doutor em Engenharia Elétrica. Approved by the Examination Committee:

Prof. Jean Pierre von der Weid
Advisor
Centro de Estudos em Telecomunicações – PUC-Rio

Prof. Walter Margulis
Centro de Estudos em Telecomunicações – PUC-Rio

Profa. Isabel Cristina dos Santos Carvalho
Departamento de Física – PUC-Rio

Prof. Anderson Stevens Leonidas Gomes
Universidade Federal de Pernambuco – UFPE

Prof. Gustavo Castro do Amaral
Technische Universiteit Delft – TUDelft

Prof. Ricardo Marques Ribeiro
Universidade Federal Fluminense – UFF

Rio de Janeiro, March the 29th, 2023

Marlon Medeiros Correia

Marlon Medeiros Correia graduated from the Universidade Federal Fluminense (Niterói, Brasil) in Telecommunications Engineering. Obtained his Master of Science title at the Programa de Pós Graduação em Engenharia Elétrica e de Telecomunicaçõe at UFF, PPGEET, focusing on the field of devices and systems for optical communications. He is a member of the Optoelectronics Laboratory of Center for Telecommunication Studies (CETUC) in PUC-Rio.

Bibliographic data

Correia, Marlon Medeiros

Mode-locked fiber lasers for optical time-domain reflectometry and sensing / Marlon Medeiros Correia; advisor: Jean Pierre von der Weid. – 2023.
139 f. : il. color. ; 30 cm

Tese (doutorado)–Pontifícia Universidade Católica do Rio de Janeiro, Departamento de Engenharia Elétrica, 2023.
Inclui bibliografia

1. Engenharia Elétrica – Teses. 2. Mode-locked. 3. Reflectômetro óptico no domínio do tempo sensível a fase. 4. Lasers de fibra aleatório. 5. Sensor acústico distribuído. 6. Sensor de temperatura distribuído. I. Weid, Jean Pierre von der. II. Pontifícia Universidade Católica do Rio de Janeiro. Departamento de Engenharia Elétrica. III. Título.

CDD: 621.3

This thesis is dedicated to the memory of my mother and sister,

Maria de Lourdes Medeiros Correia

Cristine Medeiros Correia

Acknowledgments

I would like to thank God for giving me the strength to overcome my greatest difficulties and for his constant presence in my life.

To my father, for his unlimited support, and for encouraging me along each and every step of the way.

To my advisor Jean Pierre von der Weid, for having welcomed me as a advisee, for his enormous patience in clarifying my doubts and for all the support given to me so that this work could be carried out.

To Professor Walter Margulis, my sincere and deep gratitude for all the support provided to me for this work to be carried out.

To Professor Gustavo Castro do Amaral for his assistance in the completion of this work.

To friends Pedro Tovar Braga and Felipe Calliari for useful discussions.

To all my family and friends, who directly or indirectly contributed to this work.

To my colleagues and friends of PUC–Rio for the support and friendship.

To my godfather and godmother for their unconditional support with me.

Without them, this work would not have been possible.

To the brazilian agency CNPq for the financial support (140701/2019-2) and PUC-Rio for the exemption scholarship, without which this work would not have been realized.

This study was financed in part by the Coordenação de Aperfeiçoamento de Pessoal de Nível Superior - Brasil (CAPES) - Finance Code 001.

Abstract

Medeiros Correia, Marlon; von der Weid, Jean Pierre (Advisor). **Mode-locked fiber lasers for optical time-domain reflectometry and sensing.** Rio de Janeiro, 2023. 139p. Tese de Doutorado – Departamento de Engenharia Elétrica, Pontifícia Universidade Católica do Rio de Janeiro.

Different types of lasers can be used to generate light pulses with a wide range of pulse durations, energies and peak powers. Q-switching and mode-locked techniques have been reported for years by several authors and researchers and are frequently used in the generation of ultra-short-pulse lasers with time-domain pulse durations from the nanosecond to femtosecond range. A configuration, with gain provided by a semiconductor optical amplifier (SOA) and erbium-doped fiber amplifier (EDFA) is proposed and employ the dispersion management technique to generate a train of optical pulses exhibiting high-peak-power, ultra-low repetition rate, and fast temporal width, enabling this laser to be used as a source for high-resolution optical time domain reflectometer (OTDR) applications. The mode-locking operation has been known to occur only in standard ordered lasers for a long time and until recently it was found to also occur in disordered random fiber lasers (RFL). Although progress has been made towards locking spatial and longitudinal modes in random lasers, the literature lacks reports on Fourier transform-limited pulse generation despite the many decades of the field. The author experimentally demonstrates a mode-locked random fiber laser (MLRFL) operating as a lasing phase-sensitive optical time-domain reflectometer (Φ-OTDR) based on random feedback from a sensing fiber. Here, the full output of the laser provides the sensing signal, in contrast to the small backscattered signal measured in a conventional OTDR. The laser operates as a distributed acoustic sensor (DAS) and distributed temperature sensor (DTS).

Keywords

Lasers; Mode-locked; Semiconductor optical amplifier; Erbium-doped fiber amplifier; Ultra-low repetition rate; Optical time domain reflectometer; Random fiber laser; Transform limited-pulse; Phase-sensitive optical time domain reflectometer; Distributed acoustic sensor; Distributed temperature sensor.

Resumo

Medeiros Correia, Marlon; von der Weid, Jean Pierre (Advisor). **Lasers de fibra de modo travado para reflectometria óptica no domínio do tempo e sensoriamento.** Rio de Janeiro, 2023. 139p. Tese de Doutorado –Departamento de Engenharia Elétrica, Pontifícia Universidade Católica do Rio de Janeiro.

Diferentes tipos de lasers podem ser usados para gerar pulsos de luz com uma ampla faixa de durações de pulso, energias e potências de pico. As técnicas de Q-switching e mode-locked são relatadas há anos por vários autores e pesquisadores e são frequentemente utilizadas na geração de lasers de pulso ultracurto com duração de pulso no domínio do tempo na faixa de nanossegundos até femtossegundos. Uma configuração, com ganho fornecido por um amplificador óptico semicondutor (SOA) e amplificador de fibra dopada com érbio (EDFA) é proposta e emprega a técnica de gerenciamento de dispersão para gerar um trem de pulsos ópticos exibindo alta potência de pico, taxa de repetição ultra-baixa e largura temporal curta, habilitando que este laser seja usado como uma fonte para aplicações de alta resolução em reflectometria óptica no domínio do tempo (OTDR). A operação mode-locked é conhecida por ocorrer apenas em lasers ordenados padrão por um longo tempo e até recentemente foi encontrado também em lasers de fibra aleatórios desordenados (RFL). Embora tenha havido progresso no sentido de travar modos espaciais e longitudinais em lasers aleatórios, a literatura carece de relatos sobre geração de pulsos limitada por transformada de Fourier, apesar das muitas décadas de campo. O autor demonstra experimentalmente um mode-locked random fiber laser (MLRFL) operando como um refletômetro óptico de domínio do tempo sensível à fase (Φ-OTDR). Aqui, a saída total do laser fornece o sinal de detecção, em contraste com o pequeno sinal retroespalhado medido em um OTDR convencional. O laser opera como um sensor acústico distribuído (DAS) e sensor de temperatura distribuído (DTS).

Palavras-Chave

Lasers; Mode-locked; Amplificador óptico semicondutor; Amplificador de fibra dopada com érbio; Taxa de repetição ultra-baixa; Reflectômetro óptico no domínio do tempo; Lasers de fibra aleatório; Reflectômetro óptico no domínio do tempo sensível a fase; sensor acústico distribuído; sensor de temperatura distribuído.

Table of contents

List of figures

List of tables

List of abbreviations

AM – Amplitude Modulation

ASE - Amplified spontaneous emission

CW – Continuos wave

DAS – Distributed acoustic sensor

DOFS – Distributed optical fiber sensor

DSF - Dispersion-shifted fiber

DTS – Distributed temperature sensor

DWDM - Dense wavelength division multiplexing

EDF - Erbium-doped fiber

EDFA- Erbium-doped fiber amplifier

ESA - Electrical spectrum analyzer

F8-PMLL - Figure-eight passively mode-locked laser

FBG – Fiber Bragg Grating

FSR - Free spectral range

FWHM - Full width half maximun

GVD - Group velocity dispersion

HEAR - Hybrid electronically addressable random laser

ITU- International telecommunication union

MLRFL – Mode-locked random fiber laser

MoS_2 - Molybdenum disulfide

MZI - Mach-Zehnder Interferometer

NALM - Nonlinear amplifier loop mirror

NPR - Nonlinear polarization rotation

OBPF - Optical band-pass filter

OC – Optical coupler

OSA - Optical spectrum analyzer

OSC – Oscisloscope

OTDR - Optical-time-domain-reflectometer

PBS – Polarization beam splitter

PC - Polarization controller

PC-OTDR - Photon-counting optical-time-domain-reflectometer

PDG - Polarization dependent gain

PDL – Polarization Dependent Loss

PMF - Polarization-maitening-fiber

PMLFL - Passively mode-locked fiber laser

PMLFRL - Passively mode-locked fiber ring laser

PZT – Piezoelectric

RF - Radio-frequency

RFL – Random fiber Laser

SAs - Saturable Absorbers

SESAM - Semiconductor saturable absorber mirrors

SMF – Single mode fiber

SNR – Signal-to-noise ratio

SOA- Semiconductor optical amplifier

SPM - Self-Phase-Modulation

TWA - Traveling-wave amplifiers

WDM - Wavelength division multiplexers

ϕ-OTDR - Phase-sensitive-optical-time-domain-reflectometer

"The first gulp from the glass of natural sciences will turn you into an atheist, but at the bottom of the glass God is waiting for you."

Werner Heisenberg

1
Introduction

Interest in short pulsed laser sources optics has been maintained over the past decades thanks to the development of techniques for short high-power optical pulse generation, which finds applications in several areas of science. Besides optical communications, which involves increasingly higher frequencies [1-3], intense short pulses at low repetition rates are a challenging theme with important practical applications such as: optical fiber monitoring [4-6]. One technique that attracts special attention is passive mode-locking in fibre lasers, due to both the absence of active modulation devices and the high-quality factor of fibre cavities [7]. Passively mode-locked fiber laser (PMLFLs) rely on saturable absorbers (SAs) that can be semiconductor saturable absorber mirrors (SESAMs) [8], graphene [9] and Molybdenum disulfide (MoS_2) [10] to create a fixed phase relationship (mode-locking) between the allowed spectral modes within the optical cavity. It has been demonstrated that the behaviour of SAs can be reproduced by exploiting the phenomenon of nonlinear polarization rotation (NPR) [11, 12] or nonlinear amplifier loop mirror (NALM) in a fibre ring [13, 14]. Group velocity dispersion (GVD) in optical fibres may be a limiting factor for fast mode locked optical pulses mainly in long cavity fibre rings. By combining fibres that exhibit dispersion parameters β_2 with opposite signs, i.e., positive and negative values of β_2 at the operation wavelength the total GVD of the fiber ring can be managed to minimize the GVD experienced by the optical pulse signal [15].

Random fiber lasers (RFL) generally employ the Rayleigh scattered light from an optical fiber as feedback mechanism. In some cases, the gain medium is distributed over the feedback fiber [16, 17] or separated from it as a pumped Erbium-doped fiber (EDF) [18]. Random narrow linewidth modes were reported in a semiconductor optical amplifier (SOA) based random fiber laser with Rayleigh scattering feedback from an 8-km fiber [19]. A hybrid electronically addressable random laser (HEAR) was recently presented [20], where a pulsed

SOA in a loop mirror and the Rayleigh scattering from a pumped erbium doped fiber (EDF) formed a random cavity. The proposed feedback mechanism was Rayleigh scattering from the EDF section addressed by the SOA pulse whose frequency is in resonance with the cavity roundtrip time. The backscattered light in a standard telecom fiber is very weak. Nevertheless, under Strong optical amplification, Rayleigh backscattering has been used as the feedback needed for laser action [21, 22]. A fiber laser based on the feedback from randomly distributed scattering centers has ill-defined modes and is generally described as a random fiber laser [21, 22]. Random lasers based on Raman [23, 24], Brillouin [25, 26] and Rayleigh scattering in fibers [21, 22] have been reported. They often incorporate amplifiers such as Erbium-doped fibers (EDFs), semiconductor optical amplifiers (SOAs) or both, to provide or complement the necessary gain needed for laser action [21, 22, 27-31].

Rayleigh scattering is widely exploited in distributed sensing with optical fibers in the time domain [32-35]. A weak backscattered signal is generated from the propagation of a short duration pulse along the fiber. It gives an indication of the intensity of the pulse at every fiber position, the pulse duration limiting the spatial resolution of the measurement. In Optical Time Domain Reflectometry (OTDR), the intensity-drop along the fiber and the echoes generated at discontinuities such as components, connectors and splices allow monitoring a fiber link for losses [36]. Distributed sensors based on the scattering of a coherent pulse [37] are capable of identifying disturbances such as vibrations [37, 38], perimeter intrusion [39, 40] and seismic events [41, 42]. Such disturbances affect locally the relative phases of the backscattered light from different points within the pulse, and consequently their interference. Phase-OTDR systems are widely used as distributed acoustic sensors (DASs) [38–50]. The Rayleigh scattering process in fused silica fibers is not significantly affected by external environmental conditions (e.g. temperature), but in the case of highly coherent optical probing sources, an OTDR signal forms as a result of optical interference and its intensity and phase are both responsive to fiber mechanical perturbations and refractive index changes. Thus, it is possible to monitor temperature changes and mechanical vibrations. Distributed temperature sensors (DTSs) that are capable of delivering real-time information using low-cost optical fibers as a sensing element are widely used to monitor the temperature and operating

conditions along extended infrastructure objects, such as power grid lines, oil and gas pipelines. In principle, by using specially designed fibers with optical losses sensitive to a specific external physical field, phase-sensitive OTDRs could be used to create a whole family of different distributed optical fiber sensors including DTSs [51-53].

This thesis reports a practical analysis of a figure-eight passively mode-locked laser (F8-PMLL) where periodic transmission and reflection of the optical pulses takes place as a function of the input instantaneous power and the nonlinear phase shift between the counter-propagating longitudinal modes cavity [13, 14]. As we continue to advance pulse generation techniques, we have developed passively mode-locked fiber ring laser (PMLFRL) based in a practical analysis of nonlinear polarization rotation effect in semiconductor optical amplifiers (SOAs) showing that, when high-power optical pulses reach a SOA, they undergo a nonlinear polarization (NPR) change due to polarization dependent saturation of the optical amplifier, thus, SOAs can act as NPR devices [11, 12]. This work also reports a practical analysis of a mode-locked random fiber laser (MLRFL) in which it is demonstrated that the device operates in active mode-locking regime generating Fourier-transform limited pulses combined with Rayleigh backscattering feedback. In addition, applications as distributed acoustic sensor (DAS), sometimes termed distributed vibration sensing (DVS) and distributed temperature sensor (DTS) are demonstrated and shows its operation as phase-sensitive optical time domain reflectometer (ϕ-OTDR).

1.1 Motivation

With developments in science and advanced technologies, high quality optical sources are required in many fields. Recently, the repetition rate of mode-locked lasers in the kilohertz range has also attracted much attention, and the low-repetition-rate pulse can be useful in OTDR systems [4-6]. Recently, SOAs and EDFAs have been used as the gain medium in fiber lasers [10, 11, 21, 22]. Compared to erbium-doped fibers, SOAs have the upper state lifetime ranging from nanoseconds to picoseconds and are much shorter than that of erbium-doped fibers (microseconds). As a result, the energy in the upper state and the gains of

SOAs are typically smaller than those of erbium-doped fibers, but the response of SOA is much faster. In OTDR applications, spatial resolution and dynamic range are important figures of merit in measuring long fibers length [4-6]. Pulses with low repetition rate, short temporal duration and high peak power are in high demand. Optical sources with low repetition rate and narrow temporal width are still a challenging field due to group velocity dispersion (GVD). The thesis motivation will be the search for the development of new architectures of pulsed optical sources based on the mode-locked regime capable of delivering pulses with high peak power, low repetition rate and narrow temporal width for applications in OTDR systems.

Interest in random lasers has been maintained over the past decades mainly because complex physical processes that take place in amplifying disordered systems [16, 21-26]. A laser is generally constructed from two basic elements: an optical gain medium that ensures the stimulated emission and an optical cavity that partially retains the light. When the total gain in the cavity is greater than the losses, the system reaches the threshold and achieves laser action. Currently, there are many works discussing new architectures and the complex physical processes of operation of a random fiber laser [17-26]. As these new optical source architectures are consolidated and become more common, applications with RFL also grown substantially and become their own field of research. A hybrid electronically addressable random laser (HEAR) was recently presented [20] where a pulsed SOA in a loop mirror and the Rayleigh scattering from a pumped erbium doped fiber (EDF) formed a random cavity. The author motivation is to be able to show that the HEAR laser presented in [20] can be used directly as a distributed optical fiber sensor (DOFS) within the addressable section of the fiber, with the laser intensity being sensitive to external effects on the fiber, such as stress or temperature, with the resolution given by half the modulation pulse width as in a ϕ-OTDR.

1.2 Objectives

This thesis describes and demonstrates the use of semiconductor optical amplifiers (SOAs) and erbium-doped fiber amplifiers (EDFA) as a gain medium

in optical fiber lasers. The author demonstrates experimentally optical sources in mode-locking operation and describes their importance in optical fiber monitoring applications [4-6]. In the first step, we explored an already known figure-eigth passively mode-locked laser (F8-PMLL) configuration [14] and demonstrated the entire characterization of this source and its operation in the mode-locking regime. This source is later integrated with a photon-counting optical-time-domain-reflectometer (PC-OTDR) and an analysis of the detection system is realized (not shown here). The objective of this work focuses only on the pulse generation system, however the integration with the acquisition system can be seen in the attached article (refer to annex A). In a second step, we explored the nonlinear polarization rotation (NPR) to generate short optical pulses with a low repetition rate [12]. The objective is to use NPR to initialize the mode-locking regime in conjunction with dispersion management cavity [15] to enable this laser to be a millimeter resolution source for OTDR applications. Finally, we explore a hybrid electronically addressable random fiber laser (HEAR) configuration that uses localized [19] and distributed [16] gain mechanisms. This still poorly explored random laser configuration [20] is assembled in our laboratory in order understand its mode-locking operation and demonstrate its functionality as a distributed optical fiber sensor (DOFS).

1.3 Thesis contribution

The thesis presents a study of the necessary theoretical tools and the practical approach of experimental architectures that operate as pulsed optical sources.

The figure-eigth passively mode-locked laser (F8-PMLL) based on configurations already demonstrated in works in the literature [13] is presented, however, optical band-pass filter (OBPF) is used in order to meet the bandwidth standards of dense wavelength division multiplexing (DWDM) systems. The laser generate pulses with high peak-power with a bandwidth suitable for integration with a PC-OTDR [6]. Thus, measurements long length fibers in the different DWDM channels can be realized without crosstalk effects.

The generation of pulses with low repetition rate and narrow temporal width are challenging topics, so this thesis contribute for development and improvement of the new optical sources for high resolution applications in fiber monitoring [4, 5]. PMLFRL with dispersion management is demonstrated and the results are comparable with state-of-the-art mode-locked methods. To the best of the author knowledge, this is the lowest repetition rate obtained with ps-long pulses-based PMLFL, enabling this laser to be used as a source for millimetre resolution OTDR applications.

Random lasers [54, 55] are based on a stochastic distribution of scattering centres that help form an effective cavity with laser modes, even when a laser mirror is lacking [18-21]. The random mode-spacing makes it difficult to lock the phases of the modes to each other [56-62]. Mode-locking random fiber lasers (MLRFL) where the gain and scattering coexist spatially are challenging topics. So, few random laser reports exist on locking the spatial modes [11-16] and the longitudinal modal distribution [62]. To the best of the author knowledge this is the first mode-locked random fiber laser generating Fourier-transform limit optical pulses. In addition, it's demonstrates the operation of the device as a distributed optical fiber sensor (DOFS). The big advantage here is that instead of a tiny backscattered signal measurement as it is in an OTDR, it is the full output of the laser that provides the sensing signal. Hence, no averaging is needed, and a fast response is available.

1.4 Thesis outline

This thesis shows at the optoelectronic pulse generation from optical fiber lasers, with SOA and EDFA providing gain and working as broadband emission sources. A literature review of publications and several experiments were undertaken. The comprehension of mode-locked theory is required for a thorough understanding of the work. Also, the light scattering phenomena is important for understand the feedback mechanism in random fiber lasers and distributed optical fiber sensors. Thus, this thesis is organized as follows.

Chapter 1 contextualizes the work presented in this thesis, describing the main motivations of the research, objective, relevance and main contributions.

Chapter 2 reviews the main concepts involved in laser theory, presenting the theoretical concepts necessary to understand the mode-locked regime and the physical mechanisms that govern random fiber lasers. This chapter is important for the work as it contributes to an easier understanding of the theoretical and experimental results.

Chapter 3 presents the setups and experimental results of both the figure-eigth passively mode-locked laser (F8-PMLL) and passively mode-locked fiber ring laser (PMLFRL). This chapter describes the optical pulse generation mechanisms and discusses the relevance of the results.

Chapter 4 presents the assembly and experimental results of the mode-locked random fiber laser (MLRFL) and shows its use as a distributed optical fiber sensor (DOFS) according to the addressing of dispersion shifted fiber (DSF) sections.

Chapter 5 summarizes the thesis, where we list the publications in journals and congresses of the results obtained so far, strongly indicating the relevance of the work.

2
Background

This chapter reviews the main concepts involved in this work to better understand the functioning of mode-locked lasers, random fiber lasers and OTDR systems. Reviews the basics concepts of laser and provides a better understanding of the experimental results that will be demonstrated in the following chapters.

2.1
Laser emission

The laser (light amplification by stimulated emission of radiation) is a device that produces electromagnetic radiation based on the stimulated emission of photons. The presence of a photon in a mode of specified frequency, propagation direction, and polarization stimulates the emission of a duplicate ("clone") photon with precisely the same characteristics as the original (see Figure 2.1). The photons has the same energy and wavelength (monochromatic light), are in phase (coherent light) and their associated electromagnetic waves have the same direction (collimated light) [63]. This photon amplification process is the phenomenon that underlies the operation of laser amplifiers and lasers.

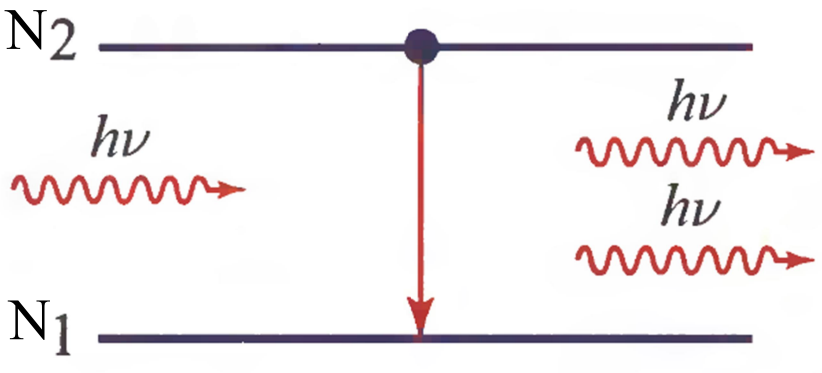

Figure 2.1. Estimulated emission [63].

$$\Delta E = E_2 - E_1 = h\nu \text{ (J) ou } \Delta E = \frac{1{,}24}{\lambda(\mu m)} \text{ (eV)} \qquad (2.1)$$

Stimulated emission is a process whereby a photon of energy hν (see equation 2.1) stimulates the atom to emit a "clone" photon as it undergoes a downward transition. The stimulated emission is characterized by population inversion and occurs when a system there is a greater amount of atoms in the excited state than in the ground state ($N_2 > N_1$). This estimulated downward transition defines the light emission that we commonly call LASER. Figure 2.2 shows an external power source (the pump) excites the active medium (represented by a collection of atoms) producing a population inversion.

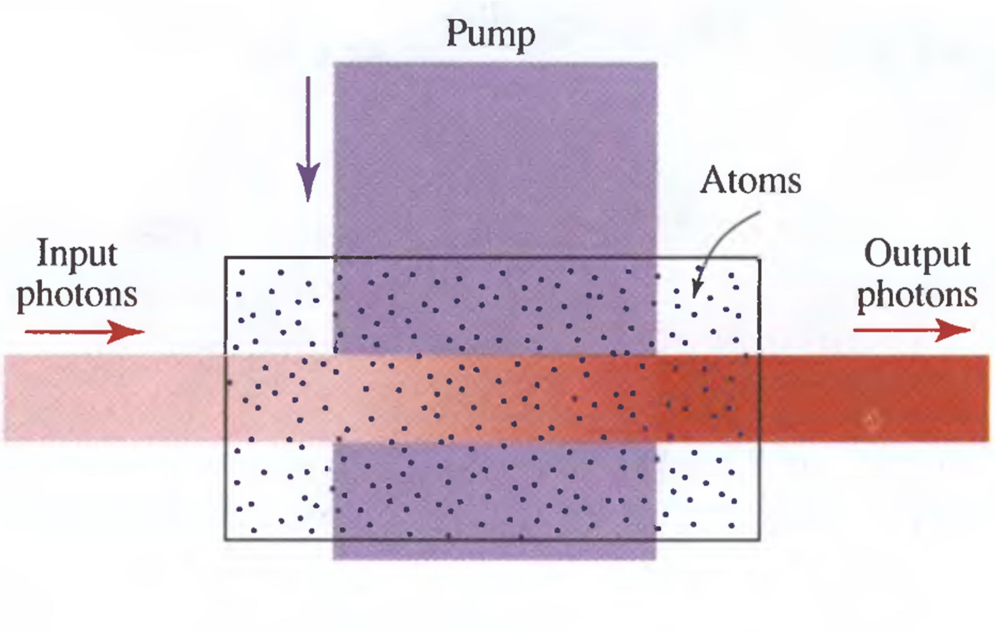

Figure 2.2. The laser amplifier. An external power source (the pump) excites the active medium (represented by a collection of atoms), producing a population inversion. Photons Interact with the atoms. [63].

2.2 Optical resonator

The laser is an optical oscillator in which the amplifier is the pumped active medium. Feedback is engendered by placing the active medium in an optical resonator, which reflects the light back and forth between its mirrors. Frequency selection is jointly achieved by the resonant amplifier and the resonator, which admits only certain modes. Output coupling is accomplished by making one of the resonator mirrors partially transmitting. There are multiple

configurations of optical resonators, including planar-mirrors, spherical-mirrors, ring-mirrors, rectangular cavity, fiber-ring and others [63].

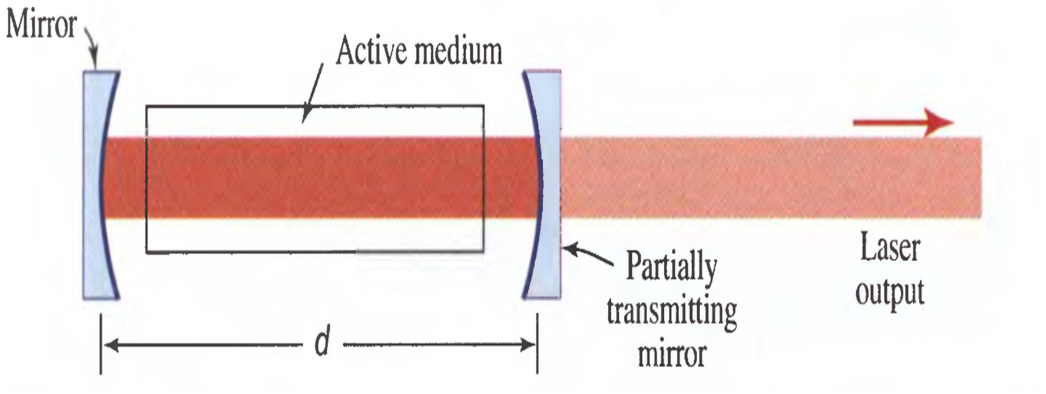

Figure 2.3. A laser consists of an active médium within an optical resonator (Fabry-Perot). The output is extracted through a partially transmitting mirror [63].

A Fabry-Perot resonator (see figure 2.3), comprising two mirrors separated by a distance d, contains the medium (refractive index n) in which the active atoms of the amplifier reside. Travel through the medium introduces a phase shift per unit length equal to the:

$$\Delta\Phi = \frac{2\pi}{\lambda}(2d) \tag{2.2}$$

The resonator sustains only frequencies (FSR, free-spectral-range) that correspond to a round-trip phase shift that is a multiple of 2π [64].

$$2q\pi = \frac{2\pi n\nu}{c}(2d) \tag{2.3}$$

$$v_q = q\frac{c}{n(2d)} \tag{2.4}$$

Then (see figure 2.4),

$$FSR = v_{q+1} - v_q = (q+1)\frac{c}{n\,(2d)} - (q)\frac{c}{n\,(2d)} = \frac{c}{n\,(2d)} \tag{2.5}$$

The Fabry-Perot is an optical resonator that also contributes to losses in the system. Absorption and scattering of light in the medium introduces a distributed loss characterized by the finesse given by equation 2.6:

$$F = \frac{FSR}{\delta v} = \frac{\pi\sqrt{|R_1 R_2|}}{1-|R_1 R_2|} \tag{2.6}$$

where R_1 and R_2 are the reflectivities of mirrors 1 and 2, respectively. The finesse is defined as the ratio of FSR and full width half maximun (FWHM) of the peaks in the interference pattern [63].

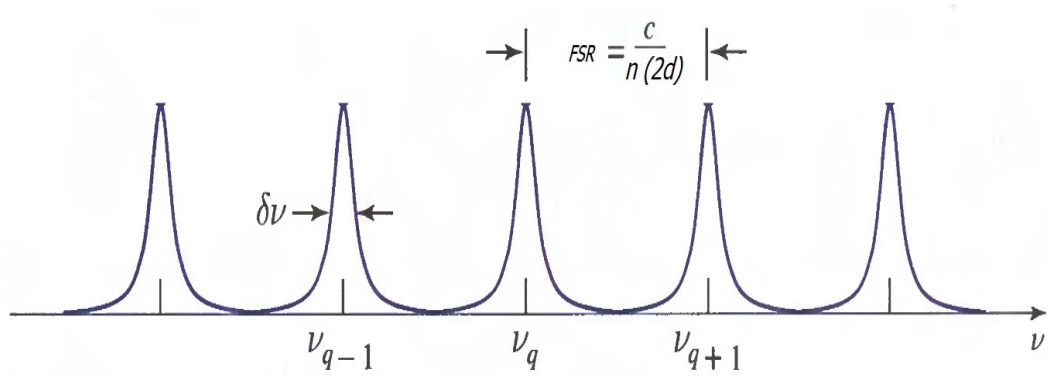

Figure 2.4. A Resonator modes are separated by the $FSR = c/n\,(2d)$ and have linewidth $\delta v = FSR/F$.

2.3 Semiconductor optical amplifier (SOA)

The semiconductor laser is a device based on a PN junction. The direct electrical polarization of the device generates the passage of an electrical current and photons emission. This emission occurs thanks to the recombination of electrons (negative charges) and holes (positive charges) in the depletion region (PN junction) [63]. This recombination allows the energy acquired by electrons to be released in the form of photons (light). Figure 2.5(a) shows the band structure of the semiconductor material. The energy bands are formed from the superposition of layers (energy levels) of atomic structures. These intrinsic structures are often previously doped with P-type and N-type materials in order to reduce the gap energy (introduction of new energy levels and approximation of the conduction band to the valence band) and formation of the depletion region

[63, 64]. Doping is a process that generates an unbalanced charges in the structure (high density of free electrons and holes) and happens thanks to the introduction of two types of impurities: Donor or Acceptor. Donor impurities are characterized by the presence of free electrons that can move freely through the semiconductor material, whereas acceptor impurities are characterized by the presence of holes that behave as positive charges. Semiconductors doped with donor impurities are of the N-type and semiconductor doped with acceptor impurities are of the P type (see figure 2.5(b)) [64]. The existence of this unbalance of charges is essential to allow the stimulated absorption of carriers, population inversion and stimulated emission of photons by the semiconductor optical amplifier.

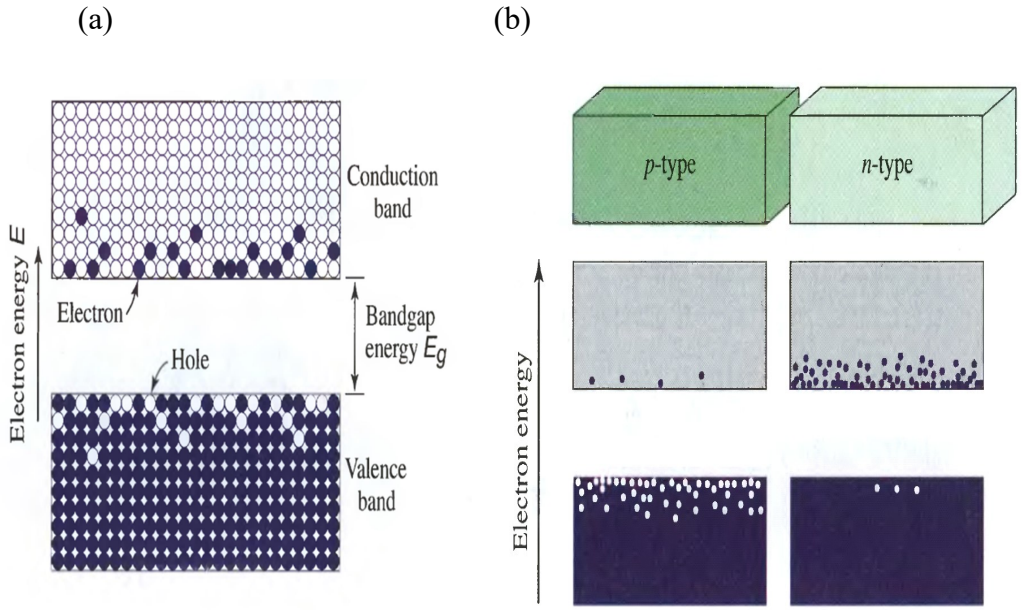

Figure 2.5. (a) Electrons in the conduction band and holes in the valence band. (b) Energy levels and carrier concentrations for a p-type and an n-type semiconductor [63].

The operation of a semiconductor optical amplifier (SOA) is the same of laser amplifiers, i.e., the creation of a population inversion leading a stimulated emission more prevalent than absorption. The population inversion is usually achieved by electric-current injection in some form of a p-n junction diode; a forward bias voltage causes carrier pairs to be injected into the junction region, where they recombine by means of stimulated emission [63]. SOAs generally consist of light output faces (mirrors) with very low reflectivity [65], then they are called Traveling-wave amplifiers (TWA), i.e., light passes only once through the gain medium. SOAs can be used in telecom systems in the form of fiber-

pigtailed components (with either normal single-mode fibers or polarization-maintaining fibers), operating at signal wavelengths near 1.3-μm or 1.5-μm, and offering a gain of up to ~20-dB, limited essentially by amplified spontaneous emission (ASE). The strong gain saturation in SOAs can be a problem for some applications, but it can also be exploited for nonlinear signal processing in telecom systems. In this work, demonstrates that when inserted in a ring, SOAs can simultaneously work as a gain medium and modulator in fiber laser configurations. In our lab, we use a SOA model SOA1013SXS [66] with FWHM bandwidth measured to be of 33-nm (see figure 2.6(a)) for an injection current of 425-mA [67]. Figure 2.6(b) shows the SOA in butterfly mount coupled to a fiber that establishes an input and an output port. This model has a low polarization dependent gain (PDG) of 1-dB, switching speed of ~1-ns and extinction ratio of ~60-dB.

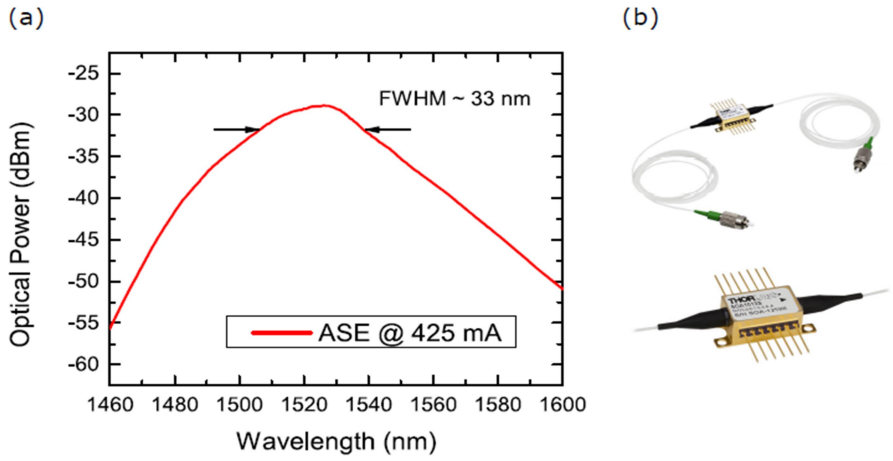

Figure 2.6. (a) Measured amplified spontaneous emission (ASE) spectrum of SOA1013SXS [67], and (b) its fiber-coupled packaged mount [66].

Figure 2.7 shows the measured gain for bias currents varying from 0 to 400 mA. For low SOA driving currents, the population inversion condition is not satisfied, such that the SOA acts as an absorption medium (negative gain). When the current starts to increase, at the point where the gain is equal to zero, establish the threshold for population inversion. Further increases will result in a single pass gain defining a transparency current (I_T). Figure 2.7 shows the transparency current is ~89-mA. For currents higher than I_T the SOA provides gain to the input signal, however, further increase in the driving current gives less gain, thus, a gain

saturation with driving current is observed. The results shown in Figure 2.7, a low power input signal had to be used, with input power of -20-dBm (small signs) [67]. For large signals, SOA saturates for smaller injection currents and consequently operates with gain compression.

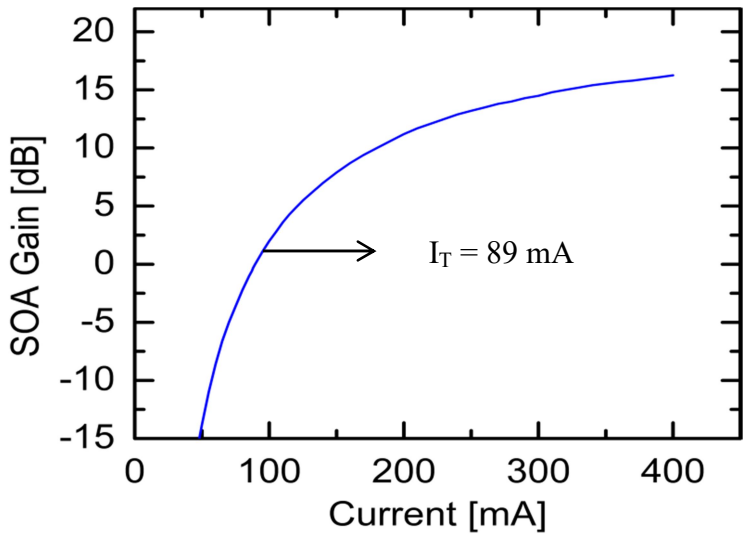

Figure 2.7. Measurement of SOA gain as a function of injection current.

2.4 Erbium-doped fiber amplifier (EDFA)

Erbium-doped fiber amplifiers (EDFAs) are the by far most important fiber amplifiers in the context of long-range optical fiber communications; they can efficiently amplify light in the 1.5-μm wavelength region, where silica-based telecom fibers have their loss minimum [68]. The core element of a fiber amplifier is a piece of rare-earth-doped fiber, which can provide laser amplification via stimulated emission when it is optically pumped with other light injected into the fiber. Among other attractive features, they offer high polarization-independent gain and low insertion loss.

The energy level refers to an amount of particular energy contained by the ion corresponding either to absorb or emitted energy. Amplification in Erbium doped fiber is closely related to the changes in energy level of Erbium ions [68]. Absorbing energy will increase its energy level and vice versa for emitting energy. In amplification terms, emitting light is associated with emitting photons. Figure

2.8 shows the possible energy levels for Erbium ions as well as possible pumping bands. Absorption of pump photons excites Erbium ions to higher energy states.

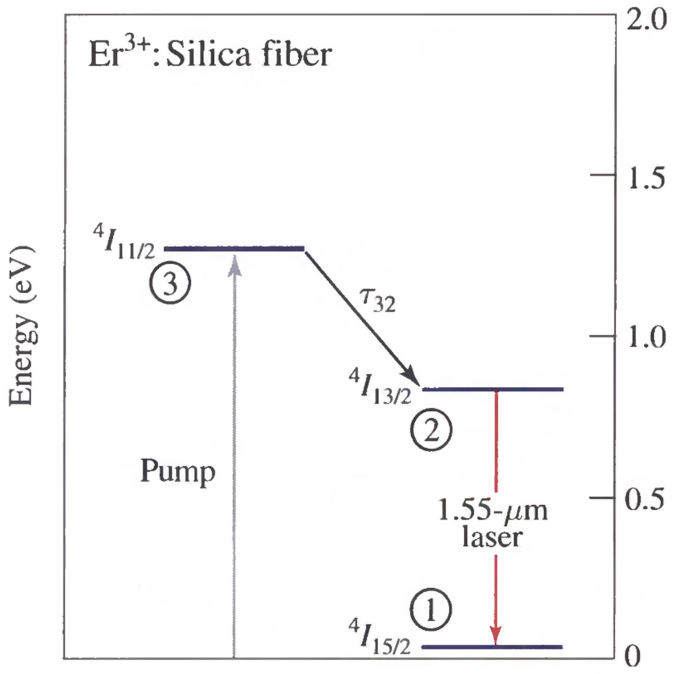

Figure 2.8. Schematic of energy-level manifolds for the Er^{3+}: silica fiber $^4I_{13/2}$→$^4I_{15/2}$ laser transition in the vicinity of 1550 nm. Pump power at 980 nm [63].

The $^4I_{13/2}$→$^4I_{15/2}$ laser transition can also be directly pumped at 1480-nm by light from InGaAsP laser diodes. This quasi-two-Ievel pumping scheme is less efficient than the three-level scheme implemented at 980-nm since the gain per unit pump power is lower and the noise is higher in the latter case [63, 68]. However, the pump transition linewidth and saturation signal power are greater at 1480-nm so that pumping at this wavelength is sometimes used for higher power amplifiers [63]. In our lab, we use a commercial EDFA (Tuolima) (see Figure 2.9) establishing an input port and an output port with average output power of ~26.5-dBm and fixed gain of 22-dB [69].

Figure 2.9. Off-the-shelf Tuolima EDFA [69].

A second commercial variable-gain EDFA (Thorlabs 100S) was characterized. The EDFA offer >20-dBm output power with a low noise figure of <5-dB [70]. The pump current of the EDFA amplifier is adjustable through the instrument's front panel, allowing the user to vary the gain and output power of the amplifier (see Figure 2.10(a)). The results shown in Figure 2.10(b), a low power input signal had to be used, with input power of -30-dBm (small signs). The amplifier provided up to 36-dB gain for full-pump power (1000-mA).

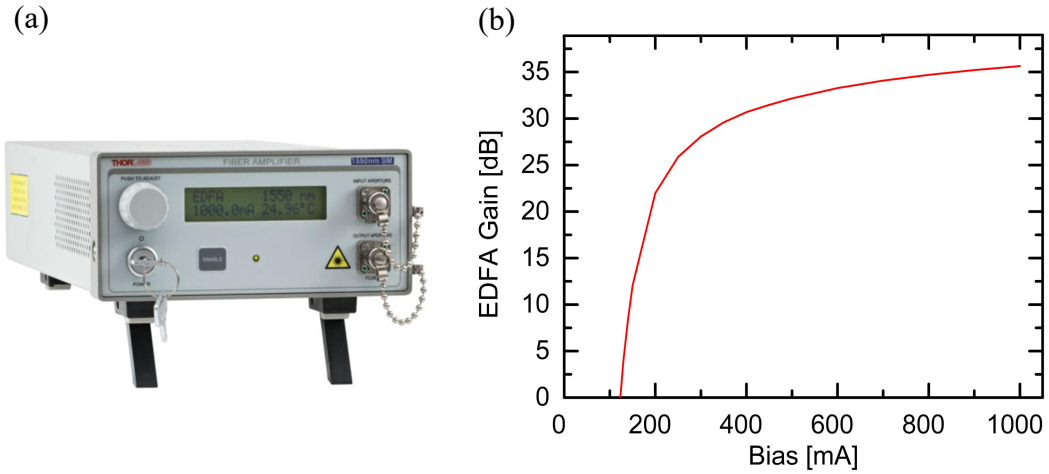

Figure 2.10. (a) Thorlabs 100s core-pumped erbium-doped fiber amplifiers [70], and (b) Measurement of EDFA gain as a function of injection current.

In our lab, we have the necessary devices to assemble an EDFA. Figure 2.11(a) shows the ASE generated from the experimental schematic shown in figure 2.11(c) in which 27-m of an erbium-doped fiber (ER 1550C3) [71] manufactured by corning, a wavelength division multiplexers (WDM) and a Thorlabs PL980P200 Pigtailed Laser Pump [72] are used. Figure 2.11(a) shows an amplification bandwidth of ~35-nm across the entire C-band of optical communications. The erbium-doped fiber ER1550C3 has an absorption of ~5-dB/m (@1550-nm) and Rayleigh backscattering intensity of ~-60-dB/m (@1550-nm) [71]. Figure 2.11(b) demonstrates the characterization of the EDF gain as a function of pump power. Gain measurements are performed with an input signal in the propagating direction of the pump power (co-pump) and in the opposite direction of the pump power (counter-pump). In a bi-directional gain system, the measured gain was 54.5-dB for a maximum pumping power of 365-mW.

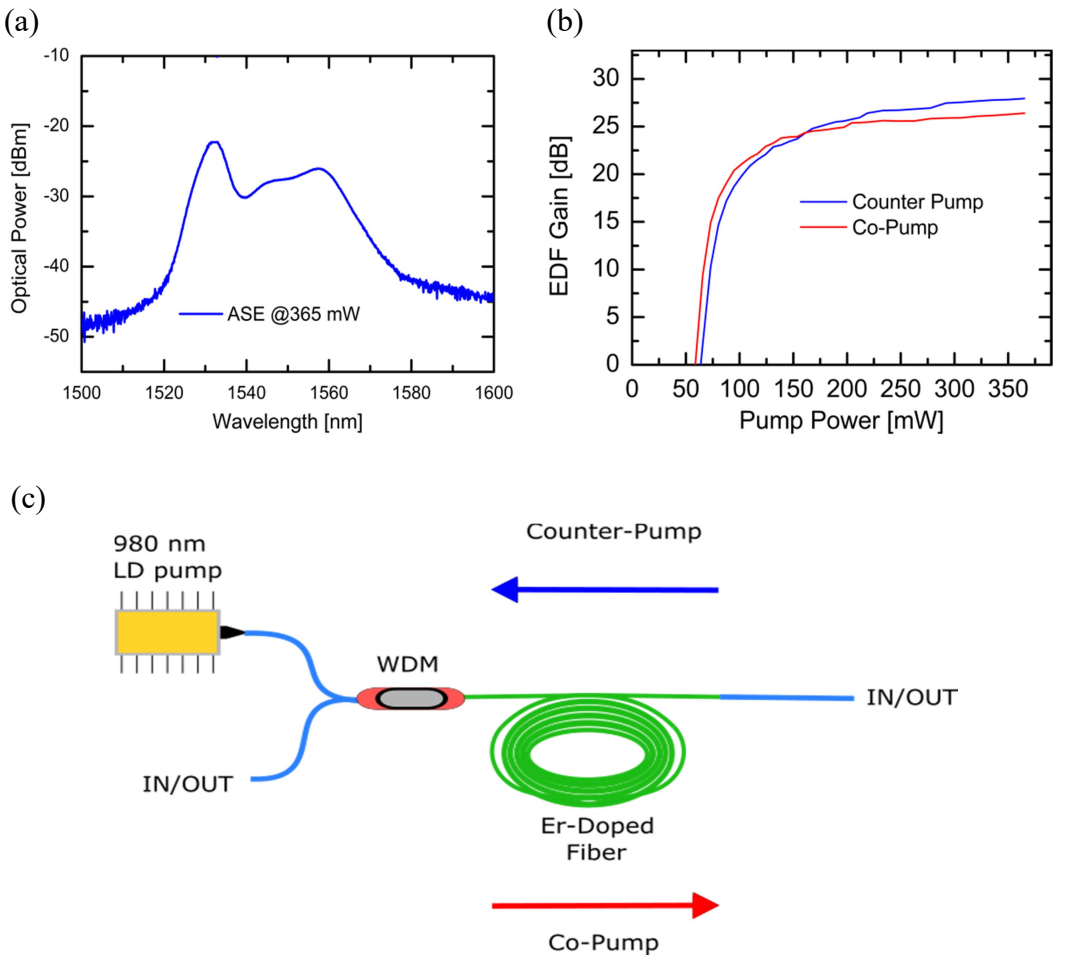

Figure 2.11. (a) Measured amplified spontaneous emission spectrum of ER1550C3; (b) Measurement of EDF gain as a function of pump power and (c) Experimental schematic of EDFA constructed from a 27-meter coil of erbium doped fiber (ER 1550C3).

2.5 Mode-locking

The mode-locking regime consists of the emission of a train of pulses with a short duration in time and a very stable repetition rate, directly dependent on the material that fills the cavity and its physical length [1-3]. In a resonant cavity, several modes can oscillate simultaneously, so the laser output will be defined as a function of time and will depend on the phase, frequency and amplitude of the longitudinal modes [64].

Mode-locked lasers rely on saturable absorber or gain/phase modulation to create a fixed phase relation between the spectral modes allowed within its optical resonator cavity [7-10]. Under the mode-locked condition, the temporal shape of

the output signal is given by a coherent weighted sum of such allowed spectral modes or, mathematically:

$$p(t) = \sum_{m=-M/2}^{M/2} c_m e^{-i2\pi(\omega_0 + nf_0)t} \tag{2.7}$$

$$f_0 = \text{FSR} = 1/T_F \tag{2.8}$$

$$\tau = T_F \,/\text{M} \tag{2.9}$$

where c_m are the individual weigths of each spectral modes (or Fourier coefficients), ω_0 is the laser's center frequency, f_0 is the optical cavity's free-spectral range (FSR), and M is the total number of allowed spectral modes within the laser bandwidth $\Delta\omega$, where $M = \Delta\omega / f_0$. Equation 2.7 shows that the cavity modes constitue a Fourier series of the output signal, which correspond to temporal pulses train since the spectrum, during mode-locked operation, takes the form of a frequency comb. So, equation 2.8 demonstrates the pulse repetition period is defined by inverse of the spectral modes frequency spacing. Already the equation 2.9, shows pulses time duration (τ) is the ratio of the repetition period in time (T_F) and the total number of modes (M) [64]. Figure 2.12 shows time pulse train and optical spectrum of mode-locked laser and the parameters of the output signal.

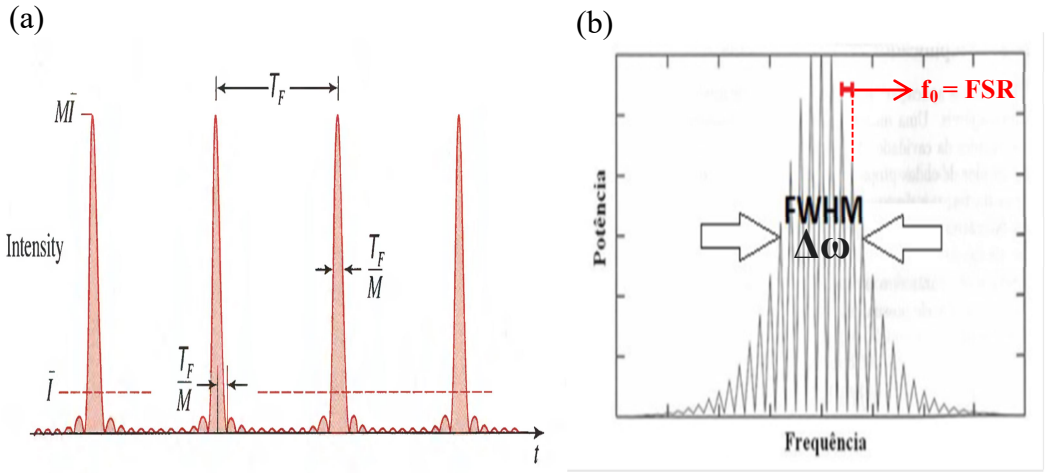

Figure 2.12. (a) Intensity of the periodic pulse train resulting from the sum of M laser modes of equal magnitudes and phases. Each pulse has a duration that is M times smaller than the period T_F and a peak intensity that is $M\bar{I}$ times greater than the mean intensity [63]; (b) longitudinal modes of the laser resonant cavity.

2.5.1
Nonlinear amplifying loop mirror (NALM)

Mode-locking can be achieved either actively (through intensity and/or phase modulation) or passively in either free-space or fiber cavities [73]. Among others, the main advantages of fiber-based mode-locked lasers include low propagation loss, the possibility of creating high Q value kilometer-long fiber cavities [12], and the fact that erbium-doped fiber amplifiers (EDFAs) and fiber-pigtailed semiconductor optical amplifiers (SOAs) can be used as the gain media [13, 14]. Figuring as physical mechanisms that guarantee mode-locking in PML fiber lasers are constructive/destructive interference of counterpropagating longitudinal modes in a so-called nonlinear amplifying loop mirror (NALM) [14, 74]. This mechanism can be easily explained from the Kerr nonlinear optical effect [63, 75]. Consider an electromagnetic wave propagating through the core of an optical fiber which is mathematically described by the equation 2.10:

$$E = E_0 \, e^{j(\omega_0 t - kz)} \tag{2.10}$$

$$E = \sqrt{I} \, e^{j\left(\omega_0 t - \frac{2\pi}{\lambda} nL\right)} \tag{2.11}$$

where I is the intensity, ω_0 is the central frequency, λ is the wavelength, n is the index of refraction and L is the distance traveled by the wave. The Kerr effect is the effect of an instantaneously occurring nonlinear response, which can be described as modifying the refractive index [63, 75]. In particular, the refractive index for the high intensity light beam itself is modified according to:

$$n(I) = n_0 + n_2 I \tag{2.12}$$

with the nonlinear index n_2 and the optical intensity I, which is proportional to the modulus squared of the electric field strength ($|E|^2$). The n_2 value of a medium is related to the third-order susceptibility χ(3) and for silica fibers, has a nonlinear index of $n_2 \approx 3 \times 10^{-16}$ cm^2/W [75]. So when we replace 2.12 in 2.11 we will have a phase dependent on the intensity of the wave:

$$E = \sqrt{I}\, e^{j\left(\omega_0 t - \frac{2\pi}{\lambda} n\,(I) L\right)} \tag{2.13}$$

$$E = \sqrt{I}\, e^{j\left(\omega_0 t - \frac{2\pi}{\lambda}(n_0 + n_2 I)\, L\right)} \tag{2.14}$$

So,

$$\phi = \frac{2\pi}{\lambda}(\, n_0 + n_2 I) L \tag{2.15}$$

$$\phi = \phi_L + \phi_{NL} = \left(2\pi \frac{L n_0}{\lambda}\right) + \left(2\pi \frac{n_2}{\lambda A_{eff}} P_0 L\right) \tag{2.16}$$

$$\phi = \phi_L + \phi_{NL} = \left(2\pi \frac{L n_0}{\lambda}\right) + (\gamma P_0 L) \tag{2.17}$$

where ϕ_{NL} is the non-linear phase shift, A_{eff} is the mode area at 1550 nm (50-μm^2) and γ is the Self-Phase-Modulation (SPM) factor:

$$\gamma = \frac{2\pi n_2}{\lambda A_{eff}} (\mathrm{W^{-1}/Km}) \tag{2.18}$$

Considering two counter-propagating optical beams in the NALM (see Figure 2.13), it can be deduced that the non-linear phase shift in the 50/50 coupler is the sum of the contributions of the SPM according to [75]:

$$\Delta\phi_{NL} = \phi_{NL_{CCw}} - \phi_{NL_{Cw}} \tag{2.19}$$

In optical fiber a typical value γ in the 1.55-μm wavelength region is 2 W^{-1}/km [75, 76]. Figure 2.13 shows an asymmetrical design of a fiber loop may contain a semiconductor optical amplifier. This configuration is called a nonlinear amplifying loop mirror (NALM). When light injected on the rigth side at a low power level, it will be mostly reflected back into the same port. In case of ultrashort pulses with a substantial peak power, however, we have substantial nonlinear phase changes in the loop [13, 14, 74, 77]. These are stronger for light propagating in counter-clockwise direction (CCw, red arrow), since this is first

amplified and then travels through passive fiber. Light in the opposite direction (clockwise, Cw, green arrow) propagates with a lower power level for most of the fiber length. As a result, the interference conditions are affected such that a power-dependent fraction of the input light reaches the upper output port.

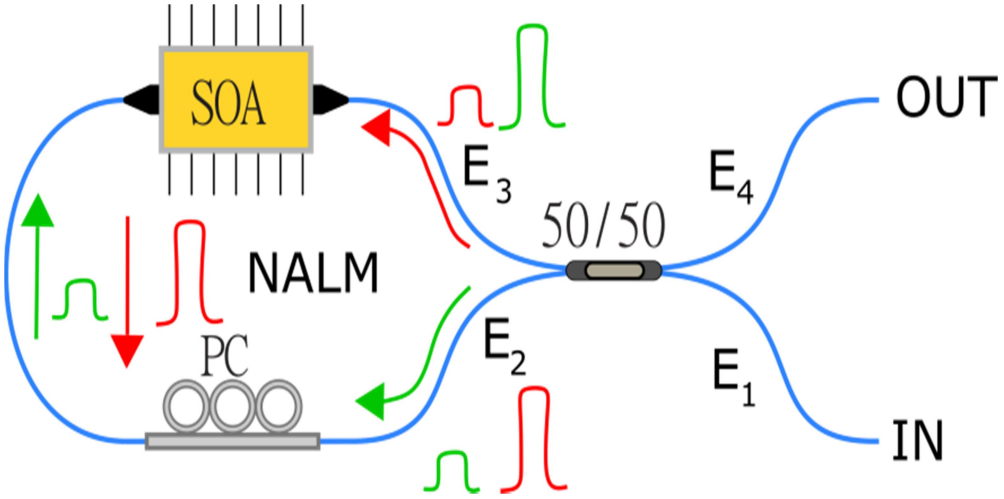

Figure 2.13. Nonlinear amplifying loop mirror (NALM).

The NALM is a known configuration and its transfer function describes the transmission (T) and reflection (R) periodic of the pulses in time and is represented by the equation 2.20 [74]:

$$T = \frac{|E_4|^2}{|E_1|^2} = \frac{I_4}{I_1} = 0.5G_{SOA}\left[1 - \cos\left(\Delta\phi_{NL}(G_{SOA} - 1)\right)\right] \quad (2.20)$$

$$R = 1 - T = \frac{|E_1|^2}{|E_1|^2} \quad (2.21)$$

where G_{SOA} is the SOA gain and $\Delta\phi_{NL}$ is the non-linear phase shift difference between counter-propagating beams. Note that when varying both the SOA gain and the polarization of the counter-propagating light beams will change in the NALM switching [13].

Works in the literature have reported the use of NALM to generate a passive mode-locked laser [13, 14, 78]. Kues *et al*. [78] used NALM to develop a figure-8 passive mode-locked laser and the experimental schematic is shown in figure 2.14.

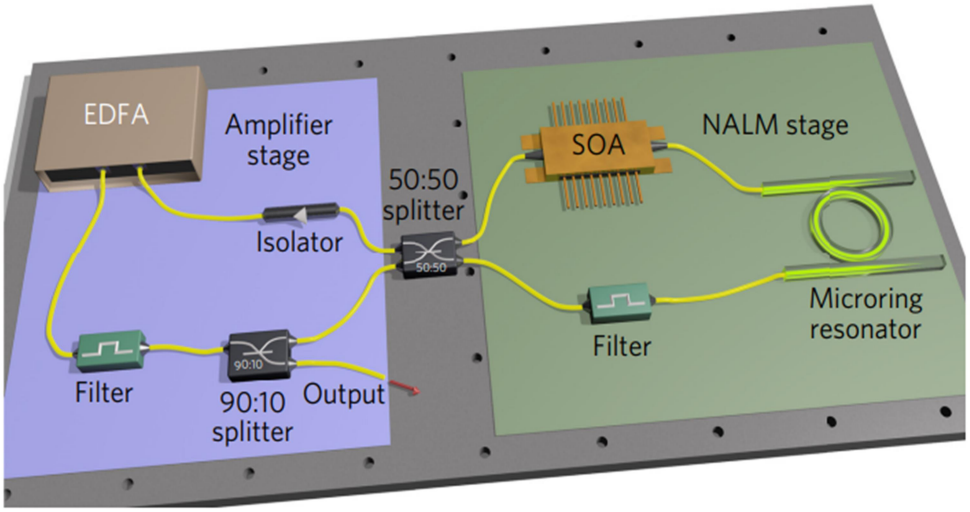

Figure 2.14. Schematic setup of the figure-eight SOA-based fiber laser [78].

Figure-8 passive mode-locked laser (F8-PMLL) similar to the shown in figure 2.14 is assembled to understand the phenomenon of optical pulses train generation and mode-locking operation. The characterization of the laser is demonstrated in chapter 3 of this thesis.

2.5.2 Nonlinear polarization rotation (NPR)

When an intense optical pulse propagates in an optical fiber which is not polarization-maintaining, there can be a nonlinear (intensity-dependent) change in the polarization state. This is usually not exactly a rotation of a linear polarization direction, but rather the change to some elliptical polarization state [79]. The physical cause of these effects is related to self-phase modulation (SPM) as well as to some birefringence ($\Delta_n = n_x - n_y$) of the fiber [75, 76]. While nonlinear polarization rotation can be disturbing in systems with fiber amplifiers, it is also often utilized for passive mode-locking of fiber lasers [11, 12]. Here, a typical configuration contains some fiber polarization controller or a set of waveplates, which can be adjusted such that the maximum transmission (minimum loss) at the polarizer occurs for the highest possible optical intensity. The configuration then serves as an artificial saturable absorber [11]. As the Kerr effect is very fast, that artificial absorber is very fast, and its strength is adjustable with the polarization

controllers [75, 76]. This makes mode-locking with nonlinear polarization rotation a powerful technique. Assuming $n_x > n_y$, n_x and n_y are the mode indices along the slow and fast axes, respectively, when low-power, continuous-wave (CW) light is launched with its polarization direction oriented at an angle with respect to the slow (or fast) axis, the polarization state of the light changes along the fiber from linear to elliptic, elliptic to circular, and then back to linear in a periodic manner (see Figure 2.15) [76, 77] over a distance known as the beat length and defined as $L_{\Delta n} = \lambda / \Delta_n$.

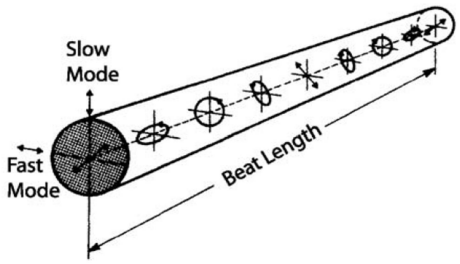

Figure 2.15. Evolution of state of polarization along of the polarization-mantaining fiber (PMF) when input signal is linearly polarized at 45◦ from the slow axis [76].

The concept is illustrated in figure 2.16 with the effect of self-phase modulation (SPM) between the orthogonally polarized eigenmodes, the linearly polarized light is initially transformed into elliptically polarization light, and then the axis of the polarization is rotated by an intensity-dependent angle [80]. Finally, if the transformed light is again linearly polarized by an analyzer, the throughput in the cavity becomes intensity-dependent. With proper polarization control on the fiber ring cavity, the architecture with aid of an analyzer plays a role like an artificial fast saturable absorber [11, 12, 81], which provides smaller loss for higher intensities and larger loss for smaller intensities to suppress the low-level radiation so as to achieve passive mode-locking in the laser cavity .

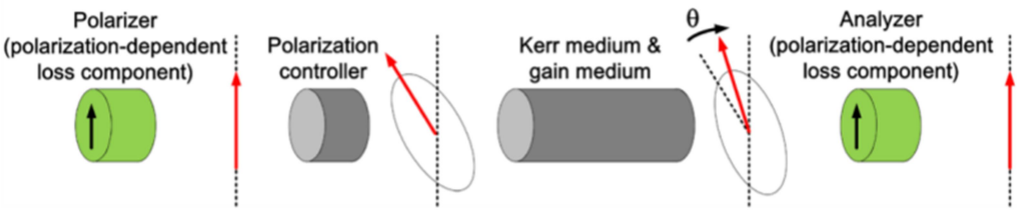

Figure 2.16. The NPR mechanism in a fiber ring laser through the set of polarizer (PDL component), polarization controller, Kerr médium and gain medium and analyzer (PDL component) [80].

From equation 2.17, the light is decomposed into orthogonal components:

$$\vec{E} = (E_x\hat{x} + E_y\hat{y})e^{-j(\phi_L+\phi_{NL})} \tag{2.22}$$

$$E_x = E_x\, e^{j(\phi_L+\phi_{NL})} \tag{2.23}$$

$$E_y = E_y\, e^{j(\phi_L+\phi_{NL})} \tag{2.24}$$

So,

$$\Delta\phi_{NL} = \phi_x + \phi_y = \gamma L\,(1-B)\big(P_x + P_y\big) \tag{2.25}$$

$$P_x = P_0 cos^2(\alpha)\ and\ P_y = P_0 sen^2(\alpha) \tag{2.26}$$

$$\Delta\phi_{NL} = \gamma L(1-B)(P_x + P_y) \tag{2.27}$$

$$B = (2 + 2\sin 2\theta)/(2 + \cos 2\theta) \tag{2.28}$$

where B is a parameter that determines the birefrigence of the medium and theta the angle of rotation [75, 76]. The coupling parameter B depends on the ellipticity angle θ and can vary from 2/3 to 2 for values of θ in the range 0 to π/2. For a linearly birefringent fiber (Polarization-maitening-fiber, PMF), θ = 0, and B = 2/3. In contrast, B = 2 for a circularly birefringent fiber (θ = π/2). Figure 2.17 shows the different polarization states that can be generated from the nonlinear polarization rotation as a function of $\Delta\phi_{NL}$ [75].

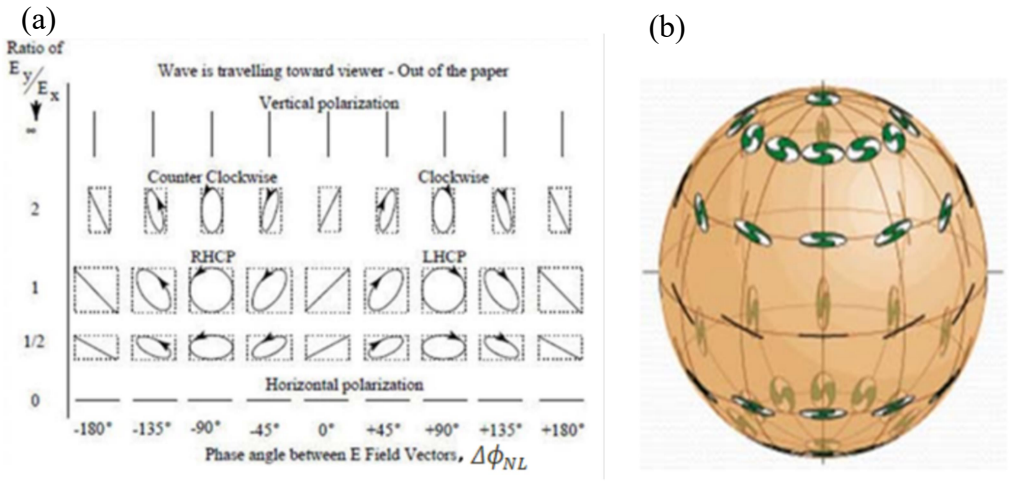

Figure 2.17. Different polarization states as a function $\Delta\phi_{NL}$; (b) Poincaré sphere [75].

The phase shift between the orthogonal fields generated from the nonlinear phase difference ($\Delta\phi_{NL}$) causes the rotation (change to a new polarization state) as shown by figure 2.17 (a). All existing polarization states are represented on the Poincaré sphere as shown in figure 2.17 (b).

Works in the literature have reported the use of nonlinear polarization rotation (NPR) to generate a passive mode-locked laser [11, 12, 80-82]. Figure 2.18 shows an experimental schematic using an SOA as an NPR device.

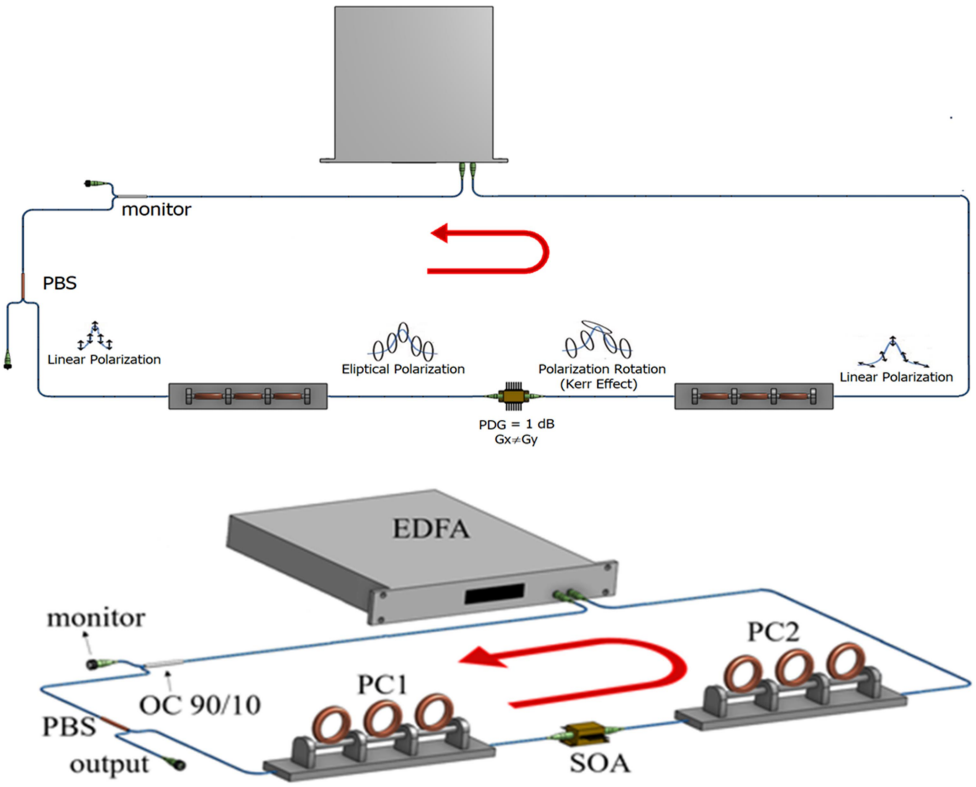

Figure 2.18. Experimental set-up of the passive mode-locked Laser based NPR.

Nonlinear polarization rotation in the SOA followed by polarization projection is employed as the mode-locking mechanism [11, 82]. In this way, the SOA not only acts as an amplifying element, but also provides the nonlinearities needed for pulse compression [12]. The linear polarization after the PBS is made elliptical using a polarization controller 1. As the pulse propagates through the SOA, the axes of the polarization ellipse rotates continuously from the peak to the edges of the pulse due to Kerr nonlinearity. At the SOA exit the polarization directions are adjusted using a polarization controller 2 so that the peak of the pulse sees high transmission and the edges are attenuated by PBS. In this way, the

NPR acts like a artificial fast saturable absorber and leads to the intensity discremination and narrowing of the pulse [11, 83].

Group velocity dispersion (GVD) in optical fibres may be a limiting factor for fast mode locked optical pulses mainly in long cavity fiber rings with low repetition rate [76]. A passive mode-locked laser fiber ring laser similar to the presented in the references [11, 12] is presented in chapter 3 of this thesis, but implemented dispersion compensating element in the ring cavity.

2.6 Group velocity dispersion (GVD)

Dispersion is the phenomenon that occurs in the propagation of electromagnetic fields in material media, causing delays in the propagation of these fields. These delays can be caused by different types of dispersion. When an electromagnetic wave interacts with the electrons that form the dielectric material, the response of the media is usually dependent on the frequency of this wave [75]. This property refers to the phenomenon of chromatic dispersion and is manifested through the dependence of the refractive index of the optical fiber on the frequency of the electromagnetic wave. The chromatic dispersion is characterized by the resonance or oscillation of electrons that form the material media when absorbing electromagnetic radiation [76]. In this case the refractive index varies depending on the propagating wavelength. Figure 2.19 shows the dependence of the refractive index in function on the wavelength.

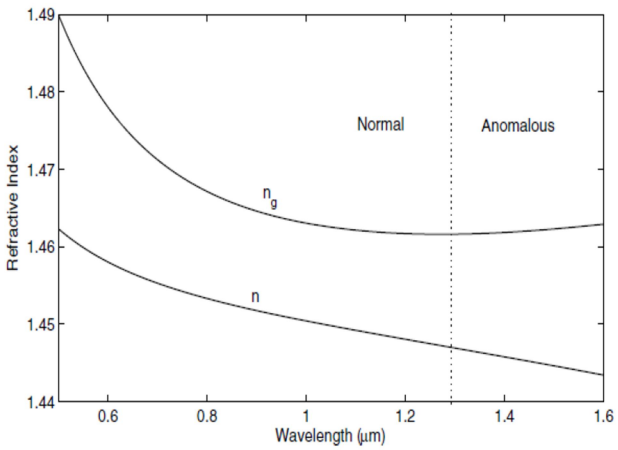

Figure 2.19. Dependence of the refractive index in function on the wavelength [75].

The chromatic dispersion causes significant changes in the propagation of ultra-short pulses along the optical fiber. This behavior is associated with fact the pulses are formed by different spectral components that travel with different speeds [75]. The speed of each spectral component is a function of the index of refraction as shown in equation 2.29:

$$v = c/n(\lambda) \tag{2.29}$$

The chromatic dispersion induces a temporal broadening of the pulse, deforming it. The dispersion can be accounted for from the expansion of the propagation constant β in a Taylor series as shown in equation 2.30:

$$\beta_m = \left(\frac{d^m\beta}{d\omega^m}\right)\omega = \omega_0 \qquad (\text{m=0,1,2,3,....}) \tag{2.30}$$

$$\beta_1 = \frac{1}{v_g} = \frac{n_g}{c} = \frac{1}{c}\left(n + \omega\frac{dn}{d\omega}\right) \tag{2.31}$$

$$\beta_2 = \frac{1}{c}\left(2\frac{dn}{d\omega} + \omega\frac{d^2n}{d\omega^2}\right) = -\frac{D\lambda^2}{2\pi c} \tag{2.32}$$

Physically these relationships show that the pulse moves with a given group velocity (v_g). D is the first order dispersion parameter and β_2 is known as the second order GVD parameter which is responsible for the temporal broadening of the pulse [75, 76]. Figure 2.20 shows the set of parameters GVD [β_2 (ps^2/Km)] and dispersion [D (ps/(km.nm))] in a silica optical fiber.

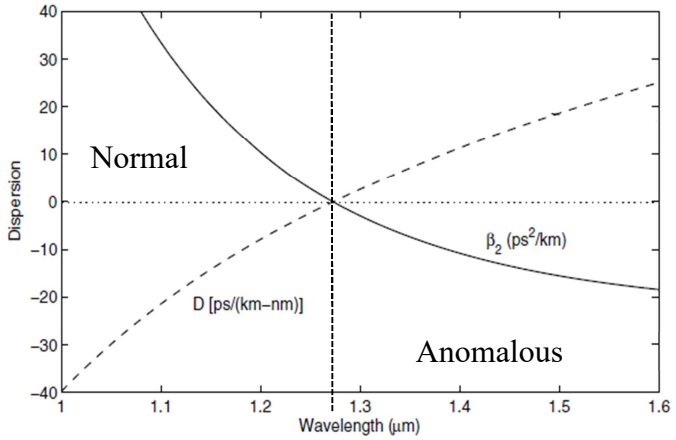

Figure 2.20. Variation of dispersion parameter and GVD parameter with wavelength [75].

Figure 2.20 shows anomalous dispersion ($\beta_2 < 0$) for wavelengths greater than 1290 nm as opposed to normal dispersion ($\beta_2 > 0$). In anomalous dispersion, electromagnetic waves with higher frequencies have a higher phase velocity compared to electromagnetic waves with lower frequencies in contrast to the normal dispersion regime.

2.7
Scattering phenomena in optical fibers

Light interacts with matter because matter contains electric charges. The time-varying electric field of light exerts forces on the electric charges and dipoles in atoms, molecules, and solids, causing them to vibrate so that they undergo acceleration [63]. Vibrating electric charges absorb and emit light. We consider in turn three scattering processes of importance in photonics: Rayleigh, Raman, and Brillouin scattering. Scattering is inherent and unavoidable under many circumstances but it can also prove useful for providing information about the characteristics of materials and for creating useful light sources.

When a pulse of light is injected into the fiber, some of the photons of light are scattered in random directions due to microscopic particle. This effect, referred to as Rayleigh scattering, provides amplitude and temporal information along the length of the fiber [76]. In addition, some of the light is scattered back in the opposite direction of the pulse. This is referred to as the backscattered signal. The scattering in the fiber optic cross section is given by equation 2.33:

$$\alpha_R = C/\lambda^4 \tag{2.33}$$

where C (0.7−0.9 dBμm⁴/Km) is the scattering constant and varies according to the fiber optic manufacturing process. Note also that the shorter the wavelength, the greater the scattering intensity. Rayleigh scattering is a process whereby a material causes na incident photon to change direction. It entails an energy-conserving (elastic) interaction so that the scattered photon has the same energy as the incident photon [76] as shown in Figure 2.21.

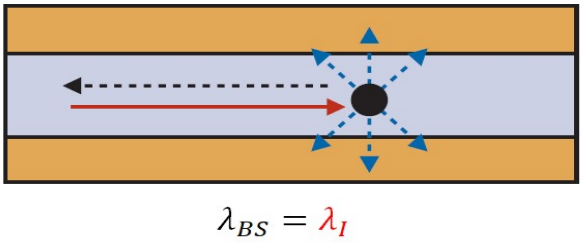

Figure 2.21. Energy-conserving interaction so that the back-scattered photon has the same energy as the incident photon.

An optical-time-domain-reflectometer (OTDR) can measure the levels of backscattering very accurately and can measure small variations in the characteristics of fiber at any point along its length [4-6]. When the scattering phenomenon involves a change in frequency, or energy change, it is said to be an inelastic scattering [63]. In addition to changes in frequency, the characterization of light scattering phenomena depends both on the properties of incident light, such as wavelength and polarization, and on those of scattering centers, mostly its size and atomic composition [76]. Table 2.1 provides an overview of light scattering phenomena, showing the classification of each phenomenon in relation to energy conservation, direction and origin.

Scattering	Type	Direction	Origin
Rayleigh	**Elastic**	**Forward / Backward**	**Microscopic Particles**
Raman	**Inelastic**	**Forward**	**Optical Phonons**
Brillouin	**Inelastic**	**Backward**	**Acoustic Phonons**

Table 2.1. Comparison of light scattering phenomena.

Raman scattering is a process by means of which a photon following an interaction with a material, emerges either at a lower frequency (Stokes scattering) or at a higher frequency (anti-Stokes scattering). Raman scattering occurs in gases, liquids, and solids [63]. Unlike Rayleigh scattering, Raman scattering is inelastic; the alteration of photon frequency is brought about by no exchange of energy with a rotational and/or vibrational mode of a molecule or solid. Brillouin scattering is similar to Raman scattering except that the exchange of energy takes place with phonons acoustic, rather than optical phonons of the médium [63, 76].

Figure 2.22 shows left peak with a downshifted frequency is called the Stokes wave, while the right one with an upshifted frequency is called the anti-Stokes wave. Both Brillouin and Raman scatterings are inelastic scatterings because they are associated with certain frequency shifts. The last mechanism that can be observed is the Rayleigh scattering attributed to fluctuations in the orientation of anisotropic molecules.

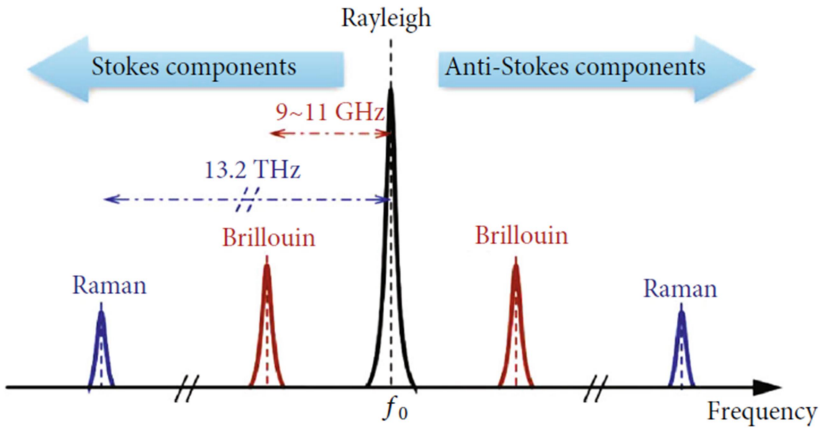

Figure 2.22. Optical spectra of Scattering phenomena in optical fiber [83].

2.8 Phase-sensitive optical time domain reflectometer (ϕ-OTDR) and modelling Rayleigh backscattering

An Optical Time Domain Reflectometer (OTDR) is a fiber optic tester for the characterization of fiber and optical networks. The purpose of an OTDR is to detect, locate, and measure events at any location on the fiber link from probe pulse. Rayleigh scattering is intrinsic to the fiber material itself and is present along the entire length of the fiber. Since Rayleigh scattering is uniform along the length of the fiber, discontinuities in Rayleigh scattering can be used to identify anomalies in the transmission along the fiber link. Some of the features obtained from this reflectometry trace are an estimation of the fiber length, fiber attenuation, fault location and loss due to connectors or splices.

The modeling of Rayleigh backscattering in optical fibers has been approached in many works, often targeting fiber monitoring applications like OTDR and Φ-OTDR [84–89]. In OTDR sections used a broadband light source,

so that the coherent length ($l_c = c/n\delta\nu_c$) is less than the pulse width spatial resolution ($R_{PW} = c\tau/2n$), and the detected signal represents intensity addition instead of field addition with interference [4-6]. Φ-OTDR configuration used a narrow linewidth laser whose coherent length is much longer than the fiber sections [38-50]. The detected signal represents field addition, which is the summing up of Rayleigh scattering of many scattering centers within the pulse width. These scattering centers are equivalent as multiple reflectors with weak reflectivity. Figure 2.23 shows the experimental schemes of an OTDR system and a ϕ-OTDR system.

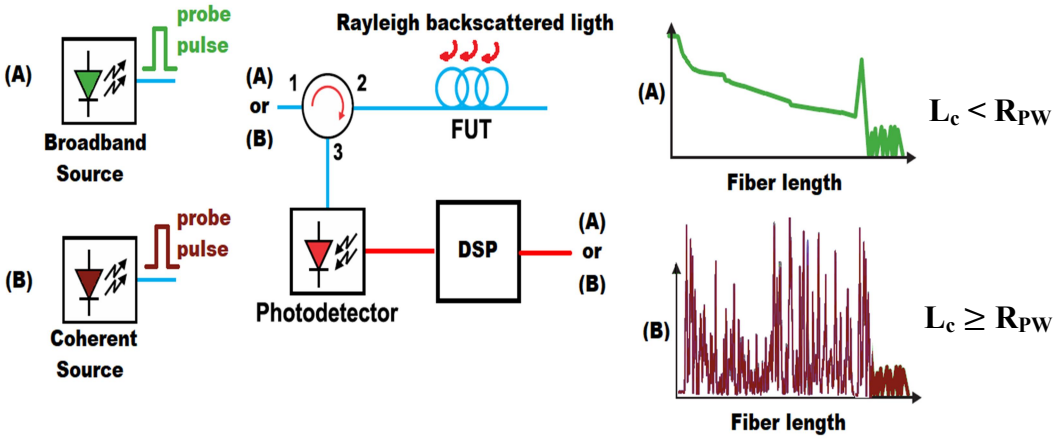

Figure 2.23. Block diagram of an OTDR and ϕ-OTDR system.

Rayleigh scattering in optical fibres is generated by random fluctuations of the refractive index at the nanoscopic scale, but the interference of Rayleigh scattered coherent light and the backscattered intensity is governed by random fluctuations of the mean refractive index on a much larger scale. Backscattering of coherent light can be modelled as the sum of the contributions from every portion of the fibre in which the phase of each contribution is randomized [90]. This allows evaluating the reflectivity of the distributed random mirror embodied by a chosen section of the backscattering fibre. The intensity spectrum of the backscattered light at the input point is frequency-dependent and fluctuations can be described as [90]:

$$I(k) \propto \left|\sum_{i=1}^{N} \exp(j\bar{n}_i kd)\right|^2 = < I > + \sum_{i \neq p} \exp\left(j\left[\overline{n_i} - \overline{n_p}\right]kd\right) \qquad (2.34)$$

where the fibre section is considered as a series of N segments of mean length d and mean refractive index $\overline{n_i}$ with random variations from segment to segment as shown in figure 2.24. The second term of (equation 2.34) is a double sum over all pairs of segments i and p and describe the fluctuations due to the interference between the optical field from all segments. The result is an intensity spectrum with strong frequency dependence, with fluctuations that can reach ~10 dB above the mean value in kilometre-long fibres [90], coming from constructive interference of the backscattered fields.

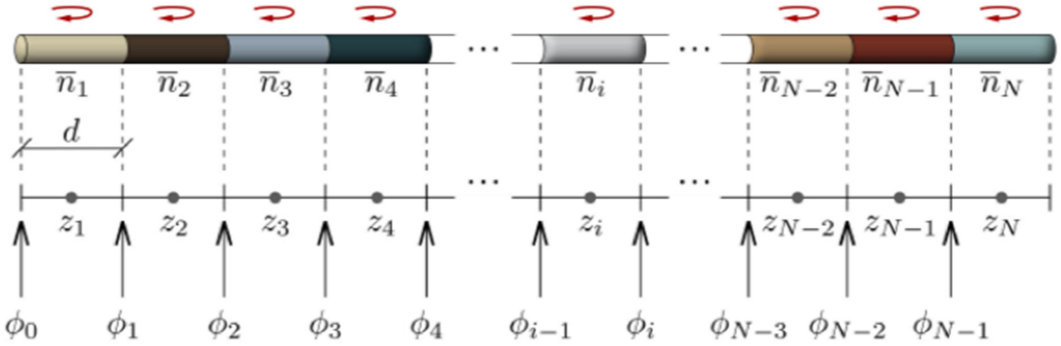

Figure 2.24. Representation of theoretical model for Rayleigh backscattering intensity fluctuations in single mode fibers [90].

The backscattered intensity spectrum calculated using Eq. (1) for typical standard single-mode fibers and d ~5 mm is shown in Figure 2.25 (a) within a 10-GHz range of optical frequencies, for illustrative fibre sections lengths of 0.5, 1 and 2-m. In the full 100-GHz used in the simulations, peaks as high as 9 dB above the mean were found. All spectra present randomly spaced relatively strong peaks, which sharpen as the length is increased. A simple approach to understanding this feature is to consider the backscattering fiber section as consisting of a long fiber Bragg grating (FBG) with a very small index depth and a random period over its length. The longer the grating, the sharper the reflection peaks [91]. The randomness of the backscattering gives rise to randomly spaced spectral peaks whose spectral width is also random. Figure 2.25(b) shows the distribution of peak widths (FWHM) of Rayleigh scattered light calculated in a 100-GHz spectral range. As expected, the mean width is inversely proportional to the length of the scattering fiber, and the longer the fiber section, the sharper the peak width

distribution. Remarkably, the most likely spectral width reflected (e.g., 50-MHz or 0.4-pm linewidth) is that of a very weak FBG of the same length (e.g., 2-m long).

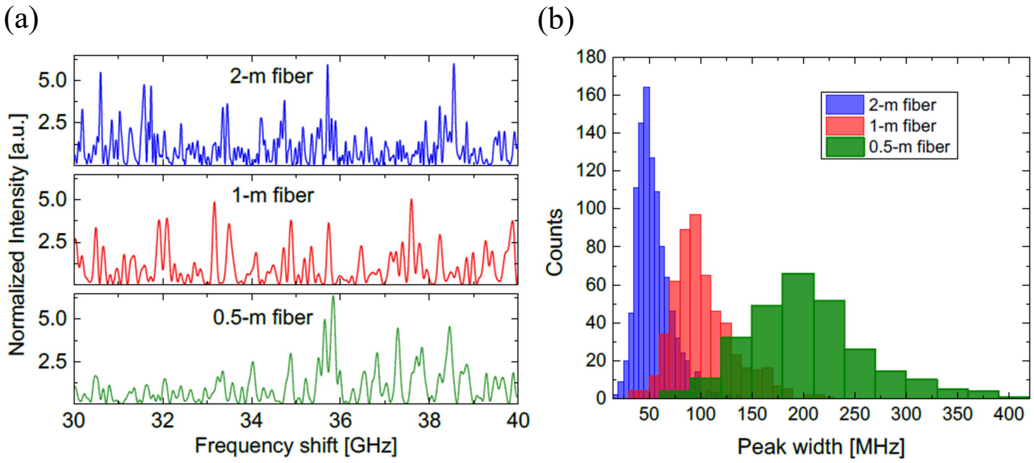

Figure 2.25. Typical simulated random backscattering spectrum in a 10 GHz range. (a) Reflection peaks are formed, narrower and more frequent for longer fibre sections (e.g., 2-m). (b) Typical occurrence of simulated peak widths for three lengths of backscattering fibre section. The most likely spectral width of the distributed random mirror (e.g., 50-MHz) predicted by Eq. (1) equals the widt of a very weak FBG of same length (2 m).

Mode locked random fiber laser (MLRFL) is demonstrated in chapter 4 of this thesis from Rayleigh backscattered light as feedback. The laser action in a random fiber laser occurs since there sufficient roundtrip gain. It is clear that with sufficiently high gain, lasing could start in any of the random spectral peaks as shown in Figure 2.25 (a). The fiber sections behave as highly selective spectral filters (see figure 2.25(b)) because backscattered light within the pulse width interferes with each other and forms a random interference pattern like a random FBG [92-95] but here with multiple reflectors of weak reflectivity (scattering center). With high enough gain and synchronous amplification (gain modulation), the laser can start at any one of the random spectral peaks and phase-locked in mode-locking regime at the random wavelength chosen.

2.9 Random Fiber Laser (RFL)

A laser is usually constructed from two basic elements: a material that provides optical gain through stimulated emission and an optical cavity that

partially traps the light. When the total gain in the cavity is larger than the losses, the system reaches a threshold and lases [54]. Random lasers work on the same principles, but the modes are determined by multiple scattering and not by a laser cavity [17-20]. Generally, RFL incorporate one optical amplifier and a fixed distributed reflector [19]. By using fiber optics as the random laser medium multiple scatters as shown in Figure 2.26 in a three-dimensional volume are confined to nearly one dimension. Confinement is caused by the difference in refractive index between the core and cladding structures, which retain light in the direction transverse to propagation. The benefits of using optical fibers as a medium for random laser action go far beyond reducing the complexity of the spatial emission, which, in this case, assumes an almost Gaussian beam [19, 20, 67, 96].

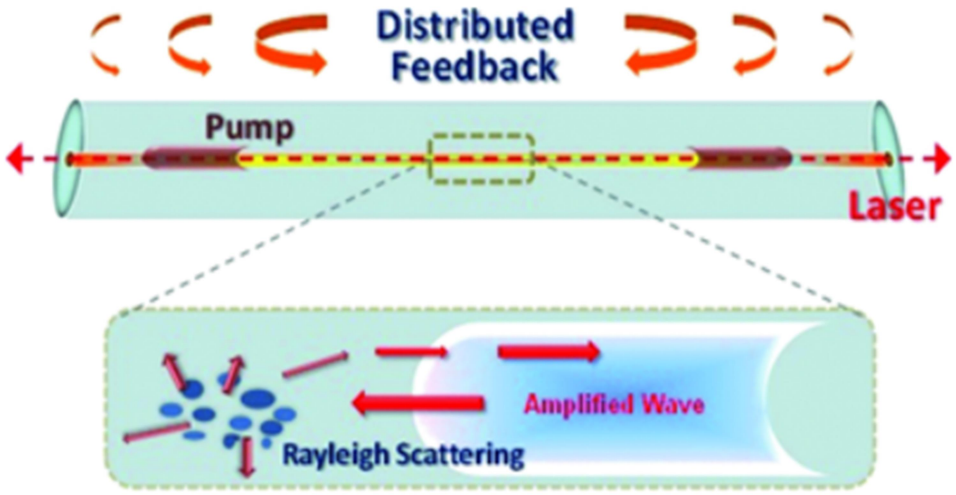

Figure 2.26. Random distributed feedback fiber laser. An optical fiber provides distributed Raman gain when pumped by two lasers. Distributed Rayleigh backscattering promotes coherent feedback along the optical fiber, defining na open optical cavity [96].

Works in the literature have reported random fiber lasers using localized (SOA) gain combined with Rayleigh scattering in single mode fibers [19, 67]. Figure 2.27 shows an example of a random fiber laser that uses an SOA as a gain medium [19, 67]. Tovar *et al.* showed that single-longitudinal-mode operation is only possible near the SOA threshold current, while multi-mode operation dominates when SOA current is increased. In this configuration, the laser cavity is defined by the Rayleigh backscattering of 8-km dispersion-shifted fiber (DSF).

While the 8-km of fibers determine the distributed feedback, the FBG acts as both a fixed mirror and an adjustable filter. The major disadvantage of this configuration occurs in the use of optical fibers of long lengths due difficult to integrate the device.

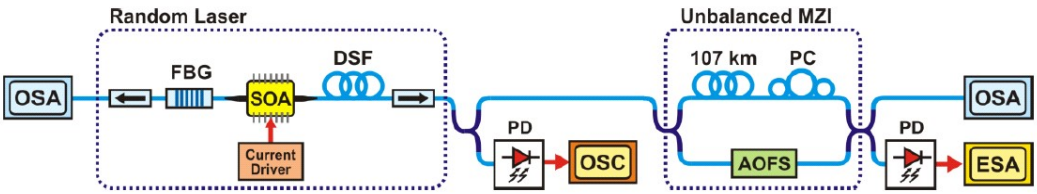

Figure 2.27. Experimental setup of the Random Fiber Laser using localized gain (SOA) [19].

Another works in the literature also reported random fiber lasers using distributed gain (Raman or EDF) [18, 96]. Margulis *et al.* demonstrated a random fiber laser using a hybrid gain mechanism using a localized system gain with an SOA and distributed gain from an EDF [20]. It was reported laser pulse by synchronizing the SOA driver to the returning amplified Rayleigh backscattered light from a selected short section of the EDF. By tuning the SOA pulse rate, random lasing was achieved by addressing selected meter-long sections of the 81-m long EDF, which was open-ended [20]. The experimental setup is shown in figure 2.28.

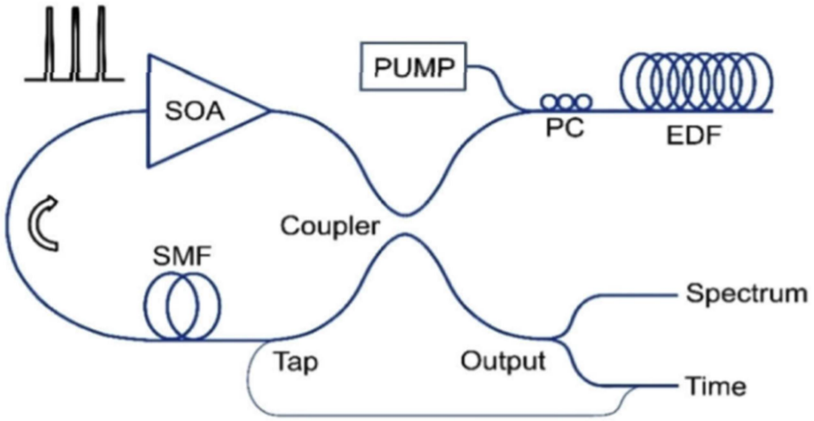

Figure 2.28. Schematic diagram for the Hybrid electronically addressable random fiber laser [20].

It was reported the tap port signal of the HEAR laser can also be seen as a optical-time-domain reflectometer (OTDR) trace of SOA probe pulses. Indeed, the modulation frequency maps the position of the resonant lasing section so that

the same fluctuations observed in a ϕ-OTDR are directly seen here in the HEAR laser intensity. Hence, the HEAR laser can be directly used as a fast distributed sensor within the addressable section of the EDF, the laser intensity being sensitive to external efects over the fiber, such as stress or temperature, with the resolution given by half the modulation pulse-width as in a ϕ-OTDR [20].

In Chapter 4 of this thesis, HEAR laser as a mode locked random fiber laser (MLRFL) is demonstrates. The device generates Fourier transform-limited pulses from the Rayleigh backscattering feedback. A mode-locked laser can generate transform-limited pulses when all modes are perfectly phase-locked. Coupling mechanisms for phase-locked can occur passively from saturable absorbers [8-10] and techniques that simulate their behavior [11-13] or actively from phase or gain modulation of the cavity modes [1, 3].

2.10 Distributed optical fiber sensor (DOFS)

A large amount of research has been undertaken on fiber optic distributed sensing technology because it allows us to determine a measurand at any point along a fiber. The Rayleigh scattering is formed by many randomly spaced scattering centers at nanometer separation, and the sum of the scattering centers can be added coherently as their spacing is much smaller than the optical wavelength [83]. This response is similar to FBG, except FBG has equal spacing, while in Rayleigh backscattering (BS), the spacing varies randomly at a range of a few nm to hundreds of nm in the spatial distance (see Figure 2.29). When the FBG is illuminated by a broadband light source, a set of beams reflected from a set of partially reflecting planes formed by the periodic core index modulation interfere with each other [97]. The interference is destructive unless each beam is in phase with all the others. According to Bragg's law which gives this condition, only one wavelength, i.e. λ_B the Bragg wavelength with reflectivity R and bandwidth ($FWHM_B$), is selected, which is given by:

$$\lambda_B = 2n\Lambda \tag{2.35}$$

$$R = tanh^2(\pi \Delta n L \eta(V) \lambda_B) \tag{2.36}$$

$$FWHM_B = \lambda_B \sqrt{\left(\frac{\Delta n}{2n}\right)^2 + \left(\frac{1}{N}\right)^2} \quad (2.37)$$

where n is the effective core index of refraction, Λ the period of the index modulation, L is the length of the grating, Δn the magnitude of the index perturbation, $\eta(V)$ a function of the fiber V parameter that represents the fraction of the integrated mode intensity comtained in the core and N is the number of grating planes [97, 98]. Already the intensity spectrum of the backscattered light (see figure 2.29(a)) at the input point is frequency-dependent and fluctuations can be described as equation 2.34 with L in this case being the length of the fiber section [90].

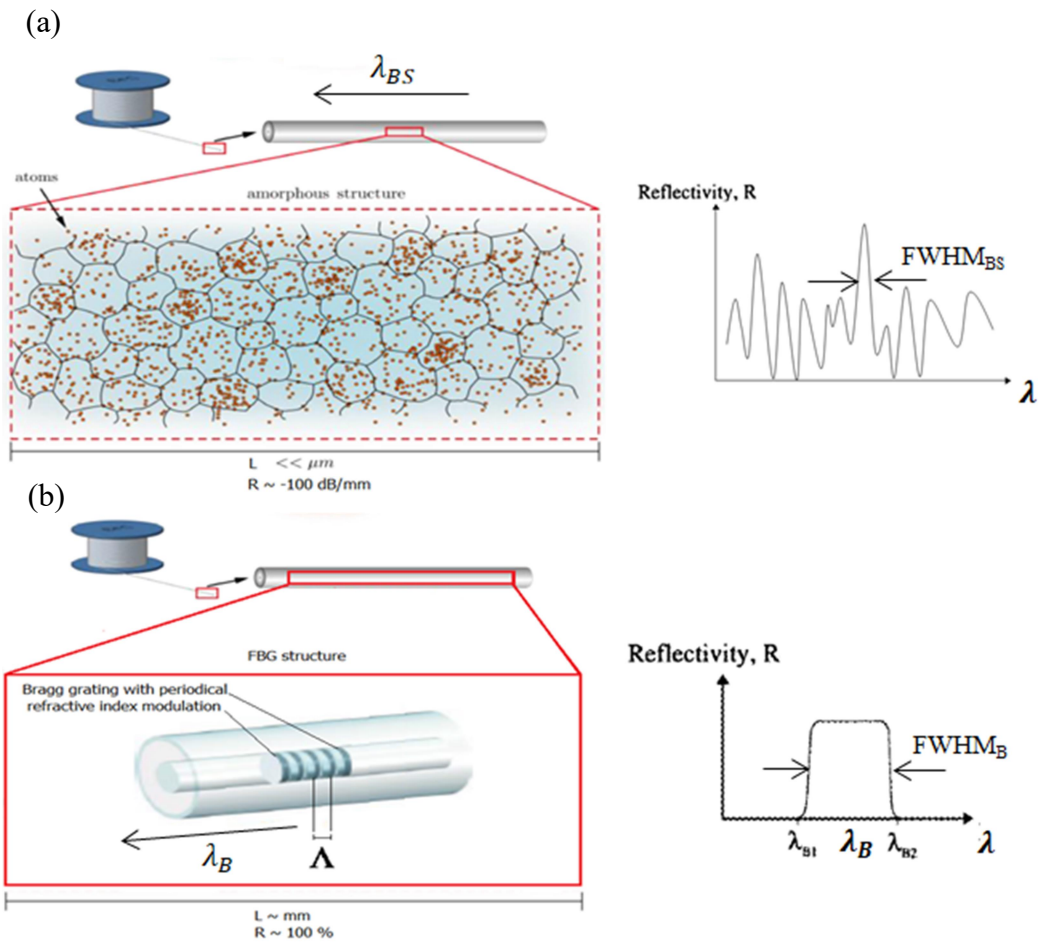

Figure 2.29. (a) Schematic of a fiber section in submicron scale and spectral response profile of Rayleigh backscattering. Atoms are represented by orange dots, and black lines define regions of constant density [90 - adapted]; (b) schematic of diagram of fiber Bragg grating and spectral response profile.

The bandwidth of the various peaks formed by the random interference pattern is a function of the length of the fiber section, which is given by:

$$FWHM_{BS} = \frac{c}{2n\mathrm{L}} \tag{2.38}$$

where c is the speed of light, n is the effective core index of refraction and L is the length of the fiber section.

A change in the temperature of the fiber produces a shift in the Bragg wavelength due to thermal expansion which changes the grating spacing, and a change in index of refraction with temperature. When the fiber is strained the Bragg wavelength varies due to the change in the grating spacing and the photoelastic efect induced change in the refractive index [97]. Just like FBG has spectral response with a profile, the wavelength shift of the Rayleigh backscattering pattern is linearly proportional to the temperature and strain with the following relation:

$$\frac{\Delta\lambda}{\lambda} = (1 - \rho_e)\varepsilon \tag{2.39}$$

$$\frac{\Delta\lambda}{\lambda} = (\alpha + \xi)\Delta T \tag{2.40}$$

where ρ_e is an effective photoelastic constant and equals 0.22, α is the thermal expansion coefficient for the fiber and equals 0.55 x 10^{-6} for silica. The quantity ξ represents the termo optic coefficient and is approximately equal to 8.3 x 10^{-6} for the germania doped sílica core. In 1989, Morey, W. W. et al measured microstrain and temperature variations in the FBG for different wavelengths, as shown in Table 2.2 [97, 98]:

Wavelength (μm)	Strain sensitivity (pm $\mu\varepsilon^{-1}$)	Temperature sensitivity (pm $^{\circ}C^{-1}$)
0.83	~0.64	~6.8
1.3	~1	~10
1.55	~1.2	~13

Table 2.2. Strain and temperature sensitivities of FBG sensors with different wavelengths [97].

Fiber optic sensing uses the physical properties of light as it travels along a fiber to detect changes in temperature, strain and other parameters. Fiber optic detection uses the fiber as a sensor to create thousands of continuous detection points along the fiber. This is called fiber optic distributed sensing. Generally, devices that measure the fiber itself are called interrogators [83]. The objective is to use a standard or specific optical fiber for strain or temperature measurements using distributed sensing based on coherent phase-sensitive OTDR (ϕ-OTDR) detection. Here, the fiber itself is the sensor. As these fiber detection method are completely intrinsic, a standard telecommunications fiber can be used as the medium as long as the expected temperature remains below 177°C (450°K) (Standard single mode fiber) and the fiber is not subjected to excessive chemicals or disruption mechanics. Figure 2.30 shows several application examples based on distributed optical fiber sensor (DOFS).

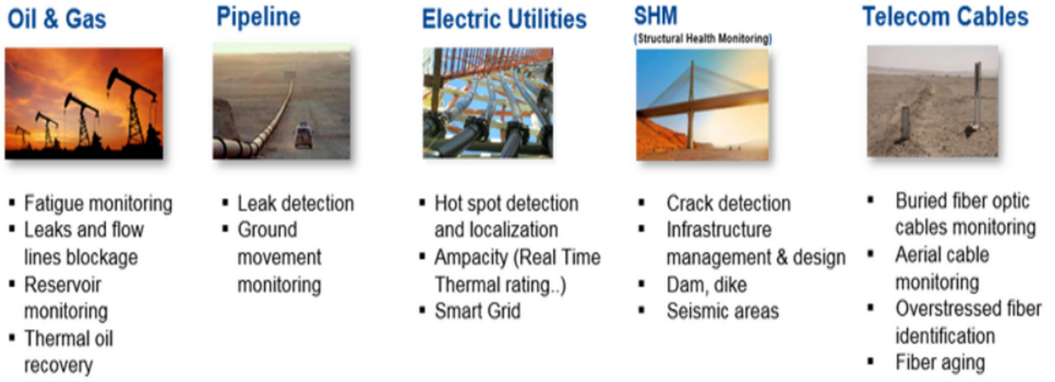

Figure 2.30. Examples of fiber optic distributed sensing applications [99].

In chapter 4 of this thesis, mode-locked random fiber laser generates tranform Fourier-limited pulses and operates as a lasing ϕ-OTDR in optical applications of distributed acoustic sensor (DAS) and distributed temperature sensor (DTS).

3
Mode-locked fiber lasers in closed cavity

This chapter presents the setups and experimental results of both the Figure-eight passively mode-locked laser (F8-PMLL) and the Passively mode-locked fiber ring laser (PMLFRL). Describes the optical pulse generation mechanisms, analyzes spectral and temporal dynamics and discusses the relevance of the results.

3.1
Figure-eight passively mode-locked laser (F8-PMLL)

The optical pulse generation is comprised of a figure-eight passively mode-locked laser (F8-PMLL). Such laser configuration has been shown to produce sub-picosecond pulses at different wavelengths [14], rendering its application for a tunable, long-reach, high-resolution time-domain reflectometer [4-6]. The physical mechanisms that guarantee mode-locked in PML fiber lasers are the constructive/destructive interference of counterpropagating longitudinal modes in a so-called nonlinear amplifying loop mirror (NALM) [14]. The latter allows for the optical switching of the input optical pulses according to the following mathematical relations shown in equation 2.20 and 2.21. When the NALM is combined with a closed fiber loop, it constitutes a figure-8 laser (F8L), an extremely versatile fiber structure that finds applications in, for instance, soliton generation, and has been first reported by Duling [100]. Recently, an F8L realized with an SOA in the NALM and na EDFA in the optical cavity has been reported [78], whose design is reproduced in this work and depicted in figure 3.1.

3.1.1
Experimental setup F8-PMLL

The NALM (left-hand side in figure 3.1) is composed by a SOA (Thorlabs-1013SXS), a Polarization Controller (PC), and single-mode fibers

totalling a length of L_1 ~8.42-meters. The optical cavity (right-hand side in figure 3.1) is formed by a PC, a 90/10 coupler (that allows one to couple a portion of the optical signal generated in the F8L to the output), a optical tunable band pass filter (OBPF, Alnair-Labs-CVF-300CL), a unidirectional EDFA (Tuolima) (incorporating an optical isolator) with 22-dB fixed gain, and single-mode fibers totaling a length of L_2 ~36,38-meters.

In the NALM, a periodic transmission and reflection of the optical pulses occurs as a function of the instantaneous input power and the non-linear phase shift between the longitudinal counter-propagating modes supported by the NALM cavity. Therefore, if an optical pulse is formed in the F8-PMLL and its peak power satisfies the transmission conditions of the NALM (see equation 2.20), it will propagate in the F8-PMLL according to the direction dictated by the optical isolator, otherwise, it will be reflected by the NALM and eliminated by the EDFA's isolator [13]. The polarization controller of the left-hand side loop (1) can be adjusted to control the birefringence in the fiber and, in turn, the non-linear phase shift factor in equation 2.20. This way, the interference of the counter-propagating longitudinal modes on the 50/50 coupler can be adjusted such that only input pulses of a certain intensity are transmitted, while lower pulses are reflected and extinguished in the EDFA's isolator. The center wavelength of emission of the F8L is dictated by the OBPF, which is tunable in the range 1530 – 1565-nm covering the telecommunication C-band.

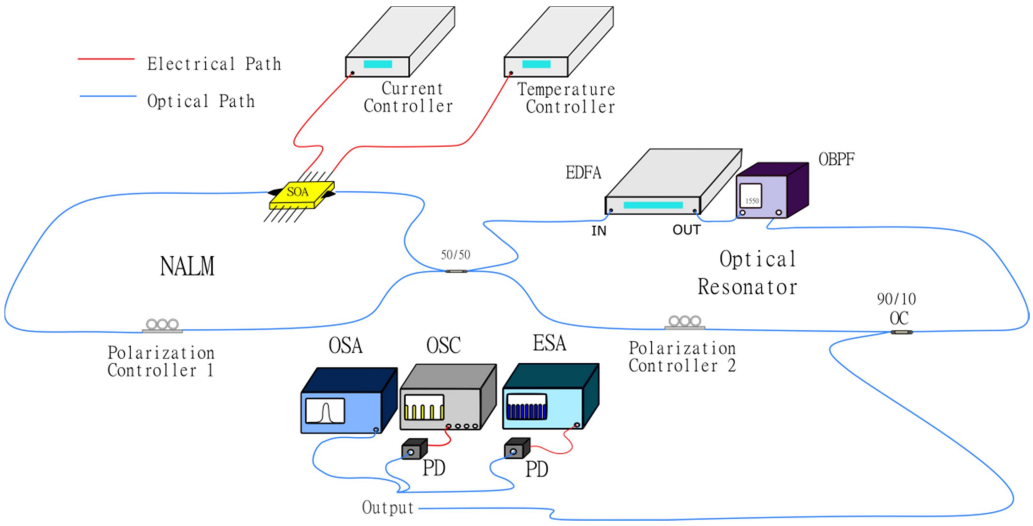

Figure 3.1. The overview of the passively mode-locked figure-8 fiber laser. On the left-hand side, the nonlinear amplifying loop mirror (NALM) is depicted. On the right-hand side, the optical cavity with an unidirectional EDFA that determines the direction of propagation, and a variable optical bandpass filter that determines the center wavelength of emission are depicted.

3.1.2
Results and discussion

Under fundamental mode operation, the F8-PMLL presented in figure 3.1 produces 303-ps wide pulses (Gaussian fit) spaced by 224-ns (repetition rate of 4.46 MHz, see equation 2.5), the former determined by a total 1.39-GHz emission bandwidth and, the latter, by the overall length of the fiber cavity of 44.8-meters. To achieve such conditions, other than correctly adjusting the PCs, the injection current of the SOA should be approximately 150-mA, which translates into optical pulses with 4-pJ energy level and 13-mW peak power. The results are shown in an oscilloscope (OSC, Tektronix-DPO7354) as describe in figure 3.2.

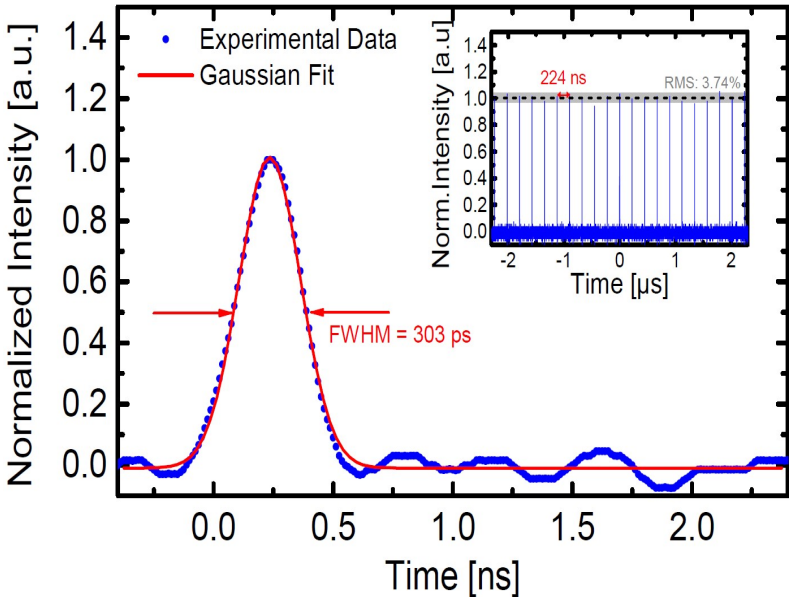

Figure 3.2. Temporal shape of the generated optical signal in the passive mode-locked figure-8 laser. Inset in Figure 3.2: The optical pulse train separation of 224-ns matches the resonator length of 44.8-meters. The pulse temporal width is 303-ps.

Under these conditions, the wavelength adjustment of the F8-PMLL is rather simple in terms of an optical bandpass filter (OBPF) which is tunable in the range covering the telecommunication C-band. The bandwidth filter was set at 0.03-nm (3.75-GHz). The F8-PMLL exhibits an full-width-half-maximum (FWHM) of 11-pm (~1.4-GHz) because the optical ring resonator together with OBPF forces coherence and performs output spectrum narrowing after several roundtrips. The results are shown in an optical spectrum analyzer (OSA, Anritsu-MS9740A) with a 0.03-nm resolution as described in figure 3.3.

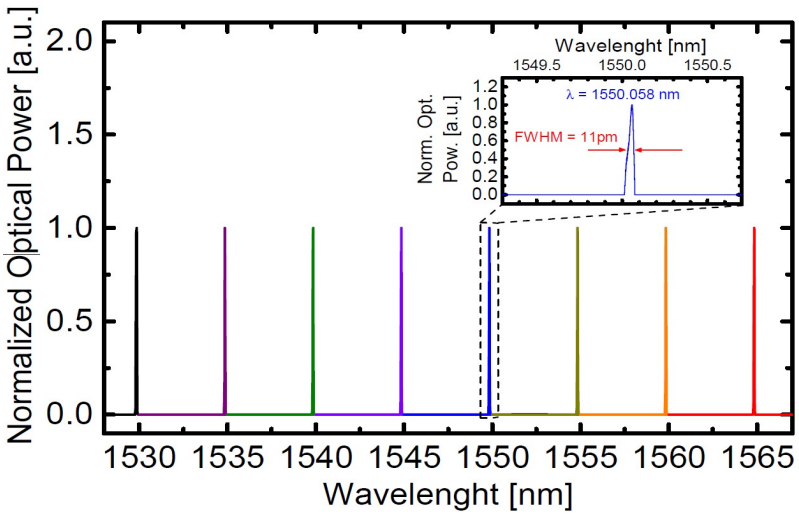

Figure 3.3. Center wavelength tunability of the employed F8-PMLL. Inset in Figure 3.3: The bandwidth, measured with a high-resolution (20 MHz) optical spectrum analyser (Apex-Technologies-AP2050A) is 11-pm at all center wavelengths.

Finally, still under the same conditions, the output spectrum is measured in an electrical spectrum analyzer (ESA, Keysight-N9344C) and corroborates the timing characteristics of the optical signal as described by equation 2.7. A frequency comb with an FSR of 4.47-MHz and a signal-to-noise ratio of 67-dB to fundamental frequency of oscillation is presented and shown in figure 3.4. The 1.39-GHz FWHM measured at the ESA is in agreement with the 11-pm FWHM measured at the OSA.

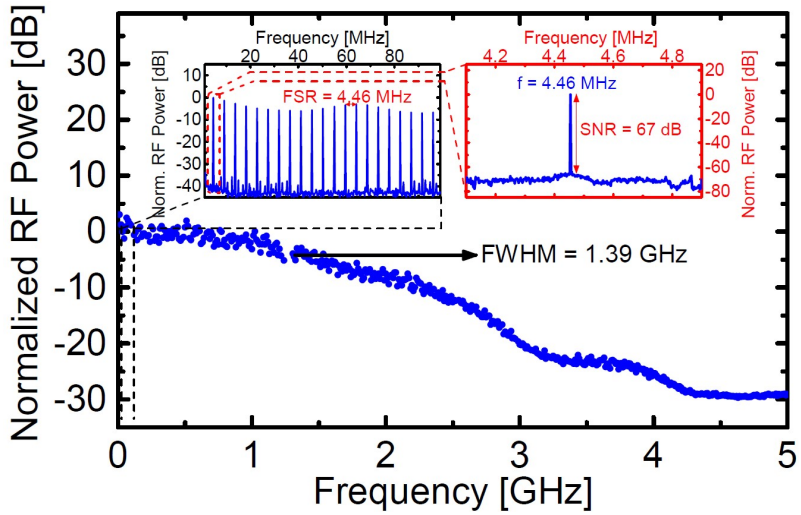

Figure 3.4. Electrical spectral characterization of the generated optical signal with respect to the central wavelength of 1550.058-nm. Inset in Figure 3.4 (left-hand side): The spectral comb-shape exhibits a free-spectral range (FSR) of 4.46-MHz (RBW = 1-kHz), which matches the resonator length of 44.8-meters. Inset in Figure 3.4 (rigth-hand side): RF spectrum of 4.46-MHz (fundamental) mode with a SNR (RBW= 10-Hz) of 67-dB.

Coherent pulsed optical sources are a required article in the Optoelectonics and Instrumentation Laboratory, particularly due to their importance in the context of DWDM systems. In such systems, a spacing between adjacent channels of 0.8-nm (100-GHz) is established, so any optical source with bandwidth broader than this threshold is seen as a source of interference for its adjacent channels (crosstalk) [76]. Furthermore, due to the Time-Bandwidth Product (TBWP) limit, we know that the broader the spectrum of an optical source, the narrower the pulse width in time can be and, thus, the greater the impact of temporal pulse stretching due to dispersive effects in the optical fiber will be [75, 76]. The F8-PMLL was specially designed to meet the requirements of: compatibility with the ITU-T (International Telecommunication Union) G.694.1 DWDM spectrum [101]; pulsed operation with high TBWP, i.e., short pulses in time with narrow spectra; and high optical pulse dynamic range, since them aim is to integrate it in a PC-OTDR experiment [6] that requires high measurement SNR. Figure 3.5 (a) shows an overview of the integration of the F8-PMLL with the data detection system. The resolution and dynamic range OTDR results are shown in figure 3.5 (b). Measurements of different lengths of fibers in different DWDM channels were performed due to the tunability of the F8-PMLL and are shown in figure 3.5 (c).

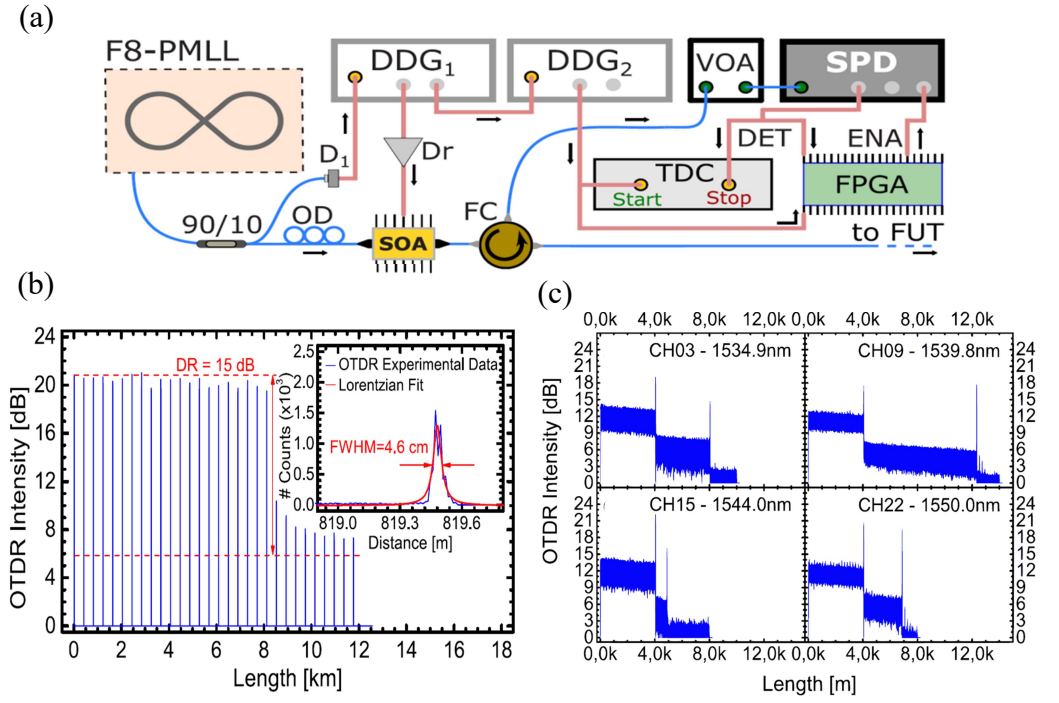

Figure 3.5. (a) Block diagram of the data acquisition system including the synchronization with the F8-PMLL; (b) Dynamic range (15 dB) and spatial resolution (4.6 cm - Inset) achieved with the proposed OTDR system; (c) Full fiber measurements of four distinct DWDM channels. The tunability of the F8-PMLL allows for each channel to be probed individually.

This work does not show the operation of the PC-OTDR acquisition system, as its focus is on the development of the pulsed optical source that enabled its construction; nevertheless, the full operation of the system is demonstrated in reference [6] (refer to Annex A).The F8-PMLL assembled in this work is an adaptation of [78], where important modifications (such as the use of the tunable optical filter and the SOA-based pulse switching) were crucial for its proper adaptation to the PC-OTDR, although the core architecture -- containing a NALM and an EDFA in the fiber cavity -- is similar. Furthermore, the study of the F8-PMLL's structure incited the pursuit of pulsed optical sources with low repetition rate and short temporal width and the realization that few works are published in this area.

3.2
Passively mode-locked fiber ring laser (PMLFRL)

The optical pulse generation is comprised of a passively mode-locked fiber ring laser (PMLFRL). Such laser configuration has been shown to produce sub-picosecond pulses [11]. The physical mechanisms that guarantee mode-locked in PML fiber lasers are the nonlinear polarization rotation [11, 79-82]. This is accomplished in a ring topology, where an SOA and an erbium doped fibre amplifier (EDFA) act as gain media while the NPR effect is enforced by the SOA. A similar experiment has been reported in [12], but with pulse durations limited to the nanosecond scale, mainly due to dispersion effects within the ultra-long cavity.

3.2.1
Experimental setup PMLFRL

The experimental setup of the passively mode-locked fiber ring laser (PMLFRL) is shown in figure 3.6. It is composed of an SOA (Thorlabs-1013SXS), a polarisation beam splitter (PBS), two polarisation controllers (PC_1 and PC_2), a unidirectional EDFA (Tuolima), a 90/10 optical coupler, a variable OBPF (Alnair-Labs-CVF-300CL) tuneable in both central wavelength and spectral bandwidth, 2.88 km of dispersion-shifted fibre and 0.125-km of standard

fiber (SMF). Mode-locking, in this configuration, is achieved by injecting a current of ~390-mA into the SOA and properly adjusting the PCs. We used an off-the-shelf EDFA with fixed 26.5-dBm average output power. When a high-power optical pulse impinges on the SOA, the pulse's leading edge can deplete the SOA gain and saturate the device, so that a much lower gain is provided for the trailing edge of the pulse. Hence, as the SOA provides polarisation dependent gain, the refractive index saturation will also be polarisation dependent so that SOA will act as a nonlinear polarization rotation device [11, 12, 79-82]. This feature can be used as a pulse compression mechanism by properly adjusting light polarisation along the cavity. In this way, the edges of the pulse are filtered by the PBS and removed from the loop. In order to repeat this operation for every roundtrip in the laser cavity, PC_1 should be adjusted so that the same state of polarisation enters the SOA after a roundtrip (see Figure 2.18). Due to its nonlinear characteristic, the NPR effect is more pronounced for higher pulse peak powers. Therefore, the use of the EDFA is essential for enhancing the pulse compression since, with higher peak power, the polarisation will change more rapidly within the optical pulse and a shorter portion of it will be aligned to the PBS. The repetition rate of the train of optical pulses at the output of the laser is determined by the length of the optical fiber cavity (see equation 2.5) and, in order to reduce the former, the latter must be increased. This is done in conjunction with dispersion management, so that the total GVD is minimised even with km-long ring lengths. Although fiber lengths were limited to the available bobbins in the lab, the operating wavelength could be selected by the tuneable filter in order to minimise the overall β_2. A minimum was found for an operating wavelength of 1558-nm, where the GVD of standard single-mode fibers (SMFs) is anomalous (β_2,SMF = −20.39-ps^2/km), in contrast to the erbium-doped fiber (EDF) and the dispersion-shifted fiber (DSF), which exhibit normal GVD (β_2, EDF = + 11.47-ps^2/km, β_2,DSF = + 2.94-ps^2/km) depending on the wavelength along the C-band (see Figure 2.20). The fiber optic ring was formed with 0.149-km SMF (0.125-km from fibre reel and 0.024-km from fibre pigtails), ~0.013-km EDF (internal to the EDFA), and 2.880-km DSF fibers. Such parameters lead to a net dispersion in the cavity of ~+5.58-ps^2 with a total length of 3.042-km.

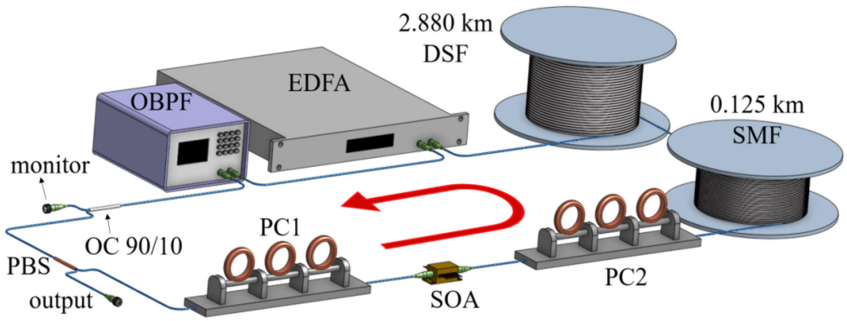

Figure 3.6. Passively mode-locked fiber ring laser (PMLFRL). The ring optical cavity with a unidirectional EDFA that determines the direction of propagation (red arrow) and a variable OBPF that determines the central wavelength at normal GVD in the dispersion-shifted fiber.

3.2.2 Results and discussion

The PMLFRL experimental results are shown in figure 3.7, where all measurements were performed on the monitor output port of figure 3.6. Figure 3.7(a) shows the pulse train, where a uniform intensity can be observed. The repetition rate of the train of optical pulses matches the measured roundtrip time of 14.88-μs and the optical fiber cavity length of 3.042-km. The pulse duration, measured with a second harmonic optical correlator and a photomultiplier (Inrad-5-14-LDA), is shown in figure 3.7(b). The full width at half maximum (FWHM) measured is 5.18-ps, corresponding to a Gaussian fit to the experimental data. The autocorrelation trace is noisy due to the very low duty cycle and the high gain set on the photomultiplier. Figure 3.7(c) shows the radio-frequency (RF) spectrum measured with an electrical spectrum analyser (ESA, Keysight-N9344C), where a frequency comb can be observed. The 67.2-kHz tone corresponding to the fundamental frequency is shown on the inset of figure 3.7(c), which exhibited a SNR of 35-dB and linewidth limited to the 10-Hz resolution bandwidth (RBW) of the spectrum analyser, meaning low phase noise and jitter on the repetition pulse rate. The optical spectrum of mode-locked pulses is shown in figure 3.7(d). The central wavelength is located at 1557.89-nm and the 3-dB spectral width is 1.82-nm (228-GHz) is compatible with Fourier nearly-transform-limited pulses. The spectrum is almost symmetric and featureless, although displaying small oscillations separated by ~25-GHz with ~1-dB modulation depth. The symmetry of the spectrum and modulation depth of the oscillations depend on the central

wavelength chosen for the filter, indicating that they are both related to the total dispersion of the fiber ring. Slight changes in the central wavelength may lead to a totally asymmetric spectrum and several dB modulation depths.

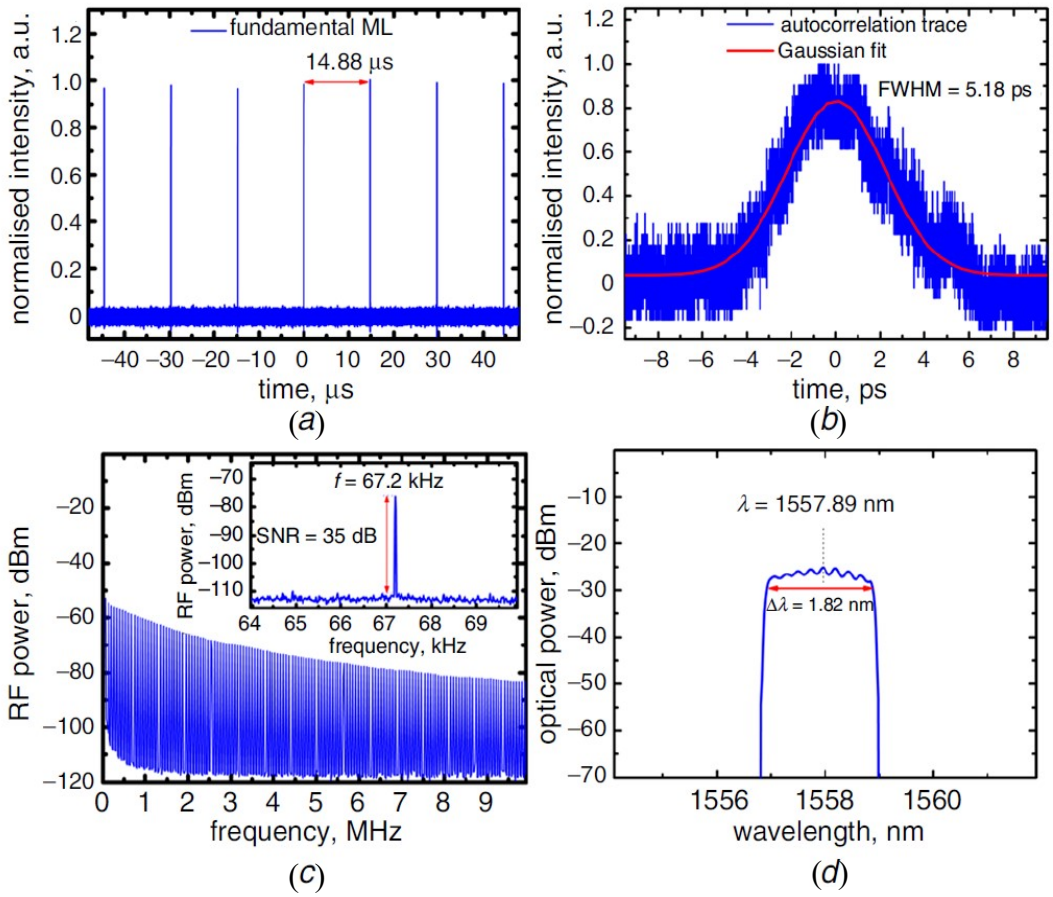

Figure 3.7. Ultra-long cavity fundamental mode-locked experimental results: (a) Temporal Pulse train; (b) Autocorrelation trace; (c) Electrical spectrum. The Inset in (c) RF spectrum of 67.2-kHz (fundamental) mode with a SNR of 35-dB (RBW = 10-Hz); (d) Optical spectrum.

Because both, repetition rate and pulse width are key features for several applications, a useful figure of merit for comparison between different achievements is the duty cycle of the optical pulse train. In optical-time-domain-reflectometry (OTDR) applications [4-6], low rates are important to allow for the measurement of long fibers, whereas pulse duration defines the spatial resolution. High-resolution in long fiber monitoring is of great interest in this context and a shorter duty cycle is very important. A comparison between duty cycle results in previous works [12, 102-105] is presented in table 3.1. The present work shows the lowest duty cycle while maintaining a low repetition rate and ps-long pulses comparable with state-of-the-art mode-locked methods.

Repetition Rate (kHz)	FWHM	Duty Cycle (10^{-4} %)	Reference
67.2	5.18 ps	0.35	This work
132.0	6.20 ps	0.82	[102]
467.2	2.90 ps	1.35	[103]
25.0	2,00 ns	50	[104]
50.7	~ ns	unknown	[12]
278.0	12.8 ns	3558.4	[105]

Table 3.1. Comparison duty-cycle results.

Figure 3.8. shows the evolution of the output pulse width of the proposed fiber optic ring laser operating in the repetition of the fundamental cavity. It shows a broad square pulse following a sharp spike at the leading edge. The duration of the square pulse can be controlled and reduced by proper adjustment of the polarization controller inside the cavity similar to what was observed in [105]. The pulse compression is evident when the operation wavelength and the polarisation are properly adjusted. From figure 3.8 we see that the width of the broad pulse is reduced from 40-ns down to 5-ns and eventually disappear by fine tuning. Besides the proper adjustment of the polarisation controllers, the central wavelength of the tuneable filter had to be properly adjusted to guarantee dispersion management, which was not possible in [105] due to their fiber choice. The final pulse width was 5.18-ps, much shorter that the scope resolution. The stable ultra-low repetition rate without CW leakage or tail in the output is of extreme importance for many applications such as high-resolution optical reflectometry. In fact, the period here corresponds to the roundtrip time in a 1.5-km long fiber, ideal for OTDR applications in avionics [4].

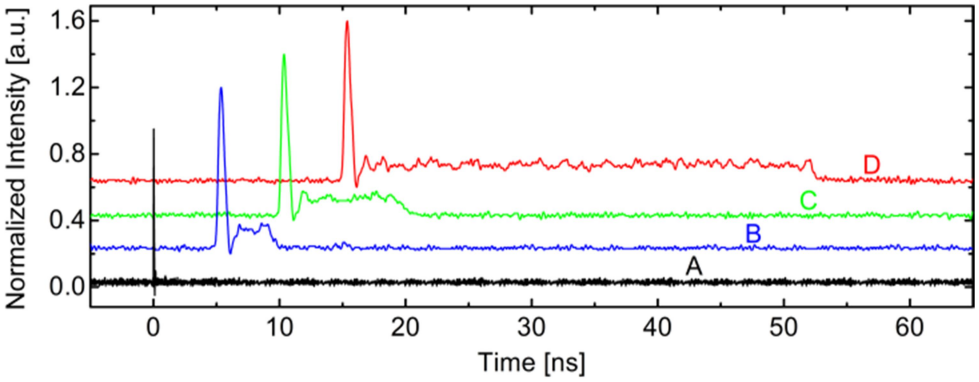

Figure 3.8. Polarisation tuning to reduce pulse width at optimum operation wavelength. Traces A to D are displaced for clarity and correspond to diferente adjustments of PC_2. Pulse A is limited by the oscilloscope bandwidth and its actual duration was measured with the autocorrelator.

The PMLFRL demontrated in this work is an adaptation of [12], where important modifications (such as the use of the tunable optical filter and bobbins fiber choice) were crucial in the dispersion management of fiber optical cavity for generate picosecond temporal pulsewidh and kHz repetition-rate. The study of PMLFRL presented relevant results allowing publication in journal that can be refer to Annex B. Adaptations of the schematic of figure 3.6 were also studied and allowed us to demonstrated different orders of harmonic mode-locking (HML) and high repetition-rate. The results were published in conference and can be refer to Annex C.

4
Mode-locked fiber laser in open cavity

This chapter presents the setups and experimental results of mode-locked random fiber laser (MLRFL). Describes the optical pulse generation mechanisms combined with Rayleigh backscattering feedback, analyzes spectral and temporal dynamics and shows its use as a distributed acoustic sensor (DAS) and distributed temperature sensor (DTS) incorporating phase-sensitive OTDR technique.

4.1
Mode-locked random fiber laser (MLRFL)

A hybrid electronically addressable random laser (HEAR) was recently presented [20], where a pulsed SOA in a loop mirror and the Rayleigh scattering from a pumped erbium doped fiber (EDF) formed a random cavity. The proposed feedback mechanism was Rayleigh scattering from the EDF section addressed by the SOA pulse whose frequency is in resonance with the cavity roundtrip time. Here, the author reproduce still poorly explored schematic presented in [20] and show that laser operates in mode-locking regime generating transform-limited optical pulses in addition to linewidth of the laser self-narrows. Random feedback from a telecom fiber lies at the heart of the mode-locked transform-limited pulse generation discussed here. The extremely faint Rayleigh backscattering in a short section of fibre arbitrarily selected within a much longer fibre spool serves as laser feedback. The chosen backscattering section of fibre is much shorter than the entire laser cavity. Periodically gated optical amplification allows synchronizing the arrival of the backscattered light from the distributed mirror to the opening of the gain window. Light scattered either too early or too late (from points lying before or after the chosen section) does not experience periodic amplification and dies off. Provided the amplification in a roundtrip compensates for the incurred loss, the laser reaches threshold. The duration of the optical pulse defines the length of the distributed laser mirror as the spatial resolution in ϕ-OTDR system.

4.2
Experimental setup MLRFL

The fiber laser cavity used in this work consisted of a loop and an open-ended section as shown in Figure 4.1. Gated amplification was provided inside the loop by driving with current pulses a semiconductor optical amplifier, Thorlabs SOA 1013SXS. A 125-m delay fibre was also included in the loop to increase the roundtrip time of the cavity to the ~1-μs range. A commercial erbium-doped fibre amplifier (EDFA, Thorlabs 100S) was also inserted in the loop. It amplified the weak backscattered signal from the distributed mirror by up to 36-dB before the SOA. An adjustable optical bandpass filter (OBPF, Alnair-Labs-CVF-300CL) was also used centered at 1532-nm to reduce the amplified spontaneous emission, and limit the feedback signal to the neighbourhood (<=20-GHz) of the wavelength of interest. The 3-dB fused fibre coupler connected the loop to the open-ended fibre section of the cavity. A large fraction of the amplification needed for the laser to go above threshold (54.5-dB) was provided by a 27-m long Corning erbium-doped fibre (1550C3) without isolators, working in both directions. Gain was provided to the EDF by a 365-mW CW-pumped diode laser at 976-nm wavelength. An open-ended 63-m long spool of single-mode fibre completed the laser cavity. The output of the laser was monitored with a 26-GHz amplified photodiode model UPD-15-IR2-FC and a 3.5-GHz 40 GSamples/s Tektronix DPO7354 oscilloscope. The optical spectrum of the laser output was measured with an Apex AP2050A optical spectrum analyser with an optical frequency resolution as narrow as 20-MHz (0.16-pm wavelength). The electrical spectrum of the laser output was measured with an Keysight-N9344C electrical spectrum analyser. The current pulses for the SOA were provided by an Avtech pulse generator (AVM-2) delivering up to 300-milliamperes with a rise time <1-ns and durations up to 20-ns. The trigger for the pulse generator came from a two-channel Keysight arbitrary function generator Model 33500B which allowed for pulse frequency tuning to the millihertz resolution. The short section of fibre providing for Rayleigh backscattering was chosen in position and in length along the fibre spool by adjusting the repetition rate and the duration of the electrical pulses driving the SOA. The single-mode fiber end was angle-cleaved and bent

sharply to prevent backscattering from the termination. Lasing was observed along the entire spool length, but the pulse amplitude and stability varied because of the random feedback.

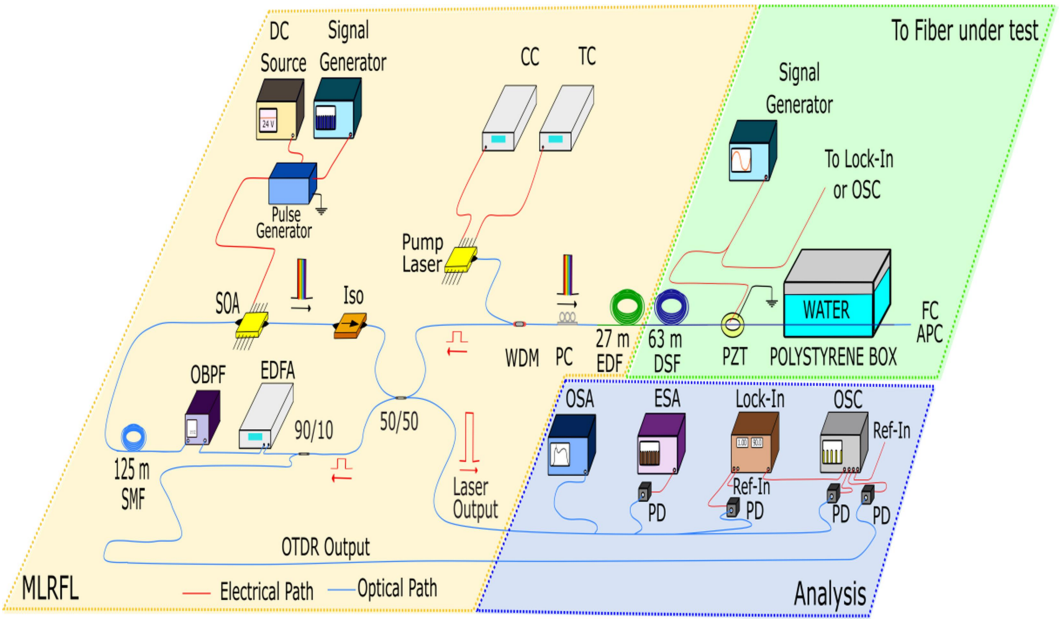

Figure 4.1. Experimental setup of mode-locked random fiber laser (MLRFL). Lasing phase-sensitive-OTDR technology allows its use as distributed acoustic sensor (DAS) and distributed temperature sensor (DTS).

4.3 Results and discussion

4.3.1 MLRFL threshold and optical spectrum output

A careful evaluation of all losses in the cavity was carried out to estimate the lasing gain threshold for better understand the gain dynamics and the limits of operation of the laser. The single pass loop connection losses added to 10-dB including 90/10 coupler, isolator and optical bandpass filter (OBPF) , whereas the double pass connections to the EDF were 13.2-dB, including 50/50 coupler and polarization controller. The roundtrip losses at the SM-EDF and EDF-DSF splice were measured to be 3.2-dB and 0.2-dB respectively. Naturally, the highest loss of the cavity was at the distributed back reflector, which amounts to the mean value of ~-69-dB/m for a typical DS fibre.

Figure 4.2(a) shows the laser output average power as a function of the EDF pump power when the system is driven at 820 kHz with square current pulses with widths 5 (green), 10 (red) and 20-ns (blue). The corresponding optical pulse durations were 4.63, 8.84 and 19.01 ns, respectively (refer annex F - supplementary information - electrical vs optical pulses). A distinct random laser threshold is observed in all cases [106, 107] with a clear sharp laser line emerging from the broadband ASE when the threshold is reached, as shown in the Figure 4.2(b). The higher feedback provided by longer, distributed random reflectors reduces the pump power needed for lasing as more power is backscattered. The MLRFL threshold at 205 mW pump power for 10-ns current pulses, correspond to a 51.5-dB double pass gain in the EDF (Corning 1550C3) (see Figure 2.11(b)), 14.5-dB single pass (@300 mA) gain in the SOA (Thorlabs 1013SXS) (see Figure 2.7) and 27-dB single pass gain (@250 mA) in the EDFA (Thorlabs 100S) (see Figure 2.10(b)). Now, considering the total cavity roundtrip losses of 95.6-dB, a random 2.6-dB reflectivity peak above the mean of the addressed section (820-kHz) is enough to fulfill the lasing gain threshold condition when this addressed section is at the end of the DSF in agreement with the model [90]. This configuration provided a maximum gain of 105 dB, which was comfortable to generate lasing pulses with durations down to ~0.3 ns. Figure 4.2(b) displays the optical spectrum of the MLRFL well above threshold for 20-ns current pulses, where the laser peak power stands 30 dB above the EDFA ASE.

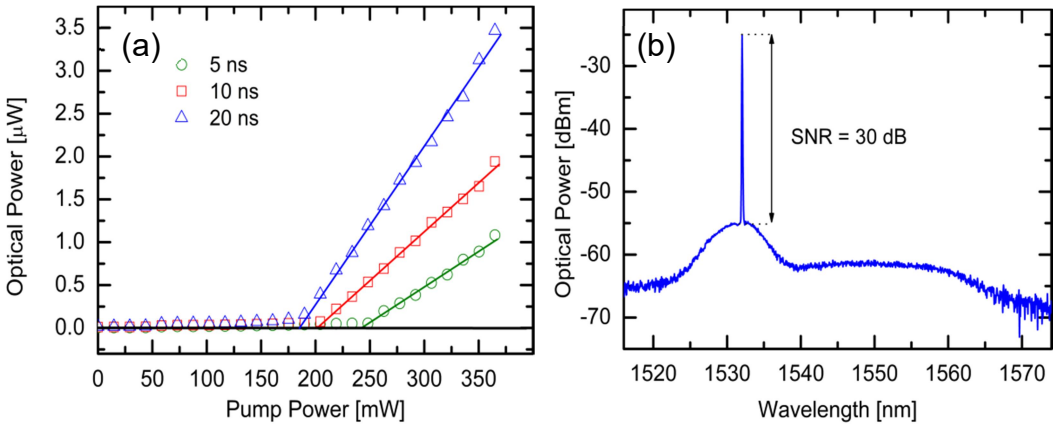

Figure 4.2. MLRFL threshold and optical spectrum output: (a) Distinct threshold for three current pulse durations. The threshold EDF pump power decreases for longer pulses; (b) The optical spectrum for 20-ns current pulses at full pump power (365-mW).

4.3.2
MLRFL temporal and electrical spectrum output

The temporal behavior of the output is measured with the 26-GHz bandwidth photodiode detector (PD) and 3.5-GHz bandwidth oscilloscope (OSC).

Figure 4.3(a) shows the temporal pulses train, where a uniform intensity can be observed. The repetition-rate of the train optical pulses is generated by the direct modulation of the SOA and matches a measured roundtrip time of 1.22-μs from a selected short section of the DSF. The electrical spectrum is measured with 26-GHz bandwidth photodiode coupled a 20-GHz bandwidth electrical spectrum analyzer (ESA) as shown in Figure 4.3(b). The inset in Figure 4.3(b) shows a series of tones repeating at 0.82-MHz interval, which are the result of the periodic gating of the laser and characteristic of the actively mode-locking regime. The interval of the frequency-comb presented corresponds to the free spectral range (FSR) of the MLRFL and matches the characteristic roundtrip time of the pulses shown in Figure 4.3(a).

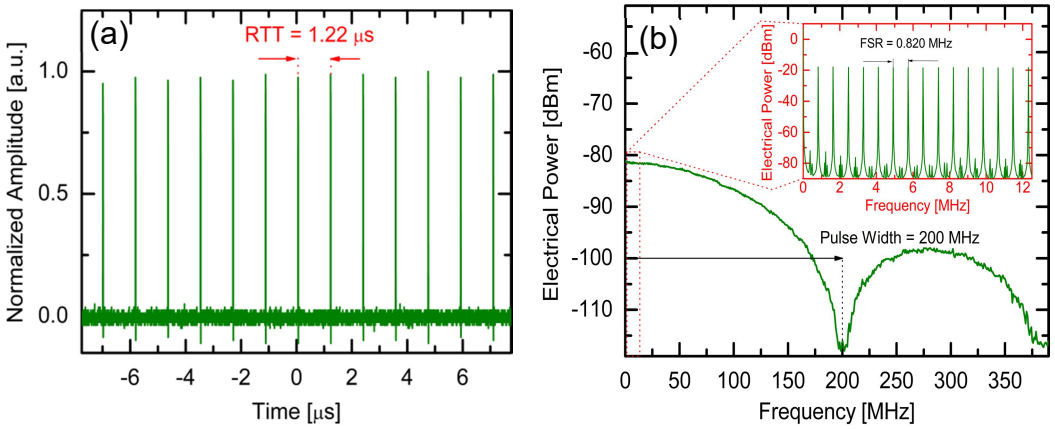

Figure 4.3. MLRFL temporal and electrical spectrum output: (a) Output OSC temporal pulses train; (b) Output ESA spectrum for 5-ns current pulses applied in SOA (RBW=1-MHz). Inset in (b) Frequency-comb with series of tones repeating at 820-kHz interval (RBW=100-Hz).

4.3.3
MLRFL generating Fourier transform-limited optical pulses

The Fourier transform-limited is understood as the lower limit for the pulse duration which is possible for a given optical spectrum of a pulse. A pulse at this limit is called transform-limited. A mode-locked laser can generate transform-

limited pulses when all modes are perfectly phase-locked to each other through a coupling mechanism such as periodic phase or amplitude modulation [1]. The minimum theoretical time–bandwidth product ($TBWP_t = \Delta\nu\Delta t$) depends on the pulse shape, and is 0.8859 for square-shaped pulses, 0.4413 for Gaussian-shaped pulses and 0.3148 for $sech^2$-shaped pulses [108].

Figure 4.4 presents generate Fourier transform-limited of MLRFL optical pulses. All measurements were performed around 1532-nm wavelength. Figure 4 (trace (a), trace (c) and trace (e)) shows time-domain and spectral-domain (trace (b), trace (d) and trace (f)) measurements for applied electrical current pulsewidths of 10-ns ((a) and (b), red), 3-ns ((c) and (d), orange) and 2-ns ((e) and (f), pink) in the SOA. The time and spectral measurements shown were taken in single sweep mode and near synchronism. The optical pulses are shorter than the electrical ones (8.84-ns, 0.874-ns and 0.336-ns of FWHM respectively) and are fitted in (a) to a square-shaped pulse, in (c) to a Gaussian-shape pulse and in (e) to a $sech^2$-shaped pulse by a dark solid line. The dark solid lines in traces (b), (d) and (f) are the corresponding Fourier-transform curves, with $Sinc^2$, Gaussian and $Sech^2$ shapes, respectively. When the duration of the pulses reduces, their shapes also change and the experimental time-bandwidth product ($TBWP_e$) reduced from 0.8902 to 0.4516 and later to 0.3325 as expected [108]. The good agreement of the Fourier-transform curves in dark line and the experimental data in red, orange and pink in traces (b), (d) and (f) respectively demonstrate that the present MLRFL can generate transform-limited pulses using the Rayleigh backscattering from a section of telecom fiber as short as 3.36-cm as cavity feedback. The good agreement is observed between the experimental data and the model predictions shown in section 2.9 [90]. The laser linewidths are the same as expected for the backscattering reflectivity peak (see Figure 2.25(b)), which is consistent with the fact that a single roundtrip is enough to sustain laser action. In fact, given the extremely low feedback of the backscattering section, almost all photons leave the cavity at every roundtrip, being filtered just once. It is worth mentioning that laser action is maintained from shot to shot by the few coherent photons backscattered from the preceding pulse. Coherence in this random laser comes from the constructive interference at the backscattering section, rather than from constructive interference at each cavity roundtrip. Cavity modes are automatically

phase-locked by the periodic pulsed gain. Even shorter pulses should be possible, but experiments here were electronics limited.

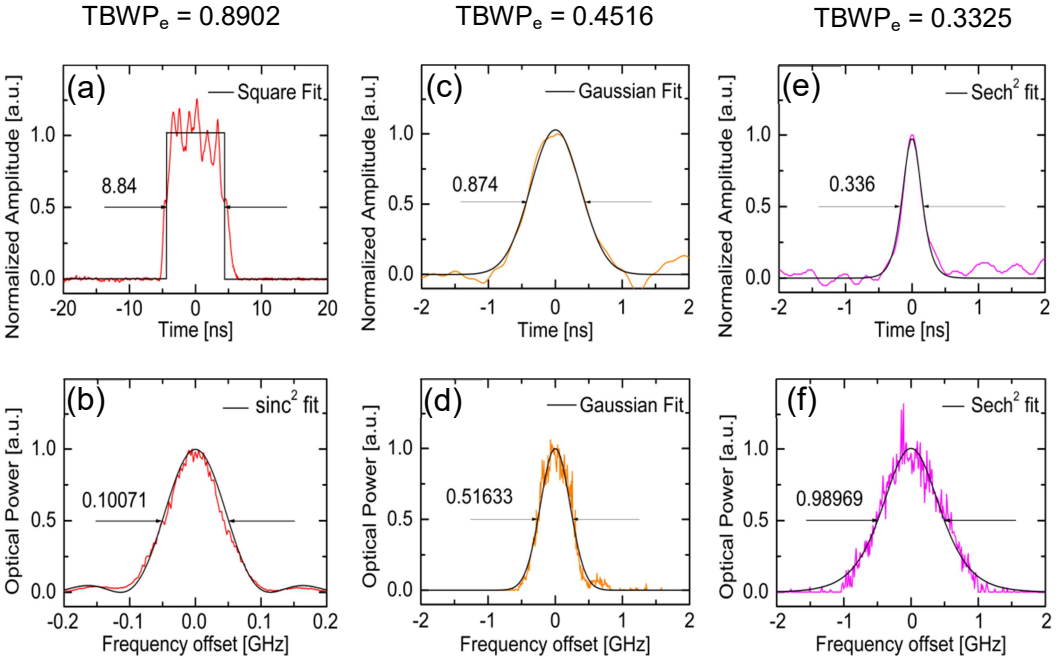

Figure 4.4. MLRFL generating Fourier transform-limited optical pulses: (a) temporal square-shaped pulse; (b) spectral features of square-shaped pulse; (c) temporal gaussian-shaped pulse; (d) spectral features of gaussian-shaped pulse; (e) temporal sech^2–shaped pulse; (f) spectral features of sech^2–shaped pulse.

4.3.4 Laser mode-hopping

Mode hopping is a phenomenon which is mostly discussed in the context of single-frequency lasers. Under some external influence, such a laser may operate on a single resonator mode for some time, but then suddenly switch to some other mode. This means that this other mode suddenly takes over all the optical power. So for some period of time, there may be power in both modes. Mode hops are originated external effects such as a drift of the temperature of the gain medium will shift the wavelength of maximum gain or internal effects such as polarization-rotation in lasers with polarization-independent gain.

Figure 4.5(a) shows multimode laser operation in the same spectral range (20-GHz) for optical fiber sections length of ~0.5, 1.0 and 2.0-m. The section length is determined by the duration of the optical pulse. The result demonstrates an increase in the number of laser peaks and a reduction in the FWHMs of the peaks as a function of the section length in agreement with the presented

theoretical model (see section 2.8) [90]. Eventually, when the pulse duration is sufficiently large and the gain is well above threshold, mode-hopping occur and other mode suddenly takes over all the optical power. So for some period of time, there may be power in both modes giving rise to simultaneous pulses at two different wavelengths as shown in Figure 4.5(b). The inset in figure 4.5(b) shows these pulses reach the detector at the same time, giving rise to optical beating at the difference between their optical frequencies. Figure 4.5(b) also shows four side-bands of the second order which probably appear due to the nonlinearities in the SOA.

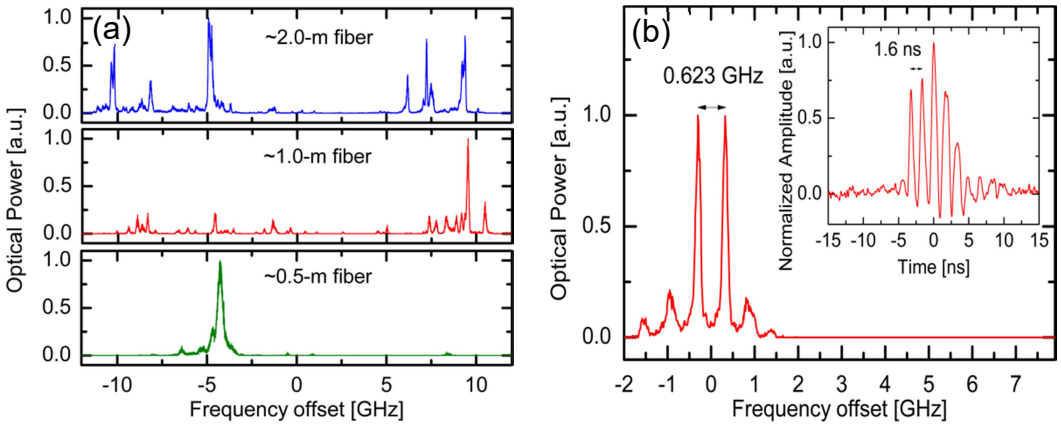

Figure 4.5. Laser mode-hopping: (a) various laser peaks according to the fiber section length; (b) double pulse generation at two different wavelengths (multimode operation). Inset in (b) optical beating in photodiode of the two wavelengths generated at the MLRFL. Polarization controller adjustments reduce the effects of mode-hopping and optimize a single or multimode emission.

4.4 Aplications

4.4.1 Optical fiber measurement and lasing Φ-OTDR

In order to characterize the system's operation parameters, OTDR profiles of different addressed section of the fiber were measured via the OTDR port in the loop. Figure 4.6 shows four OTDR profiles selecting different addressed sections of DSF for 13-ns (wine) optical pulse duration. These sections are selected according to the repetition-rate of the direct modulation pulses in the SOA. The four examples illustrated in Figure 4.6 clearly show the difference between

regimes of ASE below threshold (205-mW pump power, top trace) and lasing Φ-OTDR above threshold (365-mW pump power, three bottom traces) for different addressed fiber sections. The smooth top trace of a conventional OTDR develops into a spiky speckle-like trace characteristic of the Φ-OTDR regime when the laser is above threshold (also seen in the zoomed-in Figure 4.7(a)). This happens without the use of a narrow linewidth injection source, evidencing the strong spectral self-narrowing experienced by the laser above threshold. In contrast to the experiments reported in [20], here the source of Rayleigh backscattering is a passive fiber, not a rare-earth doped fiber. This excludes the possibility of a standing wave index-grating forming from unpumped ions [109-111]. The several peaks around the lasing peak arise from Φ-OTDR and appear due to the varying coherent superposition of Rayleigh backscattered light in agreement with the model [90].

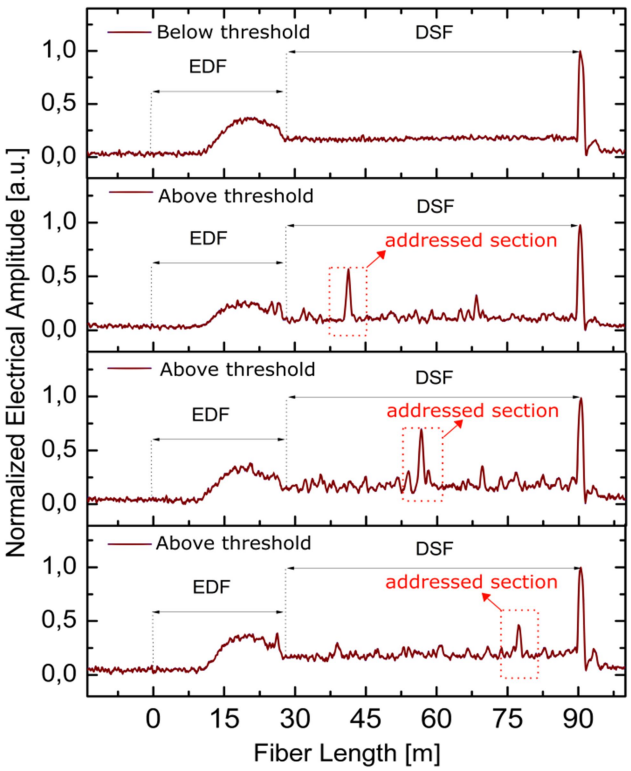

Figure 4.6. MLRFL such as lasing Φ-OTDR at different addressed section.

As shown in Figure 4.6, the single-ended passive dispersion shift fiber can be used both to provide feedback for laser action and to perform distributed sensing at various locations. Hence, the laser can be directly used as a fast

distributed sensor within the addressed section of the DSF, the laser intensity being interferometrically sensitive to external effects on the fiber, such as vibration, stress/strain or temperature, with the resolution given by half the modulation pulse-width as in a conventional Φ-OTDR. One advantage of the present set-up is that instead of a tiny, backscattered signal measurement, as is conventional in an OTDR, here it is the full output of the laser that provides the sensing signal. Hence, no averaging is needed, and a fast response is available.

4.4.2 Distributed acoustic sensor (DAS)

Prior to measuring vibrations, in order to characterize the PZT operation parameters, the PZT was placed on an arm of a balanced fiber Mach-Zehnder interferometer (MZI) to produce frequency discrimination. The modulation frequency applied to the PZT was varied while maintaining a constant drive voltage. The PZT showed resonance effects at 5-kHz. Now, with the constant resonant frequency at 5-kHz to maximize the phase change, the voltage applied to the PZT was varied. The PZT presented low harmonic distortion up to a maximum applied voltage of 1.8-Vpp.

Because of the high coherence as in a conventional Φ-OTDR, the MLRFL output is very sensitive to the phase within the addressed section and the output port shows large intensity variations as the SOA gating frequency is swept. Figure 4.7(a) shows the laser output power variation as the addressed section was displaced along a ~30-m section within the DSF, showing the strong spatial fluctuations characteristic of a Φ-OTDR [37-50] (see Figure 2.23). A 10-sec frequency sweep (1.050-MHz to 0.700-MHz) was carried out, so that the entire length of the DSF section was addressed while modulating the phase with the PZT attached to the DSF. Synchronous detection of the received signal was performed with a Lock-in amplifier, where static intensity fluctuations were eliminated. Only those fluctuations at 5-kHz were measured, and they appear with 1.37-m spatial resolution where the PZT is positioned on the DSF, at 15.8-m, as shown in Figure 4.7(b) upon a sweep over the full DSF length. Hence, the phase signals can be used for directly measuring the external vibration on fiber. The vibration frequency at 5-kHz with 1-Vpp applied to the PZT is measured, for investigating

the system performance. Although solid-state based phase-modulating schemes may allow for testing a broader range of frequencies [112, 113], the reflections may hinder their use here, and the PZT modulator is chosen. In the experiments, sinusoidal vibration signals are generated, and laser output detection is performed with a 10-MHz bandwidth photodiode with band-pass filtering in the range 1-10 kHz. Figure 4.7(c) shows the detection of the sensor signal with 1-Vpp applied (wine trace) and 2-Vpp applied (blue trace). In the latter case, the phase modulation exceeds π-rad (blue trace). Figure 4.7(d) shows the amplitude of the sensor signal measured for low voltages applied. In this regime the transfer function of the sensor has a linear phase dependence on the applied voltage, indicates that the lasing Φ-OTDR can be used as an addressable vibration sensor. Indeed, the phase disturbance introduced by the vibration on the backscattered intensity affects the sum of the optical fields of the two half sections encompassing the disturbance, hence the sinusoidal transfer function and linear dependence at low amplitudes.

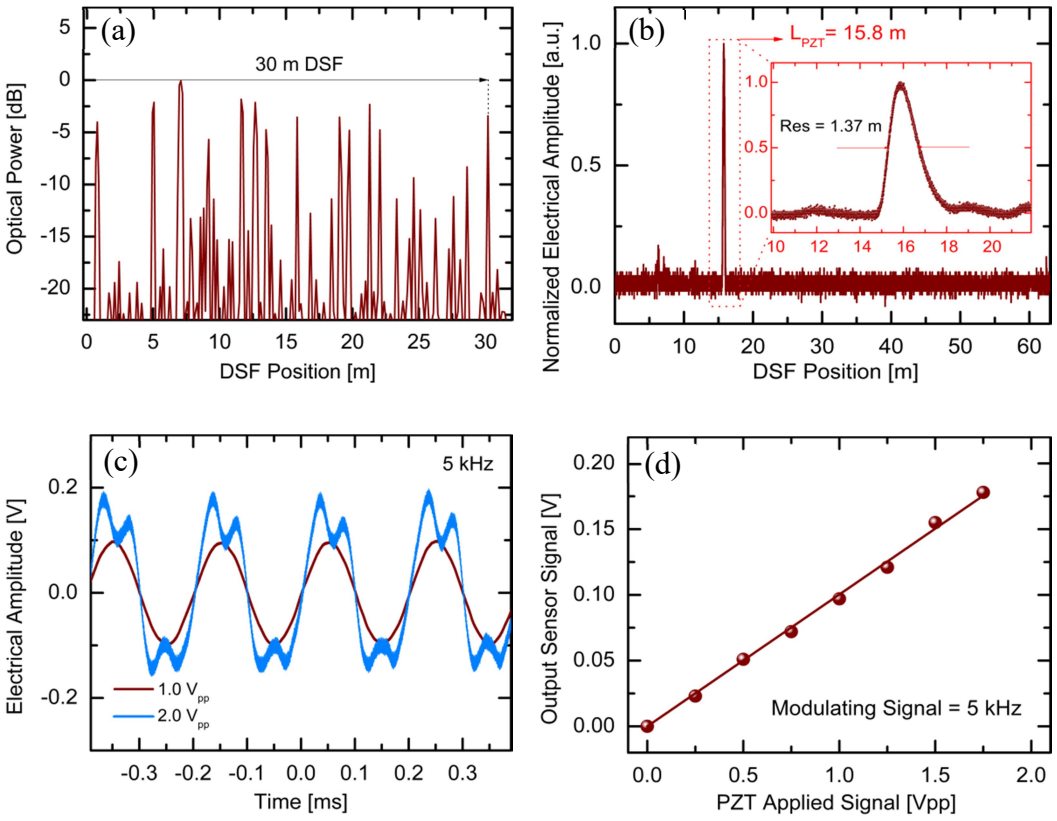

Figure 4.7. Distributed acoustic or vibration sensor performance (DAS or DVS): (a) output optical power along a ~30 m section of the DSF; (b) detection trace for vibrational wave along the full DSF. Inset in (b): Φ-OTDR resolution for 13-ns optical pulse duration; (c) sensor signal at 5-kHz; (d) detection sensitivity for different vibration intensities at 5-kHz.

4.4.3 Distributed temperature sensor (DTS)

MLRFL allows selection of the addressed section length and bandwidth of the transform-limited probe pulses, can be exploited as a Φ-OTDR in distributed temperature sensing (DTS) applications. From Eq. (1), it is clear that the frequency spectrum shifts as the mean refractive index of the considered fiber section varies with temperature. Given the sharpness of the lasing peak, even a tiny spectral shift can be detected precisely. As proof of principle, the open-ended telecom fibre was unwound from the spool, and a section ~1 m close to the end was immersed in water in an enclosed polystyrene box. The water temperature was initially raised, and the cooling process was monitored using a thermocouple-based thermometer and the laser wavelength. The repetition rate of the laser was tuned to 728.2 kHz so that optical feedback was provided from the section of fibre immersed in water. In order to avoid edge effects and to maximize temperature uniformity in the immersed fibre, the pulse duration was limited to ~900 ps (i.e., the laser feedback came from a central 9.0 cm long fibre section). An optical spectrum analyser was used to monitor the frequency (wavelength) shift, similar to monitoring the spectrum of simple intra-cavity FBG systems [97, 98].

Figure 4.8 shows the temperature evolution as a function of frequency shift, measured with ~4-MHz resolution. The frequency dependence on temperature in this small range is linear and approximately 1.19-GHz/^{o}C, similar to that found for FBG's (see Table 2.2). However, different from FBG's that only offer point sensing, distributed measurement here is accomplished by scanning the repetition rate of the laser. In addition, the MLRFL also exhibits advantages over distributed sensing techniques such as Φ-OTDR, since frequency shifts are directly measured (no post-processing), have a high signal-to-noise ratio and are robust to power fluctuations. Moreover, the spectral width of the laser line is much smaller than those of typical Bragg gratings used for local temperature measurements, so that the spectral shift can be better determined.

The robustness of the experimental set-up was verified by re-starting a measurement campaign a few days later and controlling that the peak position depends only on the sample temperature. Note that the laser cavity was protected

in the laboratory but not temperature-stabilised. The spectral measurements depend almost entirely on the temperature of the particular fiber section being addressed. Other temperature-induced fluctuations affect the cavity modes but to a large extent do not alter the spectrum of the random mirror. A temperature variation of 1 ^{o}C, over the full 200-m fibre circuit, would change the optical path of the cavity by a mere ~1-mm, well below the spatial resolution of the system. The spectral analysis of the backscattered light, however, can easily detect a variation two orders of magnitude smaller.

In the proof-of-concept application discussed here, the temperature of the water tank was initially raised to ~40 ^{o}C and the liquid stirred. Subsequently, the polystyrene lid was closed, and the system's temperature left to gradually reduce. The cooling process took several hours. The spectral acquisition and data recording took a fraction of a minute between measured points. The range of temperatures measured was chosen to be a representative temperature at a realistic warm dam location, to allow for the temperature to be in quasi-equilibrium, and to allow for data recording before the electronics instrumentation for temperature measurements showed any variation. The error bar in the temperature measurements is ±0.0125 ^{o}C. Higher precision would have been possible with better instrumentation (e.g., a nanovoltmeter to read the voltage of the immersed thermocouple). Figure 4.8 (b) exemplifies three spectra measured of 900-ps laser pulses with the optical feedback provided by the backscattering fibre section immersed in the water tank. The blue and red traces show the spectrum for a cold and a warmer temperature respectively over a range of 0.13 ^{o}C when measuring the spectrum for a reference temperature of 32.33 ^{o}C (gray). It is clear that the entire spectrum shifts with temperature, but this shift is better quantified by determining the centre position of the laser line using a Gaussian fit, considering the 70% upper part of the signal to minimise the influence of noise. The error in the determination of the peak frequency was the standard error provided by the Levenberg-Marquardt fitting algorithm and is clearly more precise than the simple determination of the maximum, which was much more affected by the noise. The spectral peak of the two data sets can be determined with a precision ~3-MHz, corresponding to a temperature 2.5-m^{o}C. The sensitivity of the technique was evaluated by considering the quality of the least squares fit over 24 independent

measurements. The average R^2-value was 0.975±0.015 while the standard error in the position of the laser line was 3.2-MHz ±750-kHz, so that the overall sensitivity of a typical spectral position in this case should be ~4-MHz or 3.3-m^{o}C in this 9 cm fibre section. Indeed, a longer fibre section used to determine the average temperature would provide sharper spectral lines whose frequency could be determined with even better precision, but the spatial resolution would be compromised accordingly. This distributed temperature measurement is Fourier Transform-limited: Dz x DT = $3x10^{-4}$ m.^{o}C. It is worth stressing that the accuracy of the measurements is significantly poorer, since the two thermometers employed for absolute measurements were not calibrated against a good temperature reference. Nevertheless, in field-applications, it is often the temperature deviation from the expected value, from for example neighbouring points, daily and seasonal variations, etc., that is most useful.

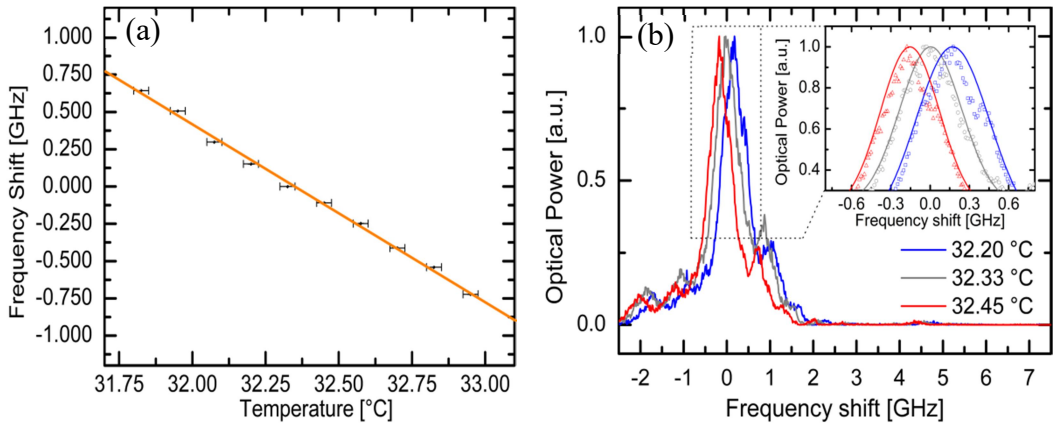

Figure 4.8. Distributed temperature sensor (DTS) performance: (a) temperature sensing using Rayleigh scattering in single-mode telecom fibre. Transform-limited pulse generation makes the laser system highly spectrally efficient. Here, ~9.0-cm resolution and 0.0033 ^{o}C precision are demonstrated. (b) Spectra of ~900-ps optical pulses measured at close temperatures. Inset in (b) shows the Gaussian fit to the 70% upper part of the spectrum, used in the determination of the central frequency.

The mode-locked random fiber laser presented relevant results allowing publications in journals and conferences that can be refer to Annex D, Annex E and Annex F.

5
Summary

This thesis described the recent and rich field of pulsed optical laser sources in mode-locking operation. We have experimentally demonstrated the generation and improvement of the F8-PMLL specially designed by us to meet DWDM system the standards requirements, as its was integrating with a high resolution PC-OTDR [6]. The author also have experimentally demonstrated the generation and improvement of the ultra-low repetition rate and picosecond-range duration optical pulses. The setup consists of a PMLFRL relying on NPR for pulse compression where dispersion management was used for GVD suppression. The final results are a stable repetition rate of 67.2 kHz, pulse duration of 5.18 ps and 1.75 nJ pulse energy with high extinction ratio. To the best of the authors' knowledge this is the lowest repetition rate obtained with ps-long pulses based PMLFRL, enabling this laser to be used as a source for millimetre resolution OTDR applications such as precision fault detection in avionics in km-long fibres [4]. Finally, a unique mode-locked random fiber laser, generating transform-limited optical pulses was demonstrated. The extremely weak Rayleigh backscattering of a short piece of telecom fibre is used as cavity feedback, leading to linewidth filtering to the Fourier limit of the laser pulses. With such weak feedback, the cavity is extremely lossy and therefore with extremely low Q-value. Consequently, a gain of the order of ~100 dB is required to compensate for the loss. These loss and gain values are amongst the most extreme ever reported for a laser An estimate of the number of photons in a 340-ps pulse backscattered in the telecom fibre gives ~102 photons. It is likely that shorter pulses, well into the picosecond regime could be generated and exploited here. This means that lasing could start with an even smaller number of photons and the system could be useful to explore more fundamental questions, such as manifestations of the quantum behaviour of the laser source and how the optical pulse evolves from white light to the coherent regime and Fourier limit. Pulses of duration under 0.3

ns were not generated for limitations in the electronics available. A Φ-OTDR system is demonstrated operates above threshold as a fiber laser. Above the threshold, the system shifts from OTDR sensing to a Φ-OTDR mode of operation. The narrow linewidth of the laser regime is uncharacteristic of conventional random lasers, which are often associated with broadband emission and lack of speckle and self-interference [114]. Here, the laser output is phase-sensitive in the addressed section, and its use as a distributed acoustic sensor (DAS) and distributed temperature sensor (DTS) is demonstrated. Very high SNR sensing application is demonstrated compared to state-of-the-art distributed sensing systems. By making use of a fiber section as a mirror for laser action, the measured sensing signal is full output of the laser, not Rayleigh light, which allows high SNR sensing over long distances. The high resolution measurements show an advance in the Φ-OTDR technique since in most of the works in the literature the resolution is often limited to 1-meter since the intensity of backscattered light is very small. Here, the author demonstrate a ten-fold increase in resolution measurements compared to state-of-the-art Φ-OTDR [37, 83]. Based on these specifications, the laser proposed should be able to as a distributed optical fiber sensor (DOFS) in severals applications as detection of soil movement along a pipeline, detection of mechanical deformation in an oil/gas pipeline, detection and location of any leak along a dam, detection and location of any critical point in an optical telecommunications network and detection location of any hot spot along the power cable (see Figure 2.30), etc. Furthermore, the physics of Rayleigh backscattering of coherent light is not restricted to single-mode fibres, and could also be applied to other scattering media. Given the sensitivity of the system to extremely low levels of backscattered light, its concept can conceivably be applied to distributed sensing of dilute scattering particles in free space, as a lasing-LIDAR with transform-limited resolution.

Bibliography

[1] Jiarong Qin, Ruihong Dai, Yao Li, Yafei Meng, Yongbing Xu, Shining Zhu, and Fengqiu Wang, "20 GHz actively mode-locked thulium fiber laser," Opt. Express 26, 25769-25777 (2018).

[2] D. Lorenser et al., "50-GHz passively mode-locked surface-emitting semiconductor laser with 100-mW average output power," in IEEE Journal of Quantum Electronics 42(8), 838-847 (2006).

[3] G. Duan et al., "High performance InP-based quantum dash semiconductor mode-locked lasers for optical communications," in Bell Labs Technical Journal 14(3), 63-84 (2009).

[4] Herrera, Luis Ernesto & Amaral, Gustavo & von der Weid, Jean Pierre, "Ultra-high-resolution tunable PC-OTDR for PON monitoring in avionics," in Optical Fiber Communication Conference (OFC), paper 10.1364/OFC.2015.W2A.39 (2015).

[5] Shuai, Wang & Fan, Xinyu & Liu, Qingwen & He, Zuyuan, "Ultra- High-Resolution OTDR based on Linear Optical Sampling with Digital Dispersion Compensation," in Asia-Pacific Optical Sensors Conference (APOS), paper Th3A.5. 10.1364/APOS.2016.Th3A.5 (2016).

[6] F. Calliari, M. M. Correia, G. P. Temporão, G. C. Amaral and J. P. v. d. Weid, "Fast Acquisition Tunable High-Resolution Photon-Counting OTDR," in Journal of Lightwave Technology 38(16), 4572-4579 (2020).

[7] P. Yan et al., "Topological Insulator Solution Filled in Photonic Crystal Fiber for Passive Mode-Locked Fiber Laser," in IEEE Photonics Technology Letters 27(3), 264-267 (2015).

[8] U. Keller et al., "Semiconductor saturable absorber mirrors (SESAM's) for femtosecond to nanosecond pulse generation in solid-state lasers," IEEE J. Sel. Topics Quantum Electron. 2(3), 435–453 (1996).

[9] J. Xu et al., "All-Polarization-Maintaining Femtosecond Fiber Lasers Using Graphene Oxide Saturable Absorber," in IEEE Photonics Technology Letters 26(4), 346-348 (2014).

[10] Li, L., Lv, R., Chen, Z. et al. “Mode-Locked Er-Doped Fiber Laser by Using MoS2/SiO2 Saturable Absorber,” Nanoscale Res Lett 14, 59 (2019).

[11] X. Yang, Z. Li, E. Tangdiongga, D. Lenstra, G. D. Khoe, and H. J. S. Dorren, "Sub-picosecond pulse generation employing an SOA based nonlinear polarization switch in a ring cavity," Opt. Express 12, 2448-2453 (2004).

[12] Liu, Tonghui & Jia, Dongfang & Yang, Jingwen & Chen, Jiong & Wang, Zhaoying & Yang, Tianxin, "An ultra-long cavity passively mode-locked fiber laser based on nonlinear polarization rotation in a semiconductor optical amplifier," Laser Physics. 23, 095005 (2013).

[13] Hou-Ren Chen, Kuei-Huei Lin, Chih-Ya Tsai, Hsiao-Hua Wu, Chih-Hsuan Wu, Chieh-Han Chen, Yu-Chieh Chi, Gong-Ru Lin, and Wen-Feng Hsieh, "12 GHz passive harmonic mode-locking in a 1.06 μm semiconductor optical amplifier-based fiber laser with figure-eight cavity configuration," Opt. Lett. 38, 845-847 (2013).

[14] Renlai Zhou, Xuanyi Liu, Dan Yu, Qian Li, and H. Y. Fu, "Versatile multi-soliton patterns of noise-like pulses in a passively mode-locked fiber laser," Opt. Express 28, 912-923 (2020).

[15] Peng, J., Boscolo, S. Filter-Based, “Dispersion-Managed Versatile Ultrafast Fibre Laser,” Sci Rep 6, 25995 (2016).

[16] Sergei K. Turitsyn et al., “Random distributed feedback fibre laser,” Nature Photonics 4, 231-235 (2010).

[17] M. Pang et al, “Frequency stabilized coherent Brillouin random fiber laser: theory and experiments,” Opt. Express 21, 27155–27168 (2013).

[18] G. Yin et al, “Tunable Er-doped fiber ring laser with single longitudinal mode operation based on Rayleigh backscattering in single mode fiber,” Opt. Express 19 (27), 25981–25989 (2011).

[19] Pedro Tovar, Guilherme Temporão, and Jean Pierre von der Weid, "Longitudinal mode dynamics in SOA-based random feedback fiber lasers," Opt. Express 27, 31001-31012 (2019).

[20] Walter Margulis, Avishek Das, J. P. von der Weid, and Anderson S. L. Gomes, "Hybrid electronically addressable random fiber laser," Opt. Express 28, 23388-23396 (2020).

[21] T. Zhu, X. Bao, and L. Chen, "A Single Longitudinal-Mode Tunable Fiber Ring Laser Based on Stimulated Rayleigh Scattering in a Nonuniform Optical Fiber," J. Lightwave Technol. 29(12), 1802–1807 (2011).

[22] G. Yin, B. Saxena, and X. Bao, "Tunable Er-doped fiber ring laser with single longitudinal mode operation based on Rayleigh backscattering in single mode fiber," Opt. Express 19(27), 25981–25989 (2011).

[23] S. K. Turitsyn, S. A. Babin, A. E. El-Taher, P. Harper, D. V. Churkin, S. I. Kablukov, J. D. Ania-Castañón, V. Karalekas, and E. V. Podivilov, "Random distributed feedback fibre laser," Nat. Photonics 4(4), 231–235 (2010).

[24] S. A. Babin, A. E. El-Taher, P. Harper, E. V. Podivilov, and S. K. Turitsyn, "Tunable random fiber laser," Phys. Rev. A 84(2), 021805 (2011).

[25] M. Pang, X. Bao, L. Chen, Z. Qin, Y. Lu, and P. Lu, "Frequency stabilized coherent Brillouin random fiber laser: theory and experiments," Opt. Express 21(22), 27155–27168 (2013).

[26] L. Zhang, Y. Xu, S. Gao, B. Saxena, L. Chen, and X. Bao, "Multi-wavelength Coherent Brillouin Random Fiber Laser with High Optical Signal-to-Noise Ratio," in Conference on Lasers and Electro-Optics (CLEO), paper SM2L.6 (2017).

[27] W. Margulis, A. Das, J. P. von der Weid, and A. S. L. Gomes, "Hybrid electronically addressable random fiber laser," Opt. Express 28(16), 23388–23396 (2020).

[28] C. J. S. de Matos, L. D. S. Menezes, A. M. Brito-Silva, M. A. M. Gamez, A. S. L. Gomes, and C. B. de Araújo, "Random fiber laser," Phys. Rev. Lett. 99(15), 153903 (2007).

[29]. C. Hong, S. Gao, M. Zhang, J. Zhang, L. Qiao, T. Wang, F. Gao, X. Hu, S. Li, and Y. Zhu, "Advances in Random Fiber Lasers and Their Sensing Application," Sensors 20(21), 6122 (2020).

[30] I. R. R. González, B. C. Lima, P. I. R. Pincheira, A. A. Brum, A. M. S. Macêdo, G. L Vasconcelos, L. de S. Menezes, E. P. Raposo, A. S. L. Gomes, and R. Kashyap, "Turbulence hierarchy in a random fibre laser," Nat. Commun. 8(1), 15731 (2017).

[31] P. Lu, S. J. Mihailov, Y. Xu, and X. Bao, "Development of femtosecond random gratings for fiber laser and sensor applications," Proc. SPIE 11739, 12 (2021).

[32] S. V. Shatalin, V. N. Treschikov, and A. J. Rogers, "Interferometric optical time-domain reflectometry for distributed optical-fiber sensing," Appl. Opt. 37(24), 5600–5604 (1998).

[33] R. Juškaitis, A. M. Mamedov, V. T. Potapov, and S. V. Shatalin, "Interferometry with Rayleigh backscattering in a single-mode optical fiber," Opt. Lett. 19(3), 225–227 (1994).

[34] V. V. Spirin, "Transmission-reflection analysis for localization of temporally successive multipoint perturbations in a distributed fiber-optic loss sensor based on Rayleigh backscattering," Appl. Opt. 42(7), 1175–1181 (2003).

[35] L. Thévenaz, "Review and Progress in Distributed Fiber Sensing," in Optical Fiber Sensors (OFS), paper ThC1 (2006).

[36] M. Barnoski, M. Rourke, S. Jensen, and R. Melville, "Optical time domain reflectometer," Appl. Opt. 16(9), 2375–2379 (1977).

[37] Y. Koyamada, M. Imahama, K. Kubota, and K. Hogari, "Fiber-Optic Distributed Strain and Temperature Sensing With Very High Measurand Resolution Over Long Range Using Coherent OTDR," J. Lightwave Technol. 27(9), 1142–1146 (2009).

[38] Y. Lu, T. Zhu, L. Chen, and X. Bao, "Distributed Vibration Sensor Based on Coherent Detection of Phase-OTDR," J. Lightwave Technol. 28(22), 3243–3249 (2010).

[39] J. C. Juarez, E. W. Maier, K. N. Choi, and H. F. Taylor, "Distributed Fiber-Optic Intrusion Sensor System," J. Lightwave Technol. 23(6), 2081–2087 (2005).

[40] J. C. Juarez and H. F. Taylor, "Polarization discrimination in a phase-sensitive optical time-domain reflectometer intrusion-sensor system," Opt. Lett. 30(24), 3284–3286 (2005).

[41] E. F.Williams, M. R. Fernández-Ruiz, R. Magalhaes, R. Vanthillo, Z. Zhan, M. González-Herráez, and H. F. Martins, "Distributed sensing of microseisms and teleseisms with submarine dark fibers," Nat. Commun. 10(1), 5778 (2019).

[42] H. F. Martins, M. R. Fernández-Ruiz, L. Costa, E. Williams, Z. Zhan, S. Martin-Lopez, and M. Gonzalez-Herraez, "Monitoring of remote seismic events in metropolitan area fibers using distributed acoustic sensing (DAS) and spatiotemporal signal processing," in Optical Fiber Communication Conference (OFC), paper M2J.1 (2019).

[43] T. Liu, H. Li, F. Ai, J. Wang, C. Fan, Y. Luo, Z. Yan, D. Liu, and Q. Sun, "Ultra-high Resolution Distributed Strain Sensing based on Phase-OTDR," in Optical Fiber Communication Conference (OFC), paper Th2A.16 (2019).

[44] Z. Romain, X. Liu, Y. Wang, J. Zhang, Y. Wang, and B. Jin, ", "Recent Progress in the Performance Enhancement of Phase-Sensitive OTDR Vibration Sensing Systems," Sensors 19(7), 1709 (2019).

[45] X. Fan, G. Yang, S. Wang, Q. Liu, and Z. He, "Distributed Fiber-Optic Vibration Sensing Based on Phase Extraction From Optical Reflectometry," J. Lightwave Technol. 35(16), 3281–3288 (2017).

[46] Z. Qin, T. Zhu, L. Chen, and X. Bao, "High Sensitivity DistributedVibration Sensor Based on Polarization-Maintaining Configurations of Phase-OTDR," IEEE Photonics Technol. Lett. 23(15), 1091–1093 (2011).

[47] Y. Muanenda, C. J. Oton, S. Faralli, T. Nannipieri, A. Signorini, and F. D. Pasquale, "Hybrid distributed acoustic and temperature sensor using a commercial off-the-shelf DFB laser and direct detection," Opt. Lett. 41(3), 587–590 (2016).

[48] Z. He and Q. Liu, "Optical Fiber Distributed Acoustic Sensors: A Review," J. Lightwave Technol. 39(12), 3671–3686 (2021).

[49] J. Tejedor, H. F. Martins, D. Piote, J. Macias-Guarasa, J. Pastor-Graells, S. Martin-Lopez, P. C. Guillén, F. De Smet, W. Postvoll, and M. González-Herráez, "Toward Prevention of Pipeline Integrity Threats Using a Smart Fiber-Optic Surveillance System," J. Lightwave Technol. 34(19), 4445–4453 (2016).

[50] M. Soriano-Amat, H. F. Martins, V. Durán, L. Costa, S. Martin-Lopez, M. Gonzalez-Herraez, and M. R. Fernández- Ruiz, "Time-expanded phase-sensitive optical time-domain reflectometry," Light: Sci. Appl. 10(1), 51 (2021).

[51] S P Nikitin et al, '"Distributed temperature sensor based on a phase-sensitive optical time-domain Rayleigh reflectometer," Laser Phys. 28, 085107 (2018).

[52] Khalid Miah and David K. Potter," A Review of Hybrid Fiber-Optic Distributed Simultaneous Vibration and Temperature Sensing Technology and Its Geophysical Applications," Sensors 17(11), 2511 (2017).

[53] Pastor-Graells, H. F. Martins, A. Garcia-Ruiz, S. Martin-Lopez, and M. Gonzalez-Herraez, "Single-shot distributed temperature and strain tracking using direct detection phase-sensitive OTDR with chirped pulses," Opt. Express 24, 13121-13133 (2016).

[54] Wiersma, D. The physics and applications of random lasers. Nature Phys 4, 359–367 (2008).

[55] Hui Cao, "Review on latest developments in random lasers with coherent feedback," J. Phys. A: Math. Gen. 38, 10497 (2005).

[56] Kalt, H, "Towards mode-locking," Nature Photon 5, 573–574 (2011).

[57] Leonetti, M., Conti, C. & Lopez, C., "The mode-locking transition of random lasers," Nature Photon 5, 615–617 (2011).

[58] Antenucci, F., Lerario, G., Fernandéz, B. S. et al., "Demonstration of Self-Starting Nonlinear Mode Locking in Random Lasers," Phys. Rev. Lett. 307(126), 173901 (2021).

[59] Trivedi, M., Saxena, D., Ng, W.K. et al., "Self-organized lasers from reconfigurable colloidal assemblies," Nat. Phys. 18, 939–944 (2022).

[60] Mujumdar, S., Türck, V., Torre, R. & Wiersma D. S., "Chaotic behavior of a random laser with static disorder," Phys. Rev. A 76, 033807 (2007).

[61] Leonetti, M., Conti, C. & López, C., "Dynamics of phase-locking random lasers," Phys. Rev. A 88, 043834 (2013).

[62] Hu, B., Cui, H., Zhang, Y. L. et al., "Mode locking of a coherent random fiber laser with selectable repetition rates," Optics Express 28, 36380 312 (2020).

[63] B. E. A. Saleh and M. C. Teich, "Fundamentals of Photonics," 2nd ed. John Wiley and Sons (2007).

[64] Wilson, J; Hawkes, J.F.B., "Lasers Principles and Applications," Prentice Hall International Series in Optoeletronics (1987).

[65] Y. Xu, L. Zhang, L. Chen and X. Bao, "Single-mode SOA-based 1-kHz-linewidth dual-wavelength random fiber laser," Optics Express 25(14), 15828-15837 (2017).

[66] Thorlabs Inc, Datasheet SOA1013SXS High-Speed Optical Shutter/Switch, Thorlabs, available in: https://www.thorlabs.com/newgrouppage9.cfm?objectgroup_id=4336&pn=SOA1013SXS.

[67] Braga, Pedro Tovar, "Modeling Rayleigh backscattering of coherent light in single-mode fibers & applications on the prediction of mode dynamics of Random DFB fiber lasers," Tese, Doutorado em Engenharia Elétrica, Pontifícia Universidade Católica do Rio de Janeiro (PUC-RIO), Rio de Janeiro (2021).

[68] Naji, Ahmed W., Belal A. Hamida, X. S. Cheng, Mohd. Adzir Mahdi, Sulaiman Wadi Harun, Sheroz Khan, Wajdi F. Al-Khateeb, A. A. Zaidan, Bilal Bahaa Zaidan and Harith Ahmad. "Review of Erbium-doped fiber amplifier." International Journal of Physical Sciences 6, 4674-4689 (2011).

[69] Tuolima, Datasheet Erbium Doped Fiber Amplifier 1550nm, Tuolima. [Online]. Available in: http://www.tuolima.com/uploads/edfa-1550.pdf.

[70] Thorlabs 100S, Datasheet Erbium Doped Fiber Amplifier 1550nm, Thorlabs. [Online]. Available in: https://www.thorlabs.com/newgrouppage9.cfm?objectgroup_id=10680&pn=EDFA100S.

[71] Corning, Datasheet Erbium-Doped Fiber ER 1550C3, Corning. [Online]. Available in: https://www.corning.com/media/worldwide/global/documents/sfiber%20Erbium-doped%20Specialty %20Fibers%20PDF.pdf.

[72] Thorlabs Inc, Datasheet PL980P200 Pigtailed Laser Pump, Thorlabs. [Online]. Available in: https://www.thorlabs.com/drawings/57f7d6bb018a016c-388DB9CF-9EC7-75F05E8B996F64DEE3C6 /PL980P200-SpecSheet.pdf.

[73] H.-G. Weber and M. Nakazawa, "Ultrahigh-speed optical transmission technology," Springer Science & Business Media, 3 (2007).

[74] M. E. Fermann, F. Haberl, M. Hofer, and H. Hochreiter, "Nonlinear amplifying loop mirror," Optics Letters 15(13), 752–754 (1990).

[75] G. P. Agrawal, "Nonlinear Fiber Optics," E.D. Academic Press, ed., (2001).

[76] G. P. Agrawal, "Fiber-optic communication systems," John Wiley & Sons, 222, (2012).

[77] RP Photonics Encyclopedia.[Online].Available in: https://www.rp-photonics.com/fiber_loop_mirrors.html#:~:text=This%20configuration%20is%20called%20a,phase%20changes%20in%20the%20loop.

[78] M. Kues, C. Reimer, B. Wetzel, P. Roztocki, B. E. Little, S. T. Chu, T. Hansson, E. A. Viktorov, D. J. Moss, and R. Morandotti, "Passively mode-locked laser with an ultra-narrow spectral width," Nature Photonics 11(3), 159 (2017).

[79] RP Photonics Encyclopedia. [Online]. Available in: https://www.rp-photonics.com/nonlinear_polarization_rotation.html#:~:text=When%20an%20intense%20optical%20pulse,change%20in%20the%20polarization%20state.

[80] Sheng-Fong Lin, Huai-Yung Wang, Yu-Chuan Su, Yu-Chieh Chi and Gong-Ru Lin, "Multi-order bunched soliton pulse generation by nonlinear polarization rotation mode-locking erbium-doped fiber lasers with weak or strong polarization-dependent loss," Laser Phys. 24, 105113 (2014).

[81] Mukhopadhyay, P.K., "Femtosecond pulse generation and amplification in Yb-doped fibre oscillator-amplifier system," Pramana - J Phys 75, 787–805 (2010).

[82] Olivier, M., Gagnon, M.D., Habel, J., "Automation of Mode Locking in a Nonlinear Polarization Rotation Fiber Laser through Output Polarization Measurements," J. Vis. Exp. (108), e53679, (2016).

[83] Xiaoyi Bao and Yuan Wang, "Recent Advancements in Rayleigh Scattering-Based Distributed Fiber Sensors," Advanced Devices e Instrumentation 2021, 869657 (2021).

[84] M. Nakazawa, "Rayleigh backscattering theory for single-mode optical fibers," J. Opt. Soc. Am., 73(9), 1175–1180 (1983).

[85] P. Healey, "Fading in heterodyne OTDR," Electronics Letters 20(2), 30–32 (1984).

[86] P. Healey, "Fading rates in coherent OTDR," Electronics Letters, 20(1), 443–444 (1984).

[87] P. Healey, "Statistics of Rayleigh backscatter from a single-mode optical fibre," Electronics Letters 21(2), 226–228 (1985).

[88] J. Zhou, Z. Pan, Q. Ye, H. Cai, R. Qu, and Z. Fang, "Characteristics and explanations of interference fading of a ϕ -otdr with a multi-frequency source," Journal of Lightwave Technology, 31(17), 2947–2954 (2013).

[89] L. B. Liokumovich, N. A. Ushakov, O. I. Kotov, M. A. Bisyarin, and A. H. Hartog, "Fundamentals of optical fiber sensing schemes based on coherent optical time domain reflectometry: Signal model under static fiber conditions," Journal of Lightwave Technology 33(17), 3660– 3671 (2015).

[90] Pedro Tovar, Bismarck Costa Lima, and Jean Pierre von der Weid, "Modelling Intensity Fluctuations of Rayleigh Backscattered Coherent Light in Single-Mode Fibers," J. Lightwave Technol. 40, 4765-4775 (2022).

[91] Kashyap, R., "Fibre Bragg gratings," Ac. Press 1st ed, 155 (1999).

[92] Mathieu Gagné and Raman Kashyap, "Random fiber Bragg grating Raman fiber laser," Opt. Lett. 39, 2755-2758 (2014).

[93] Hongwei Yin, Adenowo Gbadebo, and Elena G. Turitsyna, "Top-hat random fiber Bragg grating," Opt. Lett. 40, 3592-3594 (2015).

[94] S R Abdullina et al, "Single-frequency Yb-doped fiber laser with distributed feedback based on a random FBG," Laser Phys. Lett. 13, 075104 (2016).

[95] M.I. Skvortsov et al, "FBG array-based random distributed feedback Raman fibre laser," Quantum Electron. 47, 696 (2017).

[96] Du, X., Zhang, H., Xiao, H., Ma, P., Wang, X., Zhou, P. and Liu, Z., "High-power random distributed feedback fiber laser: From science to application," Annalen der physik 528, 649-662 (2016).

[97] Yun-Jiang Rao, "In-fibre Bragg grating sensors," Meas. Sci. Technol. 8, 355 (1997).

[98] Morey, William W, Meltz, Gerald; Glenn, William H., "Fiber optic Bragg grating sensors," Proc. SPIE 1169, 98–107 (1989).

[99] VIAVI solutions. [Online]. Available in: https://www.viavisolutions.com/pt-br/deteccao-de-fibra-optica.

[100] I. N. Duling, "All-fiber ring soliton laser mode locked with a nonlinear mirror," Optics letters 16(8), 539–541 (1991).

[101] International Telecommunication Union. [Online]. Available in: https://www.itu.int/rec/T-REC-G.694.1-202010-I/en

[102] Y. Senoo, N. Nishizawa, Y. Sakakibara, K. Sumimura, E. Itoga, H. Kataura, and K. Itoh, "Ultralow-repetition-rate, high-energy, polarization-maintaining, Er-doped, ultrashort-pulse fiber laser using single-wall-carbon-nanotube saturable absorber," Opt. Express 18, 20673-20680 (2010).

[103] L. A. Rodriguez-Morales, I. Armas-Rivera, B. Ibarra-Escamilla, O. Pottiez, H. Santiago-Hernandez, M. Durán-Sánchez, M. V. Andrés, and E. A. Kuzin, "Long cavity ring fiber mode-locked laser with decreased net value of nonlinear polarization rotation," Opt. Express 27, 14030-14040 (2019).

[104] L. Chen, M. Zhang, C. Zhou, Y. Cai, L. Ren and Z. Zhang, "Ultralow repetition rate SESAM-mode-locked linear-cavity erbiumdoped fiber laser," in Conference on Lasers & Electro Optics/Pacific Rim (CLEO), paper TUP3_11 (2009).

[105] Xiaohui Li, Xueming Liu, Xiaohong Hu, Leirang Wang, Hua Lu, Yishan Wang, and Wei Zhao, "Long-cavity passively mode-locked fiber ring laser with high-energy rectangular-shape pulses in anomalous dispersion regime," Opt. Lett. 35, 3249-3251 (2010).

[106] Samuel, D. W., Namdas, E. B. & Graham, A. T., "How to recognize lasing," Nature Photonics 3, 547 (2009).

[107] Sapienza, R.., "Determining random lasing action," Nat Rev Phys 1, 690–695 (2019).

[108] K. Sala, G. Kenney-Wallace and G. Hall, "CW autocorrelation measurements of picosecond laser pulses," in IEEE Journal of Quantum Electronics 16(9), 990-996 (1980).

[109] S. Stepanov, "Dynamic population gratings in rare-earth-doped optical fibres," J. Phys. D: Appl. Phys. 41(22), 224002 (2008).

[110] J. Frisken, "Transient Bragg reflection gratings in erbium-doped fiber amplifiers," Opt. Lett. 17(24), 1776–1778 (1992).

[111] Fischer, J. L. Zyskind, J. W. Sulhoff, and D. J. DiGiovanni, "Nonlinear wave mixing and induced gratings in erbium-doped fiber amplifiers," Opt. Lett. 18(24), 2108–2110 (1993).

[112] K. Xu, "Silicon electro-optic micro-modulator fabricated in standard CMOS technology as components for all silicone monolithic integrated optoelectronic systems," J. Micromech. Microeng. 31(5), 054001 (2021).

[113] B. M. Haas and T. E. Murphy, “A Simple, Linearized, Phase-Modulated Analog Optical Transmission System,” IEEE Photonics Technol. Lett. 19(10), 729–731 (2007).

[114] A. S. L. Gomes, A. L. Moura, C. B. de Araújo, and E. P. Raposo, “Recent advances and applications of random lasers and random fiber lasers,” Prog. Quantum Electron. 78, 100343 (2021).

Annex

Publications

In this annex all the papers developed during the doctorate are listed.

Related to this work

Papers

_ "Fast Acquisition Tunable High-Resolution Photon-Counting OTDR," published in J. Lightwave Technology in 2020.

_ “Picosecond pulse-width ultra-low repetition rate passive mode-locked fibre ring laser” published in Electronics Letters in 2020.

_ “2.5-GHz Passively Mode-Locked Fiber Ring Laser Employing a Semiconductor Optical Amplifier as Nonlinear Polarization Rotator Device” published in 20º Simpósio brasileiro de micro-ondas e optoeletrônica in 2022.

_ “Vibration Sensing with a Hybrid Electronically Addressable Random Laser” published in Conference on Lasers and Electro-Optics (CLEO) in 2022.

_ “Distributed vibration sensor with a lasing phase-sensitive OTDR” published in Optics Express in 2022.

_ “A mode-locked random fibre laser generating transform-limited optical pulses” submitted in Nature Communication in 2023.

Annex A

The paper “Fast Acquisition Tunable High-Resolution Photon-Counting OTDR” was published in the Journal of Lightwave Technology in 2020.

Fast Acquisition Tunable High-Resolution Photon-Counting OTDR

Felipe Calliari, Marlon M. Correia, Guilherme Penello Temporão, Gustavo C. Amaral, *Member, IEEE*, and Jean Pierre von der Weid, *Senior Member, IEEE*

***Abstract*—A 15 dB dynamic range and 4.6 cm spatial resolution tunable photon-counting optical time-domain reflectometer (PC-OTDR) is presented along with a Field Programmable Gate Array (FPGA)-based detection management system that allows several regions of the fiber to be interrogated by the same optical pulse, increasing the data acquisition rate when compared to previous solutions. The optical pulse generation is implemented by a tunable figure-8 passive mode-locked laser providing pulses with the desired bandwidth and center wavelength for WDM applications in the C-band. The acquisition rate is limited by the afterpulse effect and dead time of the employed gated avalanche single-photon detectors. The devised acquisition system not only allows for centimeter-resolution monitoring of fiber links as long as 12 km in under 20 minutes but is also readily adapted to other photon-counting strategy for increased acquisition rate. The system provides a 20-fold decrease in acquisition times when compared with state-of-the-art solutions, allowing affordable times for centimeter-resolution long-distance fiber measurements.**

***Index Terms*—Optical fiber monitoring, optical time domain reflectometry, single-photon detection.**

I. Introduction

OPTICAL fibers are, inarguably, one of the most important elements of modern telecommunication networks, having allowed for long-haul high-bandwidth links to be implemented around the world [1]. They offer, thus, the basis for the Open Systems Interconnection (OSI) and its reliability is fundamental for the robust operation of all the higher-level network layers. Mechanical damage, the protagonist of optical fiber transmission impairments, can cause from minor to debilitating losses and, therefore, must be evaluated timely and precisely [2].

Manuscript received October 28, 2019; revised March 28, 2020; accepted April 17, 2020. Date of publication April 27, 2020; date of current version July 28, 2020. This work was supported by brazilian agencies Coordenação de Aperfeiçoamento de Pessoal de Nível Superior (CAPES), Conselho Nacional de Desenvolvimento Científico e Tecnológico (CNPq), and Fundação de Amparo à Pesquisa do Estado do Rio de Janeiro (FAPERJ). *(Corresponding author: Felipe Calliari.)*

Felipe Calliari, Marlon M. Correia, Guilherme Penello Temporão, and Jean Pierre von der Weid are with the Center for Telecommunications Studies, Pontifical Catholic University of Rio de Janeiro, Rio de Janeiro - RJ 22451-900, Brazil (e-mail: felipe.calliari@opto.cetuc.puc-rio.br; mcorreia@opto.cetuc.puc-rio.br; temporao@opto.cetuc.puc-rio.br; vdweid@opto.cetuc.puc-rio.br).

Gustavo C. Amaral is with the Center for Telecommunications Studies, Pontifical Catholic University of Rio de Janeiro, Rio de Janeiro - RJ 22451-900, Brazil, and also with the QC2DLab, Kavli Foundation, Technical University of Delft 2628 CD, Delft, The Netherlands (e-mail: gustavo@opto.cetuc.puc-rio.br).

Color versions of one or more of the figures in this article are available online at http://ieeexplore.ieee.org.

Digital Object Identifier 10.1109/JLT.2020.2990872

One way of discovering the position and magnitude of the mechanical damage imposed into a fiber is to monitor the back-propagating light originated from an interrogation signal; the nature of such light falls into two classes: scattered light, usually associated with the Rayleigh backscattering of light from the atomic nuclei of the fiber material; and reflected light, usually associated with the discontinuity of index of refraction along the fiber or to a reflective structure placed along the fiber, such as a Bragg grating; the last of which figures as the basis of several of the proposed and implemented distributed fiber sensors [3].

When the intensity of the back-propagating light is measured over time, and the position of the mechanical damage is determined based on the speed of light inside the fiber, the method is known as Optical Time Domain Reflectometry (OTDR) [4]. In OTDR applications, spatial resolution and dynamic range come as a trade-off since strengthening the pulse for enhanced reach usually affects the pulse width and diminishes the 2-point resolution [5]. To alleviate such trade-off, a photon-counting OTDR (PC-OTDR) can be assembled, where a single-photon detector is employed and a detection management system must be integrated for consistent results [6]. In recent works [7], [8], PC-OTDR systems have been developed where a train of detection gates allows for several positions of the fiber to be interrogated with a single optical pulse. Employing the same mechanism in systems with centimeter-range resolutions, which can benefit both optical fiber monitoring and sensor applications, has been elusive. In [9], for instance, a system making use of two different PC-OTDR variants was demonstrated in order to achieve centimeter-range resolution in km-range fibers without the drawback of low data acquisition rate imposed by the high-resolution acquisition procedure. There, extra signal processing steps had to be taken into account, which reduced the total monitoring speed.

In this work, a 15 dB dynamic range and 4.6 cm spatial resolution tunable photon-counting optical time-domain reflectometer (PC-OTDR) is presented along with a joint Field Programmable Gate Array (FPGA) and Time-to-Digital Converter (TDC)-based detection management system that allows several regions of the fiber to be interrogated by the same optical pulse. The optical pulse generation is implemented by a figure-8 passively mode-locked laser containing a tunable optical filter that ensures that the probing pulses are generated within the desired bandwidth and center wavelength for WDM applications. The developed detection procedure allows increasing the data acquisition rate by a factor that depends on the operator's

choice of detection window length and detection gate train period. The results indicate that portions of the fiber separated by 200 meters can be interrogated by the same optical pulse without debilitating effects coming from the afterpulse effect. Centimeter-range monitoring of km-range fibers in under 20 minutes in a wavelength division multiplexing (WDM) scenario are demonstrated in this paper.

The paper is divided as follows. The architecture and its sub-systems are presented in Section II, where the arrangement of the devices, individual characteristics, and data management are presented and discussed. Section III approaches the characteristics of the full system with respect to its achievable spatial resolution and dynamic range, tunability, acquisition rate, and limitations on such. Section IV provides discussion on possible applications and optimizations of the system and concludes with the major contributions and future works.

II. Architecture

The basic operation of a PC-OTDR begins with the optical p[ulse] generation sub-system, which creates light pulses at a rate s[uch] that only one pulse traverses the fiber at a time. Under this c[ondi]tion, back-propagating light created due to either scattering o[r re]flection of the interrogation pulse can be collected by means o[f an] optical circulator and sent to a single-photon detector. It is t[he t]ask of the data acquisition sub-system to correctly associate d[etec]tions to time windows such that, with an estimate of the fi[ber]'s refractive index and the speed of light, one can determine t[he p]ositions where the back-propagating signals originate from. In [a ma]thematical form, $d_i = \frac{c}{2n}\, t_i$, where c is the speed of light in v[acu]um, n is the refractive index of the fiber and t_i is the round-t[rip] travel time of the i-th detected pulse, taken into account by t[he f]actor 2 in the denominator.

In order to simplify the analysis of the OTDR signal, one can i[gnor]e the non-linear effects associated to the transmission of o[ptic]al signals, which allow the employment of linear system abstractions such as the transfer function and the impulse response. In this context, and since the optical fiber is a two-port network, the OTDR procures to measure the impulse response $h(t)$ of the fiber's S_{11} parameter, or $h_{11}(t)$; in fact, optical frequency-domain reflectometry (OFDR) techniques [10] such as the Incoherent- and Coherent-OFDR attempt to assess the transfer function $H_{11}(f)$ of the fiber, which is intimately related to $h_{11}(t)$ via a Fourier transform. Due to the intrinsic attenuation of light inside an optical fiber, $h_{11}(t)$, which, when translated into distance is usually referred to as the fiber profile, exhibits an exponential decay; it is, thus, usual to display the fiber profile in logarithmic scale with a linear negative slope, where eventual breaks can be associated to power losses [11], [12].

It becomes clear that the spatial resolution achievable in the measurement of the fiber profile is limited by the temporal width of the interrogating pulse, $p(t)$, since

$$h_{11}^{\text{eff}}(t) = h_{11}(t) * p(t), \tag{1}$$

where $h_{11}^{\text{eff}}(t)$ stands for the effectively measured fiber profile. At the same time, the overall energy contained in $p(t)$ will determine the amount of attenuation that it can withold while still allowing for a higher-than-one signal-to-noise ratio (SNR > 1) measurement in the detector. Assuming saturation of the optical pulse generation structure, in order to increase the optical energy contained in the probing pulse, its width must be increased, thereby constituting the so-called trade-off between spatial resolution and dynamic range. Attempting to extract the maximum of both ends of this trade-off, one can employ sources of high-power narrow optical pulses and low noise-equivalent power (NEP) detectors. Moreover, management and synchronization of pulse generation and data acquisition is imperative for efficient long-reach high-resolution measurement. In the following sub-sections, these two sub-systems (optical pulse generation and data acquisition) are presented in detail.

A. Optical Pulse Generation

The optical pulse generation sub-system is comprised of a figure-eight passively mode-locked laser (F8-PMLL). Such laser configuration has been shown to produce sub-picosecond pulses at different wavelengths [13], rendering its application for a tunable, long-reach, high-resolution time-domain reflectometer. Mode-locked lasers rely on saturable absorbers to create a fixed phase relation between the spectral modes allowed within its optical resonator cavity. Under the mode-locked condition, the temporal shape of the output signal is given by a coherent weighted sum of such allowed spectral modes or, mathematically:

$$p(t) = \sum_{n=-N/2}^{N/2} c_n e^{-i2\pi(\omega_0 + n\cdot f_0)t}, \tag{2}$$

where c_n are the individual weigths of each spectral modes (or Fourier coefficients), ω_0 is the laser's center frequency, f_0 is the optical cavity's free-spectral range (FSR), and N is the total number of allowed spectral modes within the laser bandwidth $\Delta\omega$, where $N = \Delta\omega / f_0$. Equation 2 states that the cavity modes constitute a Fourier series of the output signal, which will correspond to periodically emitted pulses since the spectrum, during mode-locked operation, takes the form of a frequency comb.

Mode-locking can be achieved either actively (through intensity and/or phase modulation) or passively in either free-space or fiber cavities [14]. Among others, the main advantages of fiber-based mode-locked lasers include low propagation loss, the possibility of creating high Q value kilometer-long fiber cavities, and the fact that erbium-doped fiber amplifiers (EDFAs) and fiber-pigtailed semiconductor optical amplifiers (SOAs) can be used as the gain media [14]. Figuring as physical mechanisms that guarantee mode-locking in PML fiber lasers are nonlinear polarization rotation [15], dispersion-managed stretched pulse propagation [16], and the constructive/destructive interference of counter-propagating longitudinal modes in a so-called nonlinear amplifying loop mirror (NALM) [17]. The latter allows for the optical switching of the input optical pulses according to the following mathematical relations:

$$\begin{aligned} \mathcal{T} &= \tfrac{I_{\text{out}}}{I_{\text{in}}} = \tfrac{\mathrm{G}(1-\cos[\Delta\phi_{\text{NL}}(\mathrm{G}-1)])}{2} \\ \mathcal{R} &= 1 - \mathcal{T}, \end{aligned} \tag{3}$$

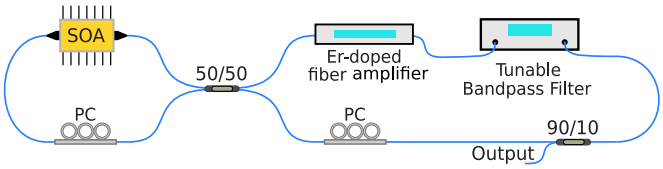

Fig. 1. The overview of the passively mode-locked figure-8 fiber laser. On the left-hand side, the nonlinear amplifying loop mirror (NALM) is depicted. On the right-hand side, the optical cavity with an unidirectional EDFA that determines the direction of propagation, and a variable optical bandpass filter that determines the center wavelength of emission are depicted. PC, Polarization Controller.

where $I_{\text{in/out}}$ are the input/output optical intensities, G is the amplifier gain, $\Delta\phi_{\text{NL}}$ is the difference in non-linear phase shift between the counter-propagating fields in the NALM, and $\mathcal{T}$ and $\mathcal{R}$ are the transmissivity and reflectivity of the NALM, respectively.

When the NALM is combined with a closed fiber loop, it constitutes a figure-8 laser (F8L), an extremely versatile fiber structure that finds applications in, for instance, soliton genera- , and has been first reported by Duling [18]. Recently, an F8L ized with an SOA in the NALM and an EDFA in the optical ity has been reported [19], whose design is reproduced in work and depicted in Fig. 1. The NALM (left-hand side in 1) is composed by an SOA, a Polarization Controller (PC), single-mode fibers totalling a length of $L_1 \approx 8.42$ meters. optical cavity (right-hand side in Fig. 1) is formed by a PC, a 10 coupler (that allows one to couple a portion of the optical al generated in the F8L to the output), a tunable band pass r (BPF),an unidirectional EDFA (incorporating an optical ator), and single-mode fibers totaling a length of $L_2 \approx 36.38$ ers.

n the NALM, a periodic transmission and reflection of the cal pulses occurs as a function of the instantaneous input er and the non-linear phase shift between the longitudinal nter-propagating modes supported by the NALM cavity. Therefore, if an optical pulse is formed in the F8-PMLL and its peak power satisfies the transmission conditions of the NALM, it will propagate in the F8-PMLL according to the direction dictated by the optical isolator; otherwise, it will be reflected by the NALM and eliminated by the EDFA's isolator [20]. The polarization controller of the left-hand side loop (1) can be adjusted to control the birefringence in the fiber and, in turn, the non-linear phase shift factor in Eq. 3. This way, the interference of the counter-propagating longitudinal modes on the 50/50 coupler can be adjusted such that only input pulses of a certain intensity are transmitted, while lower pulses are reflected and extinguished in the EDFA's isolator. The center wavelength of emission of the F8L is dictated by the BPF, which is tunable in the range 1530–1565 nm covering the telecommunication C-band as depicted in Fig. 2.

Under fundamental mode operation, the F8-PMLL presented in Fig. 1 produces 303 ps-wide pulses spaced by 224 ns (a repetition rate of 4.46 MHz), the former determined by a total 1.39 GHz emission bandwidth and, the latter, by the overall length of the fiber cavity of 44.8 meters. To achieve such conditions, other than correctly adjusting the PCs, the injection current

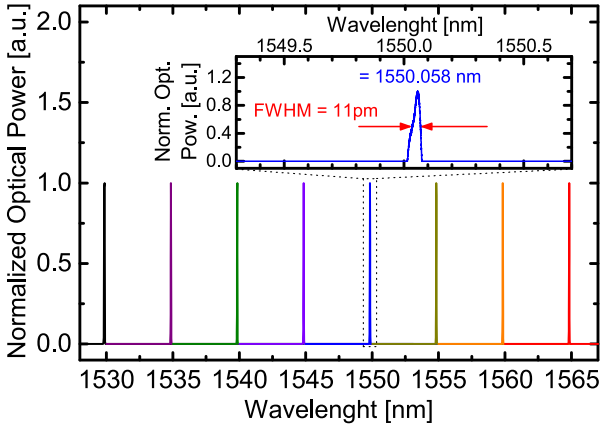

Fig. 2. Center wavelength tunability of the employed F8-PMLL. The bandwidth, measured with a high-resolution (16 MHz) optical spectrum analyzer, is 11 pm at all center wavelengths.

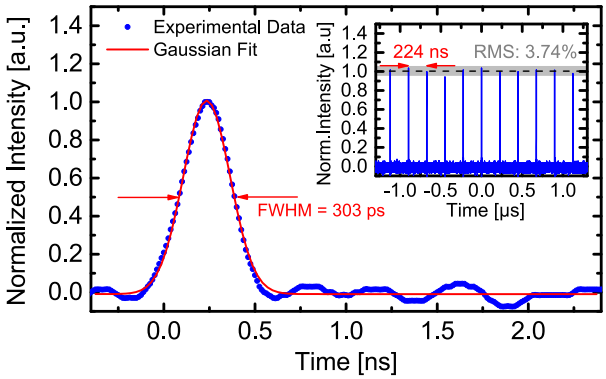

Fig. 3. Temporal shape of the generated optical signal in the passive mode-locked figure-8 laser. The pulse separation of 224 ns matches the resonator length of 44.8 meters and the pulse temporal width is 303 ps, which limits the spatial resolution of the PC-OTDR to 3.07 cm.

of the SOA should be approximately 300 mA, which translates into optical pulses with 4 pJ energy level and 13 mW peak power. Under these conditions, the wavelength tunability of the F8-PMLL is rather simple in terms of PC alignment; on the other hand, the pulse peak power limits the achievable dynamic range. In order to maintain the ease of tunability of the system while also increasing the dynamic range, the output pulses were sent to a second EDFA, which yields optical pulses with 25 pJ energy level and 83 mW peak power. Due to the broad bandwidth of the EDFA, the width of the optical pulses, after amplification, was not compromised, as presented in Fig. 3; the output spectrum, measured in a electrical spectrum analyzer (ESA), corroborates the timing characteristics of the optical signal, and is presented in Fig. 4.

B. Data Acquisition

Data acquisition is performed in synchronization with an enabling pulse from a high-speed optical switch that guarantees that a single probing pulse is traversing the fiber at a time. This is necessary since the rate of pulse emission from the PML described in the previous subsection (which is entirely

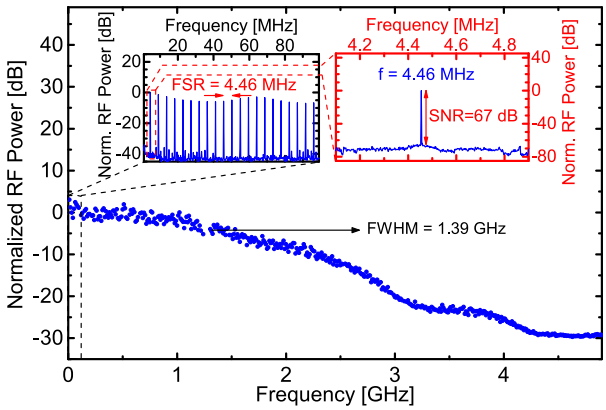

Fig. 4. Spectral characterization of the generated optical signal with respect to the central wavelength of 1550.058 nm. The spectral comb-shape exhibits a finesse $\mathcal{F} = 6371.43$, with a bandwidth (δf) of 700 Hz and a free-spectral range (FSR) of 4.46 MHz, which matches the resonator length of 44.8 meters.

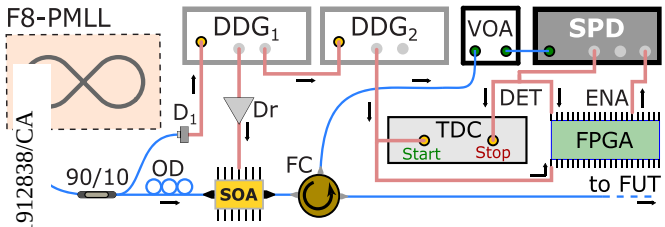

F . Block diagram of the data acquisition system including the synchro- n with the F8-MPLL; optical fibers are blue lines and pink lines are el cal signals. D_1, *p-i-n* photodetector; Dr, electronic driver; OD, optical d FC, fiber circulator; VOA, variable optical attenuator; FUT, fiber under te he black arrows indicate the direction of the electric and optical signals fo se of visualization.

d mined by the cavity length of the optical resonator) might n natch this condition. The pulse selection is accomplished th gh an SOA triggered by a short (2 ns, 300 mA) pulse, which, u r these conditions, imparts a 1 dB insertion loss on the optical pulse and creates an ASE noise level of −9.6 dBm, setting the probing pulse's extinction ratio to 27 dB. This triggering pulse, in turn, is synchronized to the incoming pulse from the PML by detecting a small portion of its output using a 90/10 beam splitter.

The block diagram of the data acquisition sub-system is depicted in Fig. 5. Synchronization is crucial not only between the PML and the SOA but, also, between these and a Field Programmable Gate Array (FPGA), a Time-to-Digital Converter (TDC), and the single-photon detector that manage the detection of the backscattered portion of the probe pulse. A Digital Delay Generator (DDG_1), triggered by detections from the F8-PMLL pulses, is responsible for reducing the rate of pulses launched into the fiber by means of an internal prescaler. It is also responsible for generating a delayed trigger (τ_p) for a second DDG (DDG_2) that works in burst mode; the importance of τ_p will be clarified further on. DDG_2 then generates a sequence of evenly-spaced (τ_b) electrical pulses that act on the TDC as a *start* pulse and are also routed to the FPGA. The FPGA is programmed such that the pulse received by DDG_2 goes through an AND gate and is enabled according to a pre-defined signal e_r, whose function will also be clarified further on; presently, e_r is considered always high, for simplicity.

The output of the FPGA's AND gate is directed to the enable input of the SPD, opening a detection window (τ_d) whose width can be tuned between 5 and 35 ns. If a detection occurs within this detection window, the detection pulse of the SPD is directed to the *stop* input of the TDC where the time difference between *start* and *stop* pulses is determined. The detection pulse is also sent to the FPGA, that records the occurrence of a detection. In case no detection occurs, the subsequent pulse from DDG_2 will reinitialize the process and the FPGA will record the absence of a detection in the previous detection window. The FPGA can, then, produce a simple binary indexed list to backtrack the detection events: 1's correspond to the occurrence of a detection; and 0's to no detection.

The fact that the system is able to reinitialize the data acquisition at every new cycle of the burst of DDG_2 allows a single optical pulse to probe regions of the fiber spaced by $d = \frac{c}{2n}\tau_b$. In order to reconstruct the fiber profile, one is required to measure the time between the pulse being launched into the fiber and any of the *stop* pulses, which can be accomplished by combining the information from the FPGA and the TDC. This is due to the TDC's data storage procedure, which piles up the time between the *start* and *stop* pulses only when a corresponding *stop* occurs; the FPGA provides, thus, a means of associating the times in the TDC to the correct detection windows which produced them. Furthermore, since τ_p represents an offset in time between the probing pulse being launched into the fiber and the opening of the detection windows, it must also be taken into account in order to write any detection time as:

$$\tau_{\text{det}} = \tau_p + i\tau_b + \tau^i_{\text{TDC}}, \tag{4}$$

where i corresponds to the index of the respective enabling pulse of DDG_2 in which a detection was recorded and τ_{TDC} is the time stored in the TDC after a detection.

Clearly, in order to probe all the points in the fiber, τ_p must be swept so that it covers the distance between two consecutive detection windows. The total number of steps for τ_p can then be calculated according to $\frac{\tau_b}{\tau_d}$ and has a direct impact on the total measurement time, as will be discussed in the next section. In order to clarify the whole procedure, Fig. 6 depicts, in (a), the time panels of all the relevant optical and electrical signals associated to the data acquisition subsystem. In (b), the event lists contained within the FPGA and the TDC are pictorially depicted as well as the procedure for combining the two lists and creating the fiber profile.

III. The Fast Acquisition Tunable High-Resolution PC-OTDR

Combining the previously described sub-systems culminates in an optical reflectometry-based measurement system that yields a spatial resolution in the centimeter range with both achievable dynamic range and data acquisition rates higher than related state-of-the-art systems; furthermore, the system is tunable around the telecommunication C-band and exhibits narrow bandwidth, making it ideal for supervision of currently

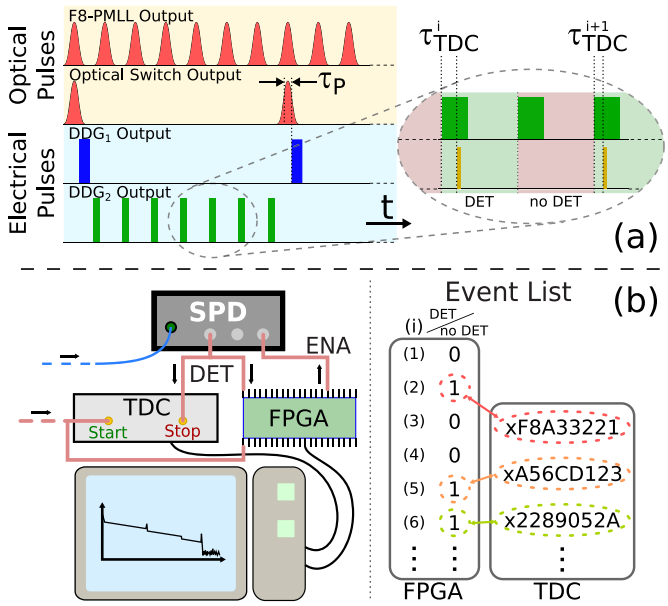

6. Data acquisition subsystem procedure. (a) Time panel of relevant rical and optical pulses. The zoomed region represents two different sit- ns, i.e., detection windows with and without an associated detection pulse. ıermore, the time between the enabling of the detector and the arrival of letection pulse (different for the two depicted events) is recorded by the ' as τ_{TDC}. (b) The detection system for reconstruction of the fiber profile d on the event lists from the FPGA and the TDC. On the left hand side, onnections between the devices is depicted as a block diagram including a ɔnal computer; optical fibers are blue lines, pink lines are electrical signals, ɔlack lines are data buses. The right hand side depicts the combination of esults from the event lists that allow for the reconstruction of τ_{det}.

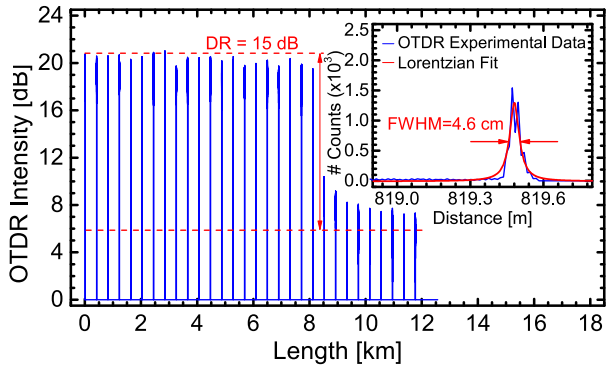

Fig. 7. Dynamic range (15 dB) and spatial resolution (4.6 cm) achieved with the proposed OTDR system. The wavelength of operation of the F8-PMLL for these results was 1550.058 nm, and the total measurement time was 5 minutes.

deployed optical networks relying on wavelength division multiplexing (WDM), such as WDM Passive Optical Networks (WDM-PON).

In order to characterize the system's operation parameters, OTDR profiles of different fibers have been measured; depending on the figure of merit of interest, the condition of the measurement also changed. This is because, even with the higher data acquisition rates propitiated by the proposed system, measurements of km-long fibers that achieve the full dynamic range of the system still require long measuring times. In Fig. 7, for instance, the dynamic range and spatial resolution are showcased using an 8-km fiber; only the measurements of detection windows associated to a fixed τ_p were acquired, however, but during an extended 5-min measurement time (t_{meas}).

For this measurement, a detection window $\tau_d = 20$ ns and a burst period $\tau_b = 2$ μs were used, yielding a 15 dB dynamic range, calculated by taking the difference, in dB, between the initial point of the profile and the 1.5-dB point below the noise level (which coincides with the average value of the noise) [21], i.e., detections associated to positions "outside" the fiber. The value of the dynamic range agrees well with the prediction based on the mean number of photons per detection window at the initial position of the fiber (0.45), the rate of emission of probing pulses into the fiber (9 KHz), and the dark count rate of the detector (5 per second). The VOA at the input of the SPD guarantees that the mean number of photons impinging on the SPD is such that multi-photon detection is reduced so that the OTDR trace exhibits no saturation effects [8]. The VOA attenuation is set to $\sim$15 dB, calculated based on the pulse peak power at the input of the fiber, the photon's energy, and the Rayleigh scattering coefficient. Under these conditions, the rate difference between detections (4100 per second) and dark counts equates to 14.5 dB, a good estimate of the achieved dynamic range in Fig. 7. The SPD operates at an efficiency of 5%, and the counting rate is 180,000 per second.

The total amount of time necessary to reproduce the results with the same dynamic range, but for all points in the fiber, would be $\frac{\tau_b}{\tau_d} t_{meas} \approx 8$ hours, which is the reason why these were not measured. The spatial resolution was determined by the full width at half maximum of a lorentzian fit into a reflection peak at the fiber's end to be 4.6 cm as shown in the inset of Fig. 7. This value, which differs from the limit induced by the temporal width of the probing pulse, is attributed, mainly, to the jitter of the SPD, although the jitter associated to the F8-PMLL and to both the TDC and DDG also contribute. These values have been experimentally determined to be 350 ps, 20 ps, 40 ps, and 45 ps, respectively, which, combined with the pulse width, amount to a spatial resolution of 4.9 cm, which agrees well with the experimentally determined values.

In order to showcase the capability of the system to perform tunable and fast fiber profile measurements with centimeter resolution, an arrayed waveguide grating (AWG) was employed. A 4-km feeder fiber (between the measurement system and the AWG) is followed by four different fibers ($L_1 = 4$ km, $L_2 = 8$ km, $L_3 = 0.9$ km, $L_4 = 3$ km) each connected to a different channel of the AWG, as follows: Ch 03, $\lambda = 1534.09$ nm, L_1; Ch 09, $\lambda = 1539.8$ nm, L_2; Ch 15, $\lambda = 1544.0$ nm, L_3; Ch 22, $\lambda = 1550.0$ nm, L_4. For these results, the measurement time for each of the values of τ_p was set to ten seconds, and the number of total steps necessary in order to cover all the points in the fiber was $\frac{\tau_b}{\tau_d} = \frac{2\mu s}{20\,\text{ns}} = 100$, totalizing a measurement time of $\sim$16.7 minutes. Interrogation of each individual channel is possible by tuning the F8-PMLL center wavelength accordingly, and the results are presented in Fig. 8.

Under these conditions, the amount of detection events are still not enough to reach the full dynamic range of the system, as previously commented, and as clearly depicted in the traces of Fig. 8. Even under such short measurement time conditions,

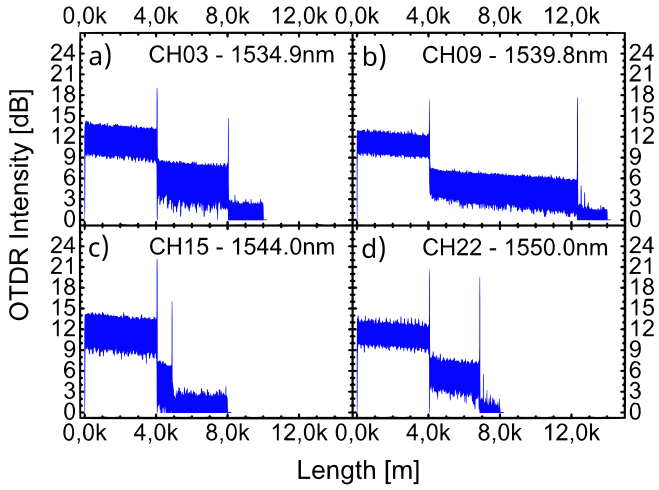

Fig. 8. Full fiber measurements of four distinct AWG channels, corresponding to different wavelengths. The tunability of the F8-PMLL allows for each channel to be probed individually. Total measurement time is ∼16.7 minutes for each of the channels. Detection peaks observed at the end of the fiber profiles correspond to afterpulsing due to the high reflection peak at the fiber end.

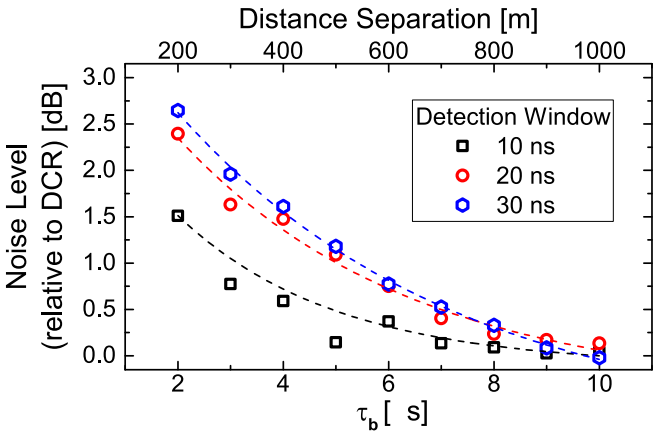

Fig. 9. Noise level, in dB, relative to the SPD's intrinsic dark count rate as the separation between detection windows and the width of such windows is varied. The exponential decay is expected from the behavior of the afterpulse probability as a function of *deadtime* [23].

h ever, the system was able to achieve a quite expressive dB dynamic range. Furthermore, the system showcases t ole centimeter-resolution measurements of km-range fibers i inute-range times, an outstanding result in comparison with s -of-the-art systems. Due to its performance, the system is d ed the Fast Acquisition High-Resolution Photon Counting C R.

A cquisition Rate and Afterpulse Probability

It is noteworthy that the burst period τ_b determines the s d-up in data acquisition of the proposed system, since a s e optical probing pulse sent into the fiber can be used to i rogate multiple regions. Enabling more detection windows p optical pulse, which corresponds to decreasing τ_b, even though positive in the sense of higher data acquisition rate, has an associated effect related to the afterpulse probability of the employed gated avalanche single-photon detectors. As the effective detector *deadtime* between two detection windows is reduced, the probability of a delayed release of a trapped carrier inside the semiconductor junction increases exponentialy [22].

For regions of the fiber where the counts associated to Rayleigh backscattered photons is above the noise (coming either from the intrinsic dark count rate of the detector of from the afterpulsing probability), the effect is not apparent; however, when one analyzes the detections outside of the fiber, where only the detector's intrinsic noise (dark count rate) should play a role, the effect becomes clear, as in positions $L \geq 8.2$ km of Fig. 7. In fact, if the separation between detection windows is too small, one can extrapolate the impact of the afterpulsing effect and expect that it completely degrades the measured OTDR profile, erasing all relevant information about the fiber.

Analyzing the impact of the afterpulse probability on the detections permits finding a set of parameters compatible with the sought after higher data acquisition rates while still minimizing as much as possible its contribution. Experimental results are presented in Fig. 9, where the difference, in dB, between the intrinsic noise level of the system, associated to the detector's dark count rate, and the noise level when the afterpulse is present, has been used as a figure of merit when the detection window length τ_d and the burst period τ_b are varied. In order to provide more insight into the results, the horizontal axis is presented in both μs and in meters, i.e., the associated distance separation, in the fiber, between two consecutive detection windows.

As can be clearly seen from Fig. 9, the afterpulse probability dominates the noise baseline level unless the separation between consecutive detection windows is longer than 1 km. Simultaneously, the number of necessary windows $\frac{\tau_b}{\tau_d}$ for complete fiber measurements increases by a factor of 5, under these conditions, with respect to the measurements of Fig. 8. Therefore, and since the impact of the afterpulse is not as critical on the noise level as the impact of increasing τ_b is on the timing, the parameters used in the measurement could be loosely selected as $\tau_b = 2$ μs and $\tau_d = 20$ ns.

B. Discussion

It is clear that one of the major benefits of the proposed system is the capability of monitoring wavelength multiplexed networks with telecom-compatible wavelengths, which is available due to the tunability of the F8-PMLL. However, short-distance high-capacity optical networks operating at the near-infrared region of the spectrum are attracting a lot of attention [24], and high-resolution monitoring is of great interest in this context. In fact, a photon-counting OTDR system operating at this wavelength and making use of a gain-switched laser was recently demonstrated [25]. There, the acquisition rate is still limited since, for each probing pulse launched into the fiber, only a single detection window is enabled. Fortunately, the herewith proposed acquisition system can be readily adapted to work in that and any other photon-counting OTDR system with equal or even higher gains, since the silicon-based single-photon detectors compatible with that system exhibit lower dark count rates, higher detection efficiency, and smaller afterpulse probability.

Systems such as the one in [26], where a superconducting nanowire single-photon detector compatible with the telecom wavelength was employed in a PC-OTDR, or the one in [27], where a 30-dB dynamic range was achieved but with a total monitoring time of 6 hours, would likewise benefit from the proposed acquisition system.

It is noteworthy that the solution found in [9] to achieve cm-resolution fault detection at long-distances would also benefit from the high-rate acquisition system. There, a *coarse* and long-reach PC-OTDR system first acquires information about the fiber profile, which is followed by a signal processing routine that identifies possible candidates that are, then, individually interrogated by a *fine* PC-OTDR system. The limitation on the acquisition system, however, causes the total monitoring time to scale with the number of identified candidates, which is overcome with the current acquisition system, since multiple fault candidates can be interrogated simultaneously.

On one hand, thus, the acquisition system proposed and demonstrated in this work enables the high-resolution monitoring of long-distance fibers by greatly increasing the rate of ı acquisition. On the other, the much higher event detection on the SPAD uncovers an application bottleneck associated ıe maximum data capacity of the employed TDC. The fact the current TDC is limited to 180 thousand samples per ɔnd caused the detection efficiency to be reduced to 5% ɔrder to avoid loss of data; for higher values of detection ɔiency the detection rate overloads the TDC. Employing DC with higher data capacity will allow for even higher ı acquisition gains and could usher the replacement of the ent avalanche single-photon detectors by superconducting owire single-photon detectors (SNSPD) that offer not only ıer detection efficiency but also free-running operation.

The gain in speed over other centimeter-resolution PC-OTDR ıtions is determined by the number of extra detection win-ws that the proposed system is capable of offering. Since this ıber will change if the fiber length increases and can also be leveraged against an increased contribution of the afterpulse effect (as shown in Fig. 9), this number is hardly determined. For the measurement conditions showcased in Fig. 7, however, 20 detection windows (within the fiber span) are available, which translates into a 20-fold factor in acquisition time in comparison with state-of-the-art solutions where only a single detection window is opened per optical pulse sent into the fiber [9], [25]. For the results of Figure 8, because the length of the fiber changes, the timing gain for the full-fiber measurement would vary between 10 and 20 using the current (limiting) devices and a reduced efficiency of the SPD. State-of-the-art (Superconducting Nanowire) Single-Photon Detectors offer absence of afterpulsing, higher than 90% detection efficiency, and as high as 100 ns deadtimes with 100 ps jitter. Allied to high-speed TDC modules, the system could perform the measurements showcased in Figs. 7 and 8 in under a minute with higher resolution (due to the reduced jitter) and higher dynamic range (due to the absence of afterpulsing).

When compared to other monitoring solutions, which do not rely on photon-counting for fiber monitoring, the Fast Acquisition Tunable PC-OTDR exhibits an unique combination of characteristics that make it competitive with respect to the state-of-the-art. For instance, a chaos-OTDR able to achieve similar (centimeter) resolution in long distance measurements has been demonstrated [28], with monitoring times as low as 2 ms. However, the technique is limited to identifying reflective events in a fiber. It is important to highlight that, even though used in a different context in [28], filtered broadband sources are not indicated for the measurements presented in Fig. 7 and 8. The fact that the demonstrated spatial resolution can be maintained for long-distance measurements is only possible due to the tunable F8-PMLL, which creates short-pulses with a relatively narrow spectral bandwidth. This way, chromatic dispersion does not severely limit the spatial resolution as more distant positions of the fiber are probed. In e.g. [29], a filtered broad band source was used to perform centimeter resolution measurements and a study of the impact of the chromatic dispersion (as the spectral bandwidth of the filter was varied) in the achievable spatial resolution was performed.

IV. Conclusion

By combining the time resolution of a TDC with the management capabilities of an FPGA, a detection system could be developed that allows for high resolution measurements with high data acquisition rates. This structure, when employed together with an optical pulse generation system that allows for wavelength tunability and high-peak-power narrow pulses culminates into the fast acquisition tunable high-resolution photon-counting OTDR, with an achievable spatial resolution of 4.6 cm and 15 dB dynamic range. The current bottleneck of the system is the throughput of the TDC, that handles a limited amount of detection events. Improving the TDC's data handling capacity, narrowing the pulse width of the F8-PMLL, and migrating the detection system in order to make use of superconducting nanowire single-photon detectors are the main future points of investigation, which have the potential to lead to sub-centimeter spatial resolution with an even higher achievable dynamic range. The realization of a system where a single optical pulse can be used to monitor distinct positions of a fiber in a high-resolution photon-counting OTDR enables dramatic gains in acquisition time and, in turn, full long-distance fiber measurements with centimeter resolution.

References

[1] S. Kumar and M. J. Deen, *Fiber Optic Communications: Fundamentals and Applications*. Hoboken, NJ, USA: Wiley, 2014.
[2] P. J. Urban, G. Vall-Llosera, E. Medeiros, and S. Dahlfort, "Fiber plant manager: An OTDR-and OTM-based PON monitoring system," *IEEE Commun. Mag.*, vol. 51, no. 2, pp. S9–S15, Feb. 2013.
[3] K. O. Hill and G. Meltz, "Fiber bragg grating technology fundamentals and overview," *J. Lightw. Technol.*, vol. 15, no. 8, pp. 1263–1276, 1997.
[4] M. Barnoski, M. Rourke, S. Jensen, and R. Melville, "Optical time domain reflectometer," *Appl. Opt.*, vol. 16, no. 9, pp. 2375–2379, 1977.
[5] G. P. Agrawal, *Fiber-optic communication systems*, vol. 222, Hoboken, NJ, USA: Wiley, 2012.
[6] G. C. Amaral, L. E. Herrera, D. Vitoreti, G. P. Temporão, P. J. Urban, and J. P. von der Weid, "Wdm-PON monitoring with tunable photon counting OTDR," *IEEE Photon. Technol. Lett.*, vol. 26, no. 13, pp. 1279–1282, Jul. 2014.
[7] L. Herrera, F. Calliari, J. Garcia, G. Amaral, and J. von der Weid, "High resolution automatic fault detection in a fiber optic link via photon counting otdr," in *Proc. Opt. Fiber Commun. Conf.*, 2016, Paper M3F–4.

[8] G. C. Amaral, J. D. Garcia, L. E. Herrera, G. P. Temporao, P. J. Urban, and J. P. von der Weid, "Automatic fault detection in wdm-pon with tunable photon counting OTDR," *J. Lightw. Technol.*, vol. 33, no. 24, pp. 5025–5031, 2015.

[9] F. Calliari, L. E. Herrera, J. P. von der Weid, and G. C. Amaral, "High-dynamic and high-resolution automatic photon counting OTDR for optical fiber network monitoring," in *Proc. 6th Int. Conf. Photon., Opt. Laser Technol.*, 2018, vol. 1, pp. 82–90.

[10] M. Wegmuller, J. P. Von Der Weid, P. Oberson, and N. Gisin, "High resolution fiber distributed measurements with coherent ofdr," in *Proc. ECOC 2000*, Munich, Germany, vol. 11, no. 4, 2000, p. 109.

[11] J. P. von der Weid, M. H. Souto, J. D. Garcia, and G. C. Amaral, "Adaptive filter for automatic identification of multiple faults in a noisy otdr profile," *J. Lightw. Technol.*, vol. 34, no. 14, pp. 3418–3424, 2016.

[12] M. Lunglmayr and G. C. Amaral, "Linearized bregman iterations for automatic optical fiber fault analysis," *IEEE Trans. Instrum. Meas.*, vol. 68, no. 10, pp. 3699–3711, Oct. 2018.

[13] M. Salhi, F. Amrani, H. Leblond, and F. Sanchez, "Analytical investigation of a figure-eight single-pulse all-fiber laser based on a nonlinear amplifying loop mirror," *Physical Rev. A*, vol. 82, no. 4, 2010, Art. no. 043834.

[14] H.-G. Weber and M. Nakazawa, *Ultrahigh-Speed Optical Transmission Technology*, vol. 3, Berlin, Germany: Springer Science & Business Media, 2007.

[15] A. Komarov, H. Leblond, and F. Sanchez, "Passive harmonic mode-locking in a fiber laser with nonlinear polarization rotation," *Opt. Commun.*, vol. 267, no. 1, pp. 162–169, 2006.

[16] Y. Chen *et al.*, "Dispersion-managed mode locking," *JOSA B*, vol. 16, no. 11, pp. 1999–2004, Nov. 1999.

[17] M. E. Fermann, F. Haberl, M. Hofer, and H. Hochreiter, "Nonlinear amplifying loop mirror," *Opt. Lett.*, vol. 15, no. 13, pp. 752–754, 1990.

[18] I. N. Duling, "All-fiber ring soliton laser mode locked with a nonlinear mirror," *Opt. lett.*, vol. 16, no. 8, pp. 539–541, 1991.

[19] M. Kues *et al.*, "Passively mode-locked laser with an ultra-narrow spectral width," *Nature Photon.*, vol. 11, no. 3, p. 159, 2017.

[20] H.-R. Chen *et al.*, "12 ghz passive harmonic mode-locking in a 1.06 μ m semiconductor optical amplifier-based fiber laser with figure-eight cavity configuration," *Opt. Lett.*, vol. 38, no. 6, pp. 845–847, 2013.

[21] D. Derickson, C. Hentschel, and J. Vobis, *Fiber optic test and measurement*, vol. 8. Englewood Cliffs, NJ, USA: Prentice Hall, 1998.

[22] S. Cova, M. Ghioni, A. Lotito, I. Rech, and F. Zappa, "Evolution and prospects for single-photon avalanche diodes and quenching circuits," *J Modern Opt.*, vol. 51, no. 9-10, pp. 1267–1288, 2004.

[23] S. Cova, A. Lacaita, and G. Ripamonti, "Trapping phenomena in avalanche photodiodes on nanosecond scale," *IEEE Electron Device Lett.*, vol. 12, no. 12, pp. 685–687, Dec. 1991.

[24] D. A. Miller, "Optical interconnects to silicon," *IEEE J. Sel. Topics Quantum Electron.*, vol. 6, no. 6, pp. 1312–1317, Nov./Dec. 2000.

[25] B. Li *et al.*, "850nm gain-switched pulse laser and its application in photon counting OTDR," in *Proc. Opt. Metrology Inspection Ind. Appl. V*, 2018, vol. 10819, Art. no. 1081915.

[26] J. Hu *et al.*, "Photon-counting optical time-domain reflectometry using a superconducting nanowire single-photon detector," *J. Lightw. Technol.*, vol. 30, no. 16, pp. 2583–2588, 2012.

[27] P. Eraerds, M. Legré, J. Zhang, H. Zbinden, and N. Gisin, "Photon counting OTDR: Advantages and limitations," *J. Lightw. Technol.*, vol. 28, no. 6, pp. 952–964, 2010.

[28] Z. Wang *et al.*, "Long-range and high-precision correlation optical time-domain reflectometry utilizing an all-fiber chaotic source," *Opt. Express*, vol. 23, no. 12, pp. 15 514–15 520, 2015.

[29] L. E. Ynoquio Herrera, G. C. Amaral, and J. P. von der Weid, "Remote fiber bragg grating-based sensor characterization with ultra-high-resolution tunable photon counting OTDR," in *Proc. SBMO/IEEE MTT-S Int. Microw. Optoelectronics Conf.*, 2017, pp. 1–4.

Annex B

The paper “Picosecond pulse-width ultra-low repetition rate passive mode-locked fibre ring laser” was published in the Electronic Letters in 2020.

Picosecond pulse-width ultra-low repetition rate passive mode-locked fibre ring laser

M.M. Correia✉, P. Tovar, F. Calliari, G.C. Amaral and J.P. von der Weid

The authors experimentally demonstrate an ultra-low repetition rate passive mode-locked fibre ring laser with a semiconductor optical amplifier works like as a gain medium and non-linear polarisation rotation. A unidirectional erbium-doped fibre amplifier provides additional gain to increase cavity power. By exploiting non-linear polarisation rotation combined with dispersion management stable 5.18 ps optical pulses with 67.2 kHz repetition rate and energy of 1.75 nJ were generated with an extinction ratio >35 dB. The central wavelength is 1557.89 nm and the optical 3-dB bandwidth 1.82 nm very appropriate for optical applications that often require high-peak-power, low repetition rate and picosecond pulses.

Introduction: Interest in short-pulsed laser sources optics has been maintained over the past decade's thanks to the development of techniques for short high-power optical pulse generation, which finds applications in several areas of science. Besides optical communications, which involves increasingly higher frequencies, intense short pulses at low repetition rates are a challenging theme with important practical applications, such as optical fibre monitoring [1, 2]. One technique that attracts special attention is passive mode-locking in fibre lasers, due to both the absence of active modulation devices and the high-quality factor of fibre cavities [3]. Passively mode-locked fibre lasers (PMLFLs) rely on saturable absorbers (SAs) to create a fixed phase relationship (mode-locking) between the allowed spectral modes within the optical cavity. It has been demonstrated that the behaviour of SAs can be reproduced by exploiting the phenomenon of nonlinear polarisation rotation (NPR) in a fibre ring [4]. This work reported theoretical analysis of NPR effect in semiconductor optical amplifiers (SOAs) showing that, when high-power optical pulses propagate an SOA, they undergo a non-linear polarisation change due to polarisation-dependent saturation of the optical amplifier, thus, SOAs can act as NPR devices [3, 4]. Group velocity dispersion (GVD) in optical fibres may be a limiting factor for fast mode-locked optical pulses mainly in long cavity fibre rings. By combining fibres that exhibit dispersion parameters β_2 with opposite signs, i.e. positive and negative values of β_2 at the operation wavelength, the total GVD of the fibre ring can be managed to minimise the GVD experienced by the optical pulse signal [5]. In this Letter, we employ the dispersion management technique to generate a train of optical pulses exhibiting high peak-power, ultra-low repetition rate, and short temporal width. This is accomplished in a ring topology, where an SOA and an erbium-doped fibre amplifier (EDFA) act as gain media while the NPR effect is enhanced by the SOA. A similar experiment has been reported in [4], but with pulse, durations limited to the nanosecond scale, mainly due to dispersion effects within the ultra-long cavity. While a number of works in the literature demonstrate either short pulse duration [6, 7] or low repetition rates [4, 8, 9], the present work employed dispersion management over the long-length ring cavity allowing for stable fundamental mode-locked pulses to be obtained with picoseconds temporal width and kHz repetition rate.

Experimental setup: The experimental setup of the passively mode-locked fibre ring laser is shown in Fig. 1. It is composed of an SOA, a polarisation beam splitter (PBS), two polarisation controllers (PC1 and PC2), a unidirectional EDFA, a 90/10 optical coupler, a variable optical band-pass filter (OBPF) tuneable in both central wavelength and spectral bandwidth, 2.88 km of dispersion-shifted fibre and 0.125 km of standard fibre (SMF). Mode-locking, in this configuration, is achieved by injecting a current of ~390 mA into the SOA and properly adjusting the PCs. We used an off-the-shelf EDFA with fixed 26.5 dBm average output power. When a high-power optical pulse impinges on the SOA, the pulse's leading edge can deplete the SOA gain and saturate the device, so that a much lower gain is provided for the trailing edge of the pulse. Hence, as the SOA provides polarisation dependent gain, the refractive index saturation will also be polarisation dependent so that SOA will act as a non-linear polarisation rotation device [3, 4]. This feature can be used as a pulse compression mechanism by properly adjusting light polarisation along the cavity. In this way, the edges of the pulse are filtered by the PBS and removed from the loop. In order to repeat this operation for every roundtrip in the laser cavity, PC1 should be adjusted so that the same state of polarisation enters the SOA after a roundtrip. Due to its non-linear characteristic, the NPR effect is more pronounced for higher pulse peak powers. Therefore, the use of the EDFA is essential for enhancing the pulse compression since, with higher peak power, the polarisation will change more rapidly within the optical pulse and a shorter portion of it will be aligned to the PBS. The repetition rate of the train of optical pulses at the output of the laser is determined by the length of the optical fibre cavity and, in order to reduce the former, the latter must be increased. This is done in conjunction with dispersion management, so that the total GVD is minimised even with km-long ring lengths. Although fibre lengths were limited to the available bobbins in the lab, the operating wavelength could be selected by the tuneable filter in order to minimise the overall β_2. A minimum was found for an operating wavelength of 1558 nm, where the GVD of standard single-mode fibres (SMFs) is anomalous ($\beta_{2,SMF} = -20.39$ ps^2/km), in contrast to the erbium-doped fibre (EDF) and the dispersion-shifted fibre (DSF), which exhibit normal GVD ($\beta_{2,EDF} = +11.47$ ps^2/km, $\beta_{2,DSF} = +2.94$ ps^2/km) depending on the wavelength along the C-band. The fibre optic ring was formed with 0.149 km SMF (0.125 km from fibre reel and 0.024 km from fibre pigtails), ~0.013 km EDF (internal to the EDFA), and 2.880 km DSF fibres. Such parameters lead to a net dispersion in the cavity of $\sim +5.58$ ps^2 with a total length of 3.042 km.

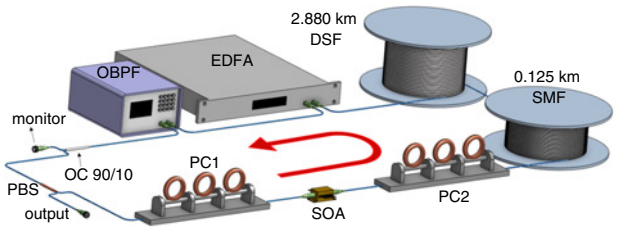

Fig. 1 *Passively mode-locked fibre ring laser (PMLFRL). The ring optical cavity with a unidirectional EDFA that determines the direction of propagation (red arrow) and a variable OBPF that determines the central wavelength at normal GVD in the dispersion-shifted fibre*

Results and discussion: The PMLFL experimental results are shown in Fig. 2, where all measurements were performed on the monitor output port of Fig. 1. Fig. 2*a* shows the pulse train, where a uniform intensity can be observed. The repetition rate of the train of optical pulses matches the measured roundtrip time of 14.88 µs and the optical fibre cavity length of 3.042 km. The pulse duration, measured with a second harmonic optical correlator and a photomultiplier, is shown in Fig. 2*b*. The full width at half maximum (FWHM) measured is 5.18 ps, corresponding to a Gaussian fit to the experimental data. The autocorrelation trace is noisy due to the very low duty cycle and the high gain set on the photomultiplier. Fig. 2*c* shows the radio-frequency (RF) spectrum measured with an electrical spectrum analyser (ESA), where a frequency comb can be observed. The 67.2 kHz tone corresponding to the fundamental frequency is shown on the inset of Fig. 2*c*, which exhibited an SNR of 35 dB and linewidth limited to the 10 Hz resolution bandwidth of the spectrum analyser, meaning low phase noise and jitter on the repetition pulse rate. The optical spectrum of mode-locked pulses is shown in Fig. 2*d*. The central wavelength is located at 1557.89 nm and the 3-dB spectral width is 1.82 nm (228 GHz) is compatible with Fourier transform-limited pulses. The spectrum is almost symmetric and featureless, although displaying small oscillations separated by ~25 GHz with ~1 dB modulation depth. The symmetry of the spectrum and modulation depth of the oscillations depend on the central wavelength chosen for the filter, indicating that they are both related to the total dispersion of the fibre ring. Slight changes in the central wavelength may lead to a totally asymmetric spectrum and several dB modulation depths.

Because both, repetition rate and pulse width are key features for several applications, a useful figure of merit for comparison between different achievements is the duty cycle of the optical pulse train. In optical-time-domain-reflectometry (OTDR) applications [1, 2], low rates are important to allow for the measurement of long fibres, whereas pulse duration defines the spatial resolution. High-resolution in long fibre monitoring is of great interest in this context and a shorter duty cycle is very important [1, 2]. A comparison between

duty cycle results in previous works [4, 6–9] is presented in Table 1. The present work shows the lowest duty cycle while maintaining a low repetition rate and ps-long pulses.

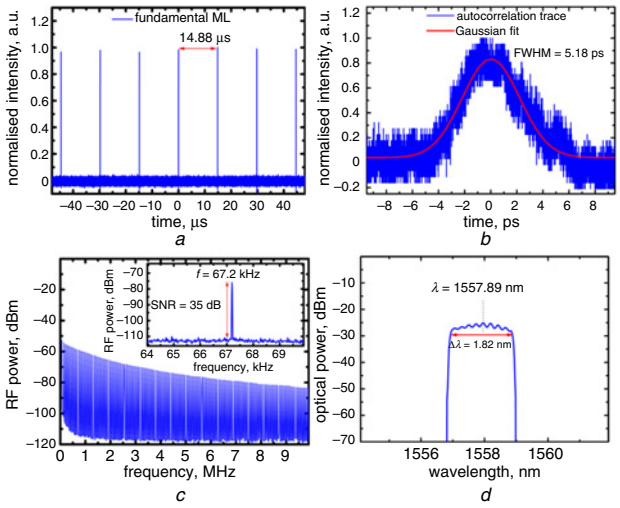

Fig. 2 *Ultra-long cavity fundamental mode-locked experimental results*

a Pulse train
b Autocorrelation trace
c Electrical spectrum
d Optical spectrum

Table 1: Comparison duty-cycle results

Repetition rate, kHz	FWHM	Duty cycle, 10^{-4}%	Reference
67.2	5.18 ps	0.35	this work
132.0	6.20 ps	0.82	[6]
467.2	2.90 ps	1.35	[7]
25.0	2.00 ns	50	[8]
50.7	~ns	unknown	[4]
278.0	12.8 ns	3558.4	[9]

Fig. 3 shows the evolution of the output pulse width of the proposed ibre optic ring laser operating in the repetition of the fundamental cavity. t shows a broad square pulse following a sharp spike at the leading edge. he duration of the square pulse can be controlled and reduced by proper djustment of the polarisation controller inside the cavity, similar to what vas observed in [9]. The pulse compression is evident when the peration wavelength and the polarisation are properly adjusted.

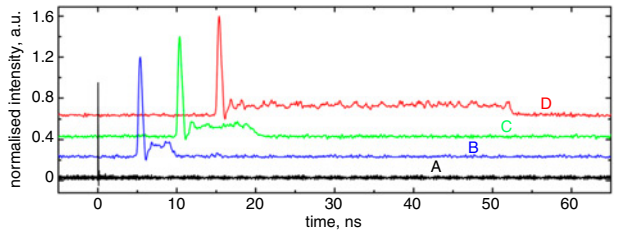

Fig. 3 *Polarisation tuning to reduce pulse width at optimum operation wavelength. Traces A to D are displaced for clarity and correspond to different adjustments of PC2. Pulse A is limited by the oscilloscope bandwidth and its actual duration was measured with the autocorrelator*

From Fig. 3 we see that the width of the broad pulse is reduced from 40 ns down to 5 ns and eventually disappear by fine-tuning. Besides the proper adjustment of the polarisation controllers, the central wavelength of the tuneable filter had to be properly adjusted to guarantee dispersion management, which was not possible in [9] due to their fibre choice. The final pulse width was 5.18 ps, much shorter than the scope resolution. The stable ultra-low repetition rate without CW leakage or tail in the output is of extreme importance for many applications such as high-resolution optical reflectometry. The period here corresponds to the roundtrip time in a 1.5 km-long fibre, ideal for OTDR applications in avionics.

Conclusion: We have experimentally demonstrated the generation and improvement of ultra-low repetition rate and picosecond-range duration optical pulses. The setup consists of a PMLFRL relying on NPR for pulse compression where dispersion management was used for GVD suppression. The final results are a stable repetition rate of 67.2 kHz, pulse duration of 5.18 ps and 1.75 nJ pulse energy with a high extinction ratio. To the best of the authors' knowledge, this is the lowest repetition rate obtained with ps-long pulses-based PMLFL, enabling this laser to be used as a source for millimetre resolution OTDR applications such as precision fault detection in avionics in km-long fibres [1, 2].

Acknowledgments: The authors acknowledge the financial support from Brazilian agencies CAPES, CNPq, and FAPERJ.

Submitted: *31 March 2020* E-first: *7 July 2020*
doi: 10.1049/el.2020.0803
One or more of the Figures in this Letter are available in colour online.

M.M. Correia, P. Tovar, F. Calliari, G.C. Amaral and J.P. von der Weid (*Centre for Telecommunications Studies (CETUC), Pontifical Catholic University of Rio de Janeiro (PUC-Rio), Rio de Janeiro 22453-900, Brazil*)

✉ E-mail: marloncorreia@opto.cetuc.puc-rio.br

References

1 Herrera, L.E., Amaral, G., and von der Weid, J.P.: 'Ultra-high-resolution tunable PC-OTDR for PON monitoring in avionics'. Optical Fiber Communication Conference, Los Angeles, CA, USA, 2015
2 Shuai, W., Fan, X., Liu, Q., *et al.*: 'Ultra-high-resolution OTDR based on linear optical sampling with digital dispersion compensation'. Asia Pacific Optical Sensors Conference, Shanghai, People's Republic of China, 2016
3 Yang, X., Li, Z., Tangdiongga, E., *et al.*: 'Sub-picosecond pulse generation employing an SOA-based non-linear polarization switch in a ring cavity', *Opt. Express*, 2004, **12**, pp. 2448–2453
4 Liu, T., Jia, D., Yang, J., *et al.*: 'An ultra-long cavity passively mode-locked fiber laser based on non-linear polarization rotation in a semiconductor optical amplifier', *Laser Phys.*, 2013, **23**, p. 095005, 10.1088/1054-660X/23/9/095005
5 Peng, J., and Boscolo, S.: 'Filter-based, dispersion-managed versatile ultrafast fibre laser', *Sci. Rep.*, 2016, **6**, p. 25995
6 Senoo, Y., Nishizawa, N., Sakakibara, Y., *et al.*: 'Ultralow-repetition-rate, high-energy, polarization-maintaining, Er-doped, ultrashort-pulse fiber laser using single-wall-carbon-nanotube saturable absorber', *Opt. Express*, 2010, **18**, pp. 20673–20680
7 Rodriguez-Morales, L.A., Armas-Rivera, I., Ibarra-Escamilla, B., *et al.*: 'Long cavity ring fiber mode-locked laser with decreased net value of non-linear polarization rotation', *Opt. Express*, 2019, **27**, pp. 14030–14040
8 Chen, L., Zhang, M., Zhou, C., *et al.*: 'Ultra-low repetition rate SESAM-mode-locked linear-cavity erbium-doped fiber laser'. Conf. on Lasers & Electro Optics & the Pacific Rim Conf. on Lasers and Electro-Optics, Shanghai, 2009, pp. 1–2
9 Li, X., Liu, X., Hu, X., *et al.*: 'Long-cavity passively mode-locked fiber ring laser with high-energy rectangular-shaped pulses in anomalous dispersion regime', *Opt. Lett.*, 2010, **35**, pp. 3249–3251

Annex C

The paper “2.5-GHz Passively Mode-Locked Fiber Ring Laser Employing a Semiconductor Optical Amplifier as Nonlinear Polarization Rotator Device” was published in the 20º Simpósio brasileiro de micro-ondas e optoeletrônica in 2022.

2.5-GHz Passively Mode-Locked Fiber Ring Laser Employing a Semiconductor Optical Amplifier as Nonlinear Polarization Rotator Device

Marlon M. Correia
Centre for Telecommunications Studies (CETUC)
Pontifical Catholic University of Rio de Janeiro (PUC-Rio)
Rio de Janeiro, Brazil
marloncorreia@opto.cetuc.puc-rio.br

Jean Pierre von der Weid
Centre for Telecommunications Studies (CETUC)
Pontifical Catholic University of Rio de Janeiro (PUC-Rio)
Rio de Janeiro, Brazil
vdweid@opto.cetuc.puc-rio.br

***Abstract* — We experimentally demonstrate a passive mode-locked fiber ring laser in which a semiconductor optical amplifier (SOA) works as a nonlinear polarization rotator whilst gain is provided by a unidirectional erbium-doped fiber amplifier. 2.30-ps optical pulses with 5.43-MHz repetition rate were generated by exploiting nonlinear polarization rotation. Different orders of harmonic mode-locking were demonstrated from 360-MHz to 2.5-GHz by changing the injection current of the semiconductor optical amplifier together with the adjustment of polarization controllers. Our results show that such a passive h ıonic mode-locked fiber ring laser has great potential in o al applications that often require high peak-power, high r ition-rate and picosecond pulses.**

eywords—Fiber Ring Laser; Harmonic Mode-Locking; conductor Optical Amplifier; Erbium-Doped Fiber Amplifier; inear Polarization Rotation.

I. INTRODUCTION

ıterest in ultrafast optics has increased over the past d des thanks to the development of techniques for ultrashort h power optical pulse generation, which finds applications i veral areas of science, such as: optical communications [1] a optical sampling [2]. One technique that attracts special a tion is passive mode-locking in fiber lasers, due to both t bsence of active modulation devices and the high-quality f r of fiber cavities [3, 4]. Passively mode-locked fiber laser rely on saturable absorbers that can be semiconductor saturable absorber mirrors [5], graphene [6] and Molybdenum disulfide (MoS_2) [7] to create a fixed phase relationship (mode-locking) between the allowed spectral modes within the optical cavity. Passive mode locking can also be obtained using techniques that simulate the behavior of a saturable absorber such as a nonlinear amplifier loop mirror (NALM) [8] or by nonlinear polarization rotation [4, 5]. It has been demonstrated that the behavior of saturable absorbers can be reproduced by exploiting the phenomenon of nonlinear polarization rotation in a fiber ring [4]. Recent works have reported theoretical analysis of nonlinear polarization rotation (NPR) effect in semiconductor optical amplifiers (SOAs) [3]. It has been shown that, when high-power optical pulses reach an SOA, they undergo a nonlinear polarization change due to polarization-dependent saturation of the optical amplifier. Thus SOAs can act as nonlinear polarization rotation devices [3].

The harmonic mode-locking (HML) regime was first observed in an erbium-doped fiber laser by Grudinin et al in 1993 [9]. In this regime, it is possible to excite harmonics of the fundamental frequency, defined by the physical dimension of the cavity, increasing the repetition rate without reducing the cavity length to unpractical levels. Recent studies showed that many erbium-doped or ytterbium-doped fiber lasers or with an SOA as a gain medium, are capable of operating in HML regime for multi-GHz pulse repetition-rates. Zhou et al in 2006, showed this capacity for the 31^{th} harmonic (1.3-GHz) with a 400-mW pumping power [10] while Chen et al in 2013, demonstrated this capacity for the 1202^{nd} harmonic (12.02-GHz) with a 660-mA current injection [8].

In this work, we present a simple experimental setup to generate passively mode-locked pulses using a 1.55-μm SOA as a nonlinear polarization switch and an erbium-doped fiber amplifier (EDFA) as a gain medium. We reached mode-locked picoseconds optical pulses with GHz repetition-rates.

II. EXPERIMENTAL SETUP

The experimental setup of the passively mode-locked fiber ring laser is shown in Fig. 1. It is composed of a multi-quantum well (MQW) SOA (1013SXS - Thorlabs), a polarization beam splitter (PBS), two polarization controllers (PC_1 and PC_2), a unidirectional EDFA (1550 nm - Tuolima) and a 90/10 optical coupler. The 37.3-m total length of the ring is given by 13-m of EDF and fiber connections within the EDFA and 24.3-m from the PCs and single mode standard fiber (SMF) pigtails.

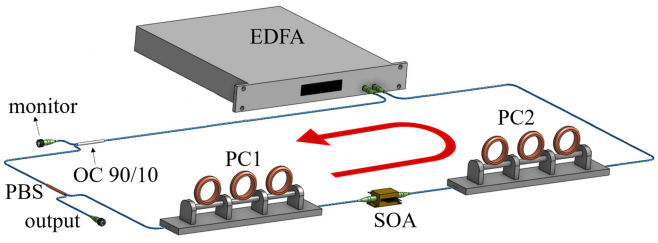

Fig. 1. Passively mode-locked fiber ring laser (PMLFRL). The ring optical cavity with a unidirectional EDFA that determines the direction of propagation (red arrow).

Mode-locking is achieved by injecting a current of approximately 55-mA into the SOA, bringing it to transparency, and properly adjusting the PCs. We used an off-the-shelf EDFA with fixed 26.5-dBm average output power as gain medium. When a high-power optical pulse impinges on the SOA, the pulse's leading edge can deplete the SOA gain and saturate the device, so that a much lower gain is provided for the trailing edge of the pulse. Hence, as the SOA provides polarization-dependent gain, the refractive index saturation will also be polarization dependent so that SOA will act as a nonlinear polarization rotation device [3, 4]. This feature can be used as a pulse compression mechanism by properly adjusting light polarization along the cavity. In this way, the edges of the pulse are filtered by the PBS and removed from the loop. In order to repeat this operation for every roundtrip in the laser cavity, PC_1 should be adjusted so that the same state of polarization enters the SOA after a roundtrip. Due to its nonlinear characteristic, the NPR effect is more pronounced for higher pulse peak-powers. Therefore, the use of the high power EDFA is essential for enhancing the pulse compression since, with higher peak-power, the polarization will change faster within the optical pulse and a shorter portion of it will be aligned to the PBS. The repetition-rate of the train of optical pulses at the output of the laser is determined by the length of the optical fiber cavity.

III. Results and Discussion

assive mode locking results are shown in Fig. 2, where all n urements were performed on the monitor output port of F 1. The optical spectrum of mode-locked pulses, measured w optical spectrum analyzer (OSA) (MS9740A - Anritsu), is sh n in Fig. 2(a). The central wavelength is located at 1 .90-nm and the 3-dB spectral width is 3.74-nm (468- C). Fig. 2 (b) shows the pulse train, where a uniform in sity can be observed. The repetition-rate of the train optical pulses matches measured roundtrip time of 184-ns and the optical fiber ring cavity length of 37.3-m. Fig. 2(c) shows the radio-frequency (RF) spectrum measured with an electrical spectrum analyzer (ESA) (N9344C - Keysight). The 5.43-MHz tone corresponds to the free spectral range (FSR) of the laser ring. The 46-dB signal-noise-to-ratio (SNR) and sharp linewidth (limited to the 10-Hz resolution bandwidth (RBW) of the spectrum analyser) mean low phase noise and jitter on the repetition pulse rate. The pulse duration, measured with a second harmonic optical correlator (5-14-LDA - Inrad) and a photomultiplier, is shown in Fig. 2(d). The full width at half maximum (FWHM) measured is 2.30-ps, corresponding to a squared hyperbolic secant ($sech^2$) fit to the experimental data. Comparison between the pulse duration and spectral width indicate that the optical pulses are Fourier transform limited.

Harmonic mode-locking experimental results are shown in Fig.3. Increasing the SOA bias current and fine tuning the polarization controllers allows the locking of only selected harmonics of the fundamental frequency. Fig. 3(a) shows the pulse repetition rates (blue circles) and output average optical power (red squares) for various SOA injection currents ranging from 65 to 125-mA. The repetition-rate could be adjusted from 363-MHz to 2.521-GHz. When modifying the configuration of the PCs, we adjust the polarization inside the cavity, which in turn changes the gain and the nonlinear phase-shift of the optical pulse as it passes through the SOA [3]. This polarization adjustment also changes the intensity-dependent switching resulting in the variation and increase of the pulse repetition rate [8]. Fig. 3(a) shows that the pulse repetition rate is proportional to the current increase above transparency whereas the output power displays a saturation behavior related to the SOA gain saturation. This means that the pulse energy decreases because the SOA is unable to provide enough energy to fulfill the needs of the increasing pulse rate. The pulse energy decreases as the repetition rate increases, as shown in Fig. 3(b).

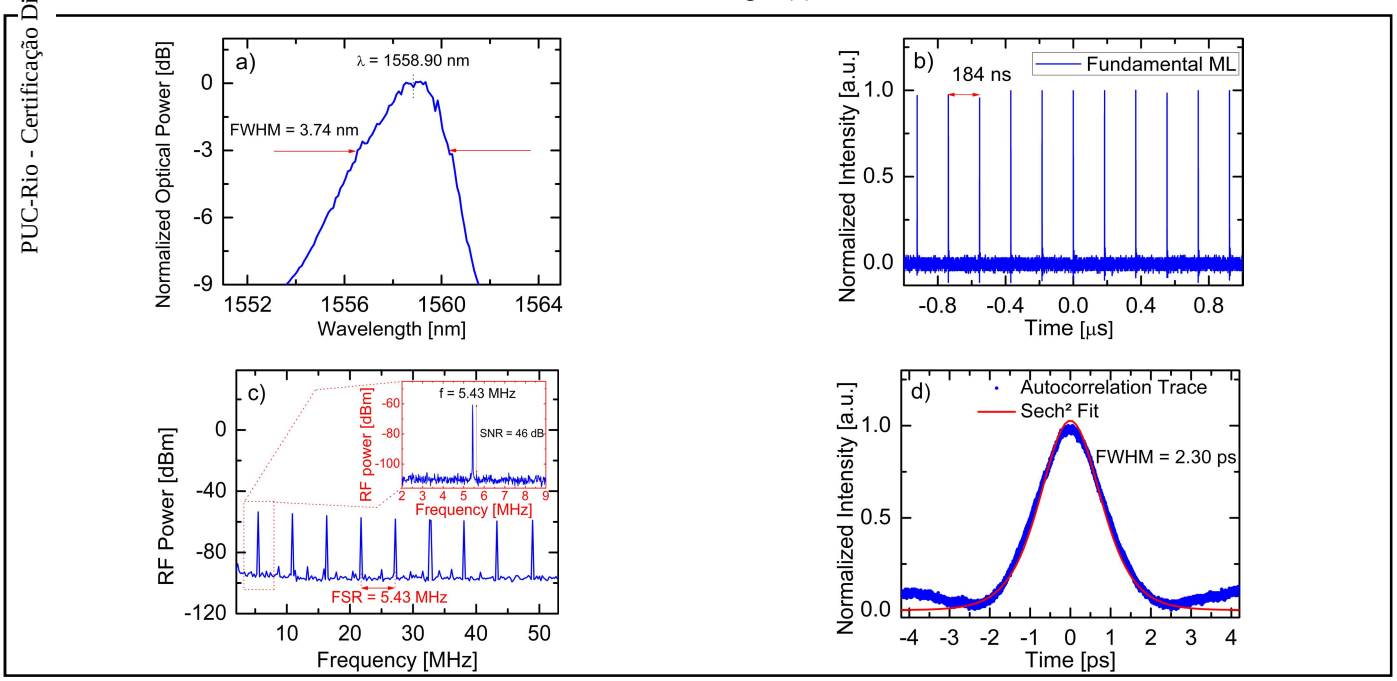

Fig. 2. Fundamental mode-locked experimental results: (**a**) optical spectrum, (**b**) output temporal pulse train, (**c**) frequency comb of fundamental mode-locked pulses (RBW=1 kHz). Inset in (**c**): RF spectrum of 5.43-MHz (fundamental) mode (RBW=10 Hz) (**d**) Autocorrelation trace of mode-locked pulses.

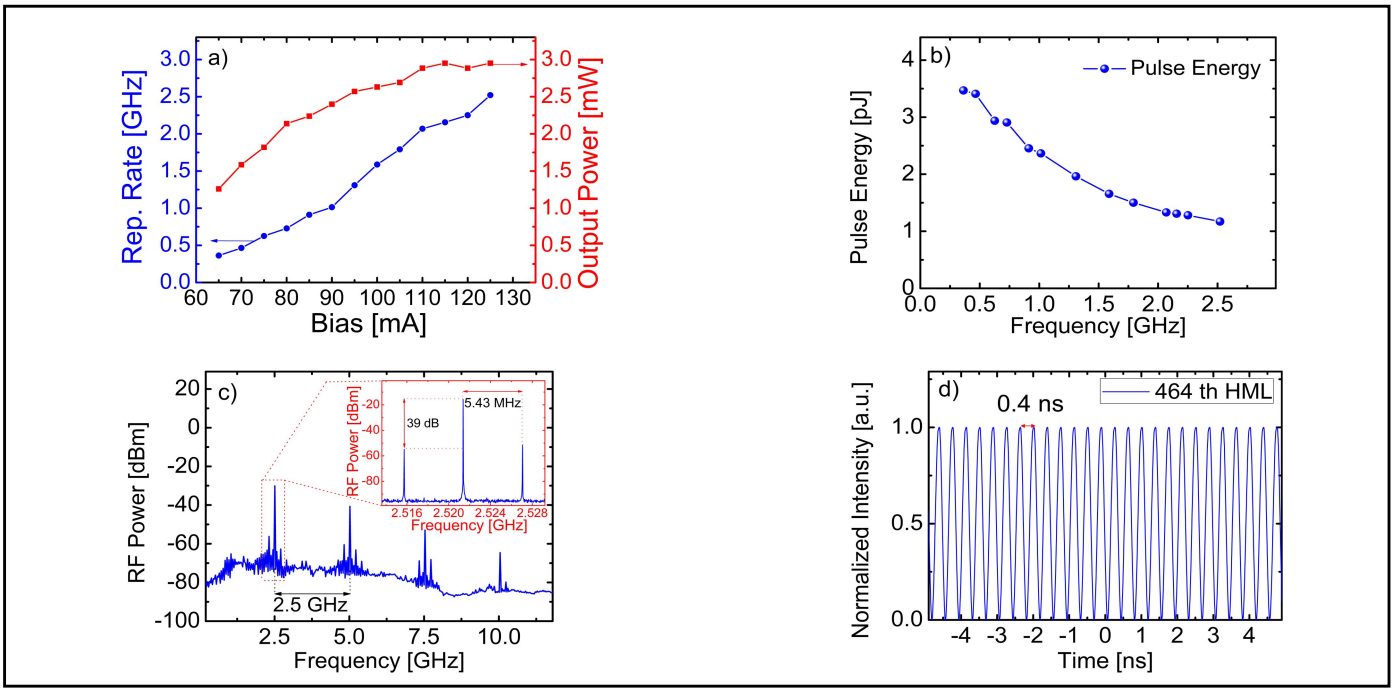

Fig. 3. Harmonic mode-locked experimental results: (**a**) repetition-rates and average output powers of PMLFRL under different SOA injection currents, (**b**) pulse energy, **(c)** frequency comb of HML pulses (RBW=1 MHz). Inset in (**c**): RF spectrum of 2.521-GHz (464th harmonic) mode (RBW=10 Hz), (**d**) output temporal pulse train of 464th HML.

The RF spectrum corresponding to the locking at the 4 harmonic of the fundamental frequency (2.521-GHz) is sh n in Fig. 3(c). It is clear that none but the 464th h onic and its multiples are present, with a suppression ra of 39-dB to the closest fundamental harmonic other th the locked ones. It should be noted that the RF spectrum is nited here by the 5-GHz photodetector (DET08CFC - T labs) bandwidth, while the optical spectrum and pulse w n remains the same as in Fig. 2. The stable pulse train fo his 464th harmonic mode-locking is shown in fig 3(d), n further limited by the 3.5-GHz oscilloscope (DPO7354 - tronix) bandwidth.

n our experiment, the system remained stable for up to o our with the fine tuning of the polarization controllers a the environment temperature control. The optimum p ization settings can drift with temperature and fiber v tion, so that readjustment may sometimes become n ssary. The use of polarization-maintaining fibers (PMF) and the arrangement of the experiment in an isolated chamber for thermal stabilization will significantly increase the stability of the system.

IV. Conclusion

In conclusion, we have investigated a passively mode locked fiber ring laser with 2.30-ps temporal pulse width at 1558.9-nm using a simplified experimental setup based in nonlinear polarization rotation at an SOA device. The pulse repetition rate can be adjusted from 360-MHz to 2.5-GHz by tuning the SOA bias current and the intracavity polarization controllers. The maximum HML repetition-rate obtained in this setup was 2.521-GHz, corresponding to the 464th harmonic of the fundamental mode-locking frequency. To the best of the author's knowledge, this is the highest repetition-rate obtained for this experimental setup. A future suggestion is to replace the off-the-shelf EDFA by variable pump EDFA, allowing better control of the intracavity power and repetition rate of the device. Replacing standard SMF by PMF (Polarization-Maintaining Fiber) will remove PBS and the need of its adjustment, as well as reducing cavity losses and improving the polarization switching performed by the SOA [8]. Therefore, it can be a promising device to be used in optical communications [1] and optical sampling [2].

Acknowledgments

The authors acknowledge the financial support from Brazilian agencies CNPQ (Award 140701/2019-2) and FAPERJ.

References

[1] G. Duan et al., "High performance InP-based quantum dash semiconductor mode-locked lasers for optical communications," in Bell Labs Technical Journal, vol. 14, no. 3, pp. 63-84, Fall (2009).

[2] Tetsuya Kanada and Douglas L. Franzen, "Optical waveform measurement by optical sampling with a mode-locked laser diode," Opt. Lett. 11, 4-6 (1986).

[3] X. Yang, Z. Li, E. Tangdiongga, D. Lenstra, G. D. Khoe, and H. J. S. Dorren, "Sub-picosecond pulse generation employing an SOA-based nonlinear polarization switch in a ring cavity," Opt. Express 12, 2448-2453 (2004).

[4] Liu, Tonghui & Jia, Dongfang & Yang, Jingwen & Chen, Jiong & Wang, Zhaoying & Yang, Tianxin, "An ultra-long cavity passively mode-locked fiber laser based on nonlinear polarization rotation in a semiconductor optical amplifier," Laser Physics. 23. 095005. 10.1088/1054-660X/23/9/095005 (2013).

[5] U. Keller et al., "Semiconductor saturable absorber mirrors (SESAM's) for femtosecond to nanosecond pulse generation in solid-state lasers," IEEE J. Sel. Topics Quantum Electron., vol. 2, no. 3, pp. 435–453, Sep. (1996).

[6] J. Xu et al., "All-Polarization-Maintaining Femtosecond Fiber Lasers Using Graphene Oxide Saturable Absorber," in IEEE Photonics Technology Letters, vol. 26, no. 4, pp. 346-348, Feb.15, (2014).

[7] Li, L., Lv, R., Chen, Z. et al. Mode-Locked Er-Doped Fiber Laser by Using MoS2/SiO2 Saturable Absorber. Nanoscale Res Lett 14, 59 (2019).

[8] Hou-Ren Chen, Kuei-Huei Li n, Chih-Ya Tsai, Hsiao-Hua Wu, Chih-Hsuan Wu, Chieh-Han Chen, Yu-Chieh Chi, Gong-Ru Lin, and Wen-Feng Hsieh, "12 GHz passive harmonic mode-locking in a 1.06 μm semiconductor optical amplifier-based fiber laser with figure-eight cavity configuration," Opt. Lett. 38, 845-847 (2013).

[9] A. B. Grudinin, D. J. Richardson, and D. N. Payne, “Passive harmonic mode-locking of fibre soliton ring lasers”, Electronics Letters, 29, 1860, (1993).

[10] S. Zhou, D. G. Ouzounov, and F. W. Wise, “Passive harmonic mode-locking of a soliton Yb fiber laser at repetition rates to 1.5 GHz”, Opt. Lett. 31, 1041 (2006).

Annex D

The paper “Vibration Sensing with a Hybrid Electronically Addressable Random Laser” was published in the Conference on Lasers and Electro-Optics (CLEO) in 2022.

Vibration Sensing with a Hybrid Electronically Addressable Random Laser

Marlon M. Correia[1], Walter Margulis[1], Anderson S. L. Gomes[2] and Jean Pierre von der Weid[1]
[1]*Center for Telecommunications Studies*
Pontifical Catholic University of Rio de Janeiro, Rio de Janeiro, Brazil
[2]*Physics Department*
Federal University of Pernambuco, Recife, Brazil
marloncorreia@opto.cetuc.puc-rio.br

Abstract: The operation of a Hybrid Electronic Addressable Random laser is analyzed. The laser operates as a ϕ-OTDR distributed vibration sensor in a transform-limited mode-locked regime with 41 MHz FWHM bandwidth and <7-kHz mode linewidth.

1. Introduction

Fiber random lasers generally employ the Rayleigh scattered light from an optical fiber as feedback mechanism. In some cases, the gain medium is distributed over the feedback fiber [1, 2] or separated from it as a pumped Erbium-doped fiber (EDF) [3]. Random narrow linewidth modes were reported in a semiconductor optical amplifier (SOA) based random fiber laser with Rayleigh scattering feedback from an 8-km fiber [4]. A hybrid electronically addressable random laser (HEAR) was recently presented [5], where a pulsed SOA in a loop mirror and the Rayleigh scattering from a pumped erbium doped fiber (EDF) formed a random cavity. The proposed feedback mechanism was Rayleigh scattering from the EDF section addressed by the SOA pulse whose frequency is in resonance with the cavity roundtrip time. Here, we show that the HEAR laser operates in a mode-locked regime generating transform-limited pulses, and that it can be used as a phase-OTDR distributed vibration sensor.

2. Experimental Setup

The schematic of the HEAR fiber laser is shown in Fig. 1, in a hybrid configuration with a SOA and EDF as gain media. The random laser cavity is defined by the Rayleigh backscattering from a 27-m EDF and unidirectional fibre amplifying loop mirror containing a SOA, an isolator and a 125-m passive standard single mode fiber (SMF). The fiber loop acts as an amplifying mirror while the EDF provides gain and distributed feedback. Isolator-2 ensures that undesired reflections are eliminated. The SOA was used for modulation, biased at 50 mA, blocking light circulating in the cavity except when driven by 300 mA square current pulses (12 ns, 15 V @50Ω). Laser pulses were obtained by synchronizing the SOA driver to the returning amplified Rayleigh backscattered light from a selected short section of the EDF, CW-pumped by a 980 nm laser diode. By tuning the SOA pulse rate, random lasing was achieved from selected 2.4-m sections of the ~27-m EDF [5]. A piezoelectric element was attached to the EDF and driven at 5 kHz, vibrating the fiber at this frequency. Measurements were performed on an optical spectrum analyzer (OSA), oscilloscope (OSC), lock-in amplifier and electrical spectrum analyzer (ESA).

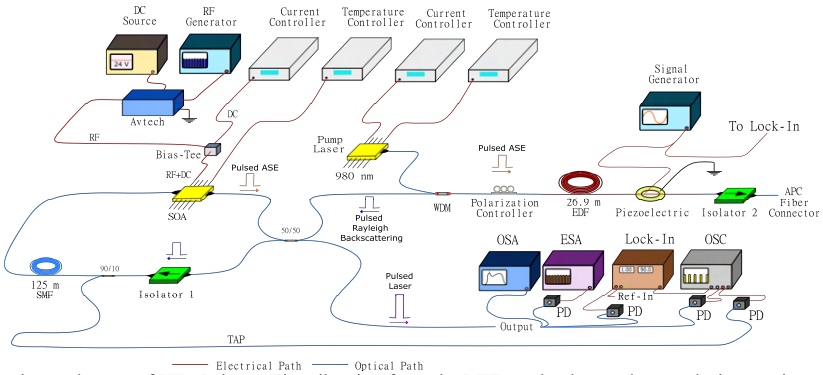

Fig. 1. Experimental setup of HEAR laser. The vibration from the PZT can be detected at any lasing section of the EDF.

3. Results and Discussion

A careful evaluation of all losses in the cavity was carried out to estimate the lasing gain threshold for the 12 ns pulses. The single pass loop connection losses added to 1.5 dB including 90/10 coupler, whereas the double

pass connections to the EDF were 2x3.6 dB, including 50/50 coupler. The roundtrip loss at the SM-EDF splice was measured to be 4.3 dB. Fig 2a shows the HEAR laser threshold at 205 mW pump power, corresponding to a 51.2-dB double pass gain in the EDF and 15.8-dB (@350 mA) gain in the SOA. Considering the 13 dB roundtrip losses, and the –56.2-dB mean Rayleigh reflectivity of the EDF (2.4-m sections), a random 2.2-dB reflectivity peak above the mean of the addressed section is enough to fulfill the lasing gain threshold condition when this addressed section is at the end of the EDF [4]. Figure 2b displays the optical spectrum of the HEAR laser just below and well above threshold, where the laser peak power stands 22 dB above the EDF ASE.

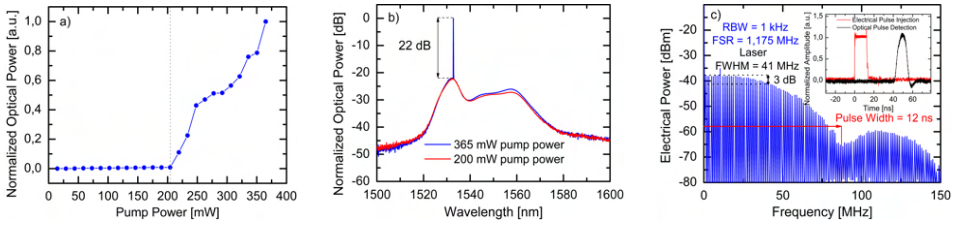

Fig. 2. a) Transfer function of the HEAR laser; b) OSA spectrum of the HEAR laser. c) ESA spectrum of the HEAR laser.

The fine spectral features of the laser were characterized with an ESA and an unbalanced Mach-Zehnder Interferometer (MZI) with 12.5 km delay between arms in a self-homodyne arrangement. Fig. 2c displays the detected signal after the unbalanced MZI for a detuned frequency. Pulses arrive at the detector from each arm without overlap. The series of tones repeating at 1.175 MHz interval is the result of the periodic gating of the HEAR laser. The 3 dB laser linewidth is 41 MHz, which gives a time-bandwidth product 0.49, similar to the value 0.44 expected for Gaussian transformed limited pulses. This is noteworthy because the random laser here lacks spectral filtering elements. Pulses overlap when fine tuning the repetition rate to 1.175230 MHz. The mode linewidth ranges from 6.9 to 4.4 kHz as the pump power increases. This sharp linewidth corresponds to a coherence time much larger than the pulse duration due to the active mode-locking regime in which the HEAR laser operates.

Because of the high coherence, the laser output is very sensitive to the phase within the addressed section and the output shows large intensity variations as the SOA gating frequency is swept. Fig. 3a shows the output power along the ~13.5-m addressable part of the EDF (at the very beginning the gain is not enough for lasing), showing the strong spatial fluctuations characteristic of a ϕ-OTDR. Modulating the phase with the PZT attached to the EDF and synchronously detecting the received signal with a Lock-in Amplifier eliminates all static intensity fluctuations, leaving only those corresponding to the 1.2-m section where the PZT is placed, as shown in Fig. 3b. Because the phase change varies linearly with the applied voltage, there is a linear dependence on the signal amplitude as in Fig. 3c, clearly proving that the HEAR laser can be used as an addressable vibration sensor.

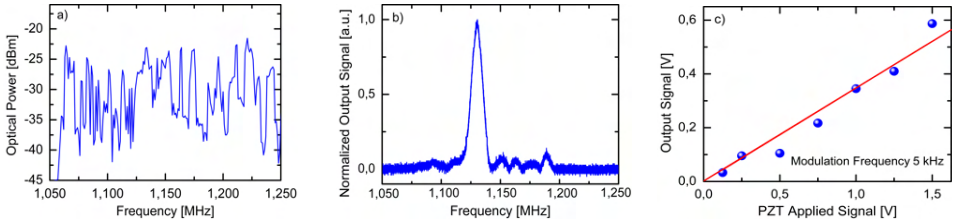

Fig. 3. a) Output power along the addressable part of the EDF; b) detection trace for vibrational wave; c) detection sensitivity for different intensities vibration at 5 kHz.

Hybrid Electronically Addressable Random Feedback Fiber Laser results were presented. The laser operates in active mode-locking regime with transform-limited pulses and high coherence given by the 4.4 kHz mode linewidth at full power. The HEAR laser output is phase sensitive in the addressed section, and its use as an acoustic vibration sensor is demonstrated.

5. References

[1] Sergei K. Turitsyn et al., “Random distributed feedback fibre laser,” Nature Photonics 4, 231-235 (2010).
[2] M. Pang et al, “Frequency stabilized coherent Brillouin random fiber laser: theory and experiments,” Opt. Express 21, 27155–27168 (2013).
[3] G. Yin et al, “Tunable Er-doped fiber ring laser with single longitudinal mode operation based on Rayleigh backscattering in single mode fiber,” Opt. Express 19(27), 25981–25989 (2011).
[4] Pedro Tovar et al, "Longitudinal mode dynamics in SOA-based random feedback fiber lasers," Opt. Express 27, 31001-31012 (2019).
[5] Walter Margulis et al, "Hybrid electronically addressable random fiber laser," Opt. Express 28, 23388-23396 (2020).

Annex E

The paper “Distributed vibration sensor with a lasing phase-sensitive OTDR” was published in the Optics Express in 2022.

Research Article | Vol. 30, No. 22 / 24 Oct 2022 / Optics Express 40243

Optics EXPRESS

Distributed vibration sensor with a lasing phase-sensitive OTDR

MARLON M. CORREIA,[1,*] WALTER MARGULIS,[1] ANDERSON S. L. GOMES,[2] AND JEAN PIERRE VON DER WEID[1]

[1]Center for Telecommunication Studies, Pontifical Catholic University of Rio de Janeiro, Rio de Janeiro, 22451-900, RJ, Brazil
[2]Departamento de Física, Universidade Federal de Pernambuco, Recife, 50670-901, PE, Brazil
[*]marloncorreia@opto.cetuc.puc-rio.br

Abstract: The authors experimentally demonstrate the operation of a lasing phase-sensitive optical time-domain reflectometer (Φ-OTDR) based on random feedback from a sensing fiber. Here, the full output of the laser provides the sensing signal, in contrast to the small backscattered signal measured in a conventional OTDR. In this proof-of-principle demonstration, the laser operates as a distributed vibration sensor with signal-to-noise ratio of 23-dB and 1.37-m spatial resolution.

1. Introduction

Rayleigh scattering is widely exploited in distributed sensing with optical fibers in the time domain [1–4]. A weak backscattered signal is generated from the propagation of a short duration pulse along the fiber. It gives an indication of the intensity of the pulse at every fiber position, the pulse duration limiting the spatial resolution of the measurement. In Optical Time Domain Reflectometry (OTDR), the intensity-drop along the fiber and the echoes generated at discontinuities such as components, connectors and splices allow monitoring a fiber link for losses [5]. Distributed sensors based on the scattering of a *coherent* pulse [6] are capable of identifying disturbances such as vibrations [6,7], perimeter intrusion [8,9] and seismic events [10,11]. Such disturbances affect locally the relative phases of the backscattered light from different points within the pulse, and consequently their interference. Phase-OTDR systems are widely used as distributed acoustic sensors [7–19].

The backscattered light in a standard telecom fiber is very weak. Nevertheless, under strong optical amplification, Rayleigh backscattering has been used as the feedback needed for laser action [20–22]. A fiber laser based on the feedback from randomly distributed scattering centers has ill-defined modes and is generally described as a random fiber laser [20–22]. Random lasers based on Raman [23,24], Brillouin [25,26] and Rayleigh scattering in fibers [20–22] have been reported. They often incorporate amplifiers such as Erbium-doped fibers (EDFs), semiconductor optical amplifiers (SOAs) or both, to provide or complement the necessary gain needed for laser action [20–22,27–31].

The use of the distributed sensor fiber as part of a laser cavity has recently been demonstrated for Raman [32] and Brillouin [33] sensor systems. Since the sensor fiber is used in a reflection mode, i.e, operating as an open-ended fiber mirror, all instrumentation can be gathered on one side of the set-up and the sensor fiber deployed where needed. To the best of our knowledge, the operation of a phase-OTDR in a lasing mode has not been studied, where the backscattered light is not simply detected, but is recirculated in a laser cavity with synchronous amplification. A lasing distributed fiber sensor based on Rayleigh scattering has some interesting physics and it could be advantageous because of the potential improvement in signal-to-noise ratio (SNR) that could be expected from a strong laser output, when compared with the conventional configuration. In this letter, we describe the implementation of a lasing phase-OTDR based on Rayleigh scattering.

#476182 https://doi.org/10.1364/OE.476182
Journal © 2022 Received 23 Sep 2022; revised 5 Oct 2022; accepted 6 Oct 2022; published 14 Oct 2022

Optics EXPRESS

Short pulse amplification takes place by gating a SOA in synchronism with the return of the backscattered light from a particular chosen section of the fiber being probed. We show that the linewidth of the laser self-narrows, allowing for sensor operation as a Φ-OTDR without the injection of a high-coherence laser source. In this proof-of-principle demonstration, we illustrate the use of the laser as a distributed vibration sensor with good SNR.

2. Experimental setup

The schematic of the lasing Φ-OTDR is shown in Fig. 1, in a hybrid configuration with a SOA and EDF as gain media [27]. The random optical feedback is produced by the Rayleigh backscattering from a 63-m piece of dispersion shifted fiber (DSF). Short pulses are generated by an unidirectional amplifying loop mirror containing a SOA, an isolator (Iso-1) and a 125-m spool of passive standard single mode fiber (SMF). Additional two-way optical amplification between the fiber loop and the distributed feedback sensing fiber is provided for by a piece of Erbium-doped fiber (EDF). The fiber loop acts as a time-gated amplifying mirror, the EDF provides two-way continuous wave (CW) gain and the DSF provides distributed feedback. The EDF is CW-pumped by a 980-nm laser diode. Isolator-2 ensures that undesired reflections after the sensing fiber are eliminated. The SOA was used for modulation, blocking light circulating in the cavity except when driven by 300-mA square current pulses (13-ns, 15-V @50Ω). Laser pulses were obtained by synchronizing the SOA current driver to the returning amplified Rayleigh backscattered light from a selected short section of the DSF. By tuning the SOA pulse rate in the range 1.050-MHz to 0.650-MHz, random feedback lasing was achieved from selected 2.6-m sections of the 63-m DSF. Adjustment of the repetition rate of the current pulses allows choosing the roundtrip time of the cavity and addressing any particular section of the fiber for optical feedback [27]. For the sensing proof-of-principle demonstration, a piezoelectric (PZT) element

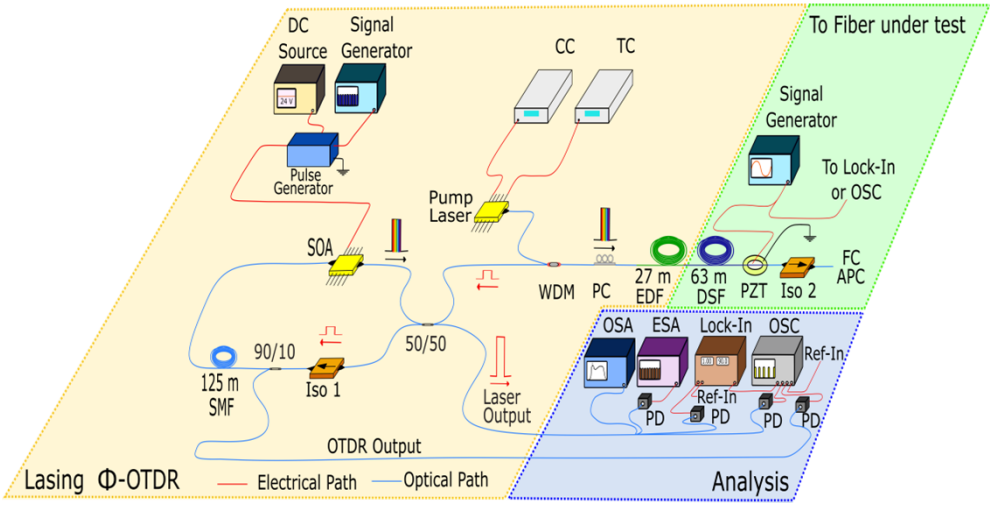

Fig. 1. Experimental setup of the lasing Φ-OTDR. The vibration from the PZT can be detected at any lasing section of the DSF. DC: Direct Current; CC: Current Controller; TC: Temperature Controller; SOA: Semiconductor Optical Amplifier; ISO: Isolator; SMF: Single Mode Fiber; OTDR: Optical Time-Domain Reflectometry; WDM; Wavelength Division Multiplex; PC: Polarization Controller; EDF: Erbium Doped Fiber; DSF: Dispersion Shifted Fiber; PZT: Piezoelectric; FC/APC: Angled Physical Contact Fiber Connector; OSA: Optical Spectrum Analyzer; ESA: Electrical Spectrum Analyzer; Lock-In: Lock-In Amplifier; OSC: Oscilloscope; PD: Photodiode Detector; Ref-In: Reference-In.

Optics EXPRESS

was attached to the DSF and driven at 5-kHz, imposing a vibration to the fiber at this frequency. Measurements were performed on an optical spectrum analyzer (OSA), oscilloscope (OSC), lock-in amplifier and electrical spectrum analyzer (ESA).

3. Results and discussion

Lasing Φ-OTDR threshold is achieved at a pump power ~205-mW into the EDF and properly adjusting the polarization controller (PC). The experimental results are shown in Fig. 2, where all measurements were performed on the laser output port of Fig. 1. The temporal behavior of the output is measured with the 125-MHz bandwidth photodiode detector (PD) and 3.5-GHz bandwidth oscilloscope (OSC). Figure 2(a) shows the temporal pulse train, where a uniform intensity can be observed. The repetition-rate of the train optical pulses is generated by the direct modulation of the SOA and matches a measured roundtrip time of 1.43-μs from a selected short section at the end of the DSF. Figure 2(b) shows a 13-ns duration square current pulse applied to the SOA and a 13-ns duration optical pulse detected, showed in Fig. 2(a). The electrical spectrum is measured with 125-MHz bandwidth photodiode and a 20-GHz bandwidth electrical spectrum analyzer (ESA). Figure 2(c) shows a series of tones repeating at 0.7-MHz interval, which are the result of the periodic gating of the lasing Φ-OTDR. The interval of the frequency-comb presented corresponds to the free spectral range (FSR) of the laser and matches the characteristic roundtrip time of the pulses shown in Fig. 2(a). The output optical spectra were analyzed with a 0.03-nm resolution optical spectrum analyzer (OSA). Figure 2(d) displays the optical spectra emitted by the laser just below (200 mW pump power) and well above threshold (365 mW pump power). In the latter case, the laser peak power stands 23-dB above the EDF amplified spontaneous emission (ASE) and the narrow lasing peak is measured at wavelength ~1557-nm.

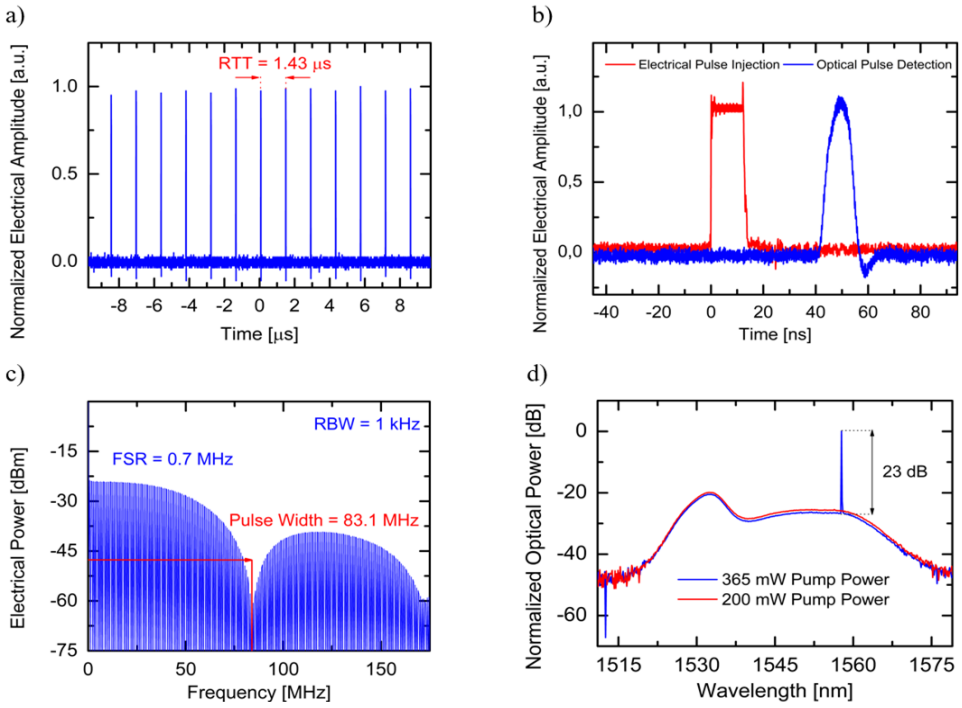

Fig. 2. Lasing Φ-OTDR experimental results: Laser output OSC temporal pulse train (a). Temporal square electrical pulse injection and optical pulse detection (b). Laser output ESA spectrum (c). Laser output OSA spectrum (d).

Optics EXPRESS

In order to characterize the system's operation parameters, OTDR profiles of different addressed section of the fiber were measured via the OTDR port in the loop. Figure 3 shows four OTDR profiles selecting different addressed sections of DSF. These sections are selected according to the repetition-rate of the direct modulation pulses in the SOA. The four examples illustrated in Fig. 3 clearly show the difference between regimes of ASE below threshold (205-mW pump power, top trace) and lasing Φ-OTDR above threshold (365-mW pump power, three bottom traces) for different addressed fiber sections. The smooth top trace of a conventional OTDR develops into a spiky speckle-like trace characteristic of the Φ-OTDR regime when the laser is above threshold (also seen in the zoomed-in Fig. 4(a)). This happens without the use of a narrow linewidth injection source, evidencing the strong spectral self-narrowing experienced by the laser above threshold. In contrast to the experiments reported in [27], here the source of Rayleigh backscattering is a passive fiber, not a rare-earth doped fiber. This excludes the possibility of a standing wave index-grating forming from unpumped ions [34–36]. The several peaks around the lasing peak arise from Φ-OTDR and appear due to the varying coherent superposition of Rayleigh backscattered light. As shown in Fig. 3, the single-ended passive dispersion compensating fiber can be used both to provide feedback for laser action and to perform distributed sensing at various locations. Hence, the laser can be directly used as a fast distributed sensor within the addressed section of the DSF, the laser intensity being interferometrically sensitive to external effects on the fiber, such as vibration or stress/strain, with the resolution given by half the modulation pulse-width as in a conventional Φ-OTDR. One advantage of the present set-up is that instead of a tiny, backscattered signal measurement, as is conventional in an OTDR, here it is the full output of the laser that provides the sensing signal. Hence, no averaging is needed, and a fast response is available.

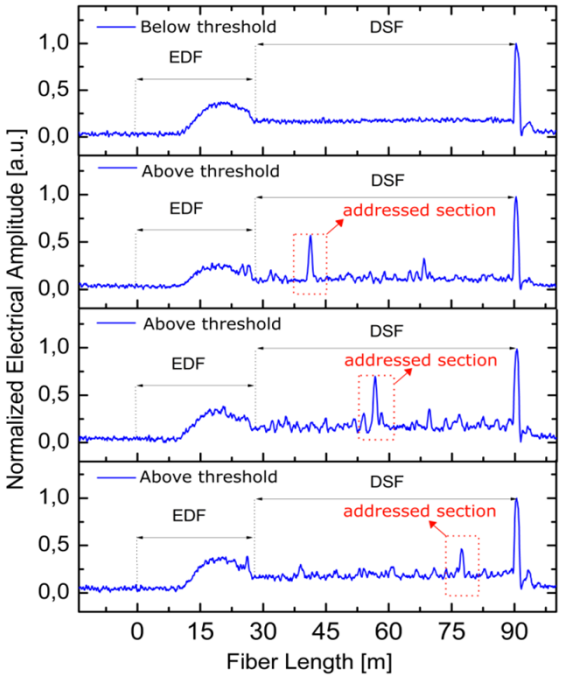

Fig. 3. Lasing Φ-OTDR at different addressed section.

Prior to measuring vibrations, in order to characterize the PZT operation parameters, the PZT was placed on an arm of a balanced fiber Mach-Zehnder interferometer (MZI) to produce frequency discrimination. The modulation frequency applied to the PZT was varied while

Optics EXPRESS

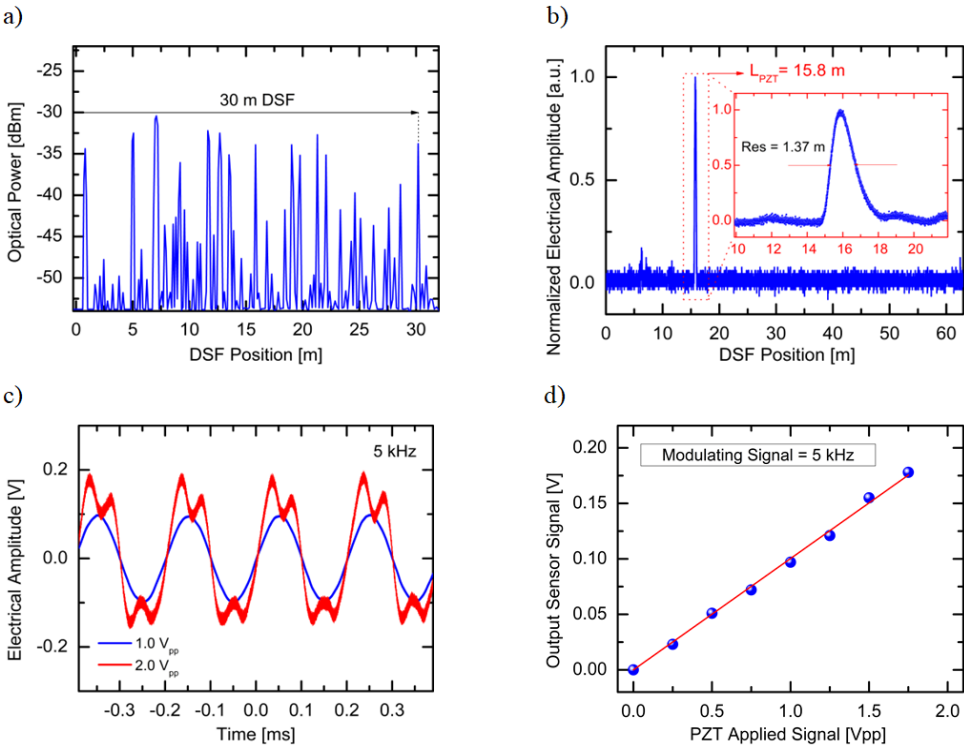

Fig. 4. Lasing Φ-OTDR performance: Output optical power along a ~30 m section of the DSF (a). Detection trace for vibrational wave along the full DSF (b). Inset in (b): Lasing Φ-OTDR resolution. Sensor signal at 5-kHz (c). Detection sensitivity for different vibration intensities at 5-kHz (d).

maintaining a constant drive voltage. The PZT showed resonance effects at 5-kHz. Now, with the constant resonant frequency at 5-kHz to maximize the phase change, the voltage applied to the PZT was varied. The PZT presented low harmonic distortion up to a maximum applied voltage of 1.8-V_{pp}.

Because of the high coherence as in a conventional Φ-OTDR, the laser output is very sensitive to the phase within the addressed section and the output port shows large intensity variations as the SOA gating frequency is swept. Figure 4(a) shows the laser output power variation as the addressed section was displaced along a ~30-m section within the DSF, showing the strong spatial fluctuations characteristic of a Φ-OTDR [11–16]. A 10-sec frequency sweep (1.050-MHz to 0.650-MHz) was carried out, so that the entire length of the DSF section was addressed while modulating the phase with the PZT attached to the DSF. Synchronous detection of the received signal was performed with a Lock-in amplifier, where static intensity fluctuations were eliminated. Only those fluctuations at 5-kHz were measured, and they appear with 1.37-m spatial resolution where the PZT is positioned on the DSF, at 15.8-m, as shown in Fig. 4(b) upon a sweep over the full DSF length. Hence, the phase signals can be used for directly measuring the external vibration on fiber.

The vibration frequency at 5-kHz with 1-V_{pp} applied to the PZT is measured, for investigating the system performance. Although solid-state based phase-modulating schemes may allow for testing a broader range of frequencies [37,38], the reflections may hinder their use here, and the PZT modulator is chosen. In the experiments, sinusoidal vibration signals are generated, and laser output detection is performed with a 10-MHz bandwidth photodiode with band-pass

Optics EXPRESS

filtering in the range 1-10 kHz. Figure 4(c) shows the detection of the sensor signal with 1-V_{pp} applied (blue trace) and 2-V_{pp} applied (red trace). In the latter case, the phase modulation exceeds π-rad (red trace). Figure 4(d) shows the amplitude of the sensor signal measured for low voltages applied. In this regime the transfer function of the sensor has a linear phase dependence on the applied voltage, indicates that the lasing Φ-OTDR can be used as an addressable vibration sensor. Indeed, the phase disturbance introduced by the vibration on the backscattered intensity affects the sum of the optical fields of the two half sections encompassing the disturbance, hence the sinusoidal transfer function and linear dependence at low amplitudes.

4. Conclusions

In conclusion, a phase-OTDR system is demonstrated that operates above threshold as a fiber laser. Here, Rayleigh backscattered light in the sensing fiber is fed back into the optical amplifier(s), instead of the light reflected by a laser's output mirror. It is found that it is possible to use a passive fiber to provide for the random distributed feedback mechanism needed to achieve laser action. Since passive fibers have very low loss compared with the Er-doped fibers used previously, this finding opens the way to address and interrogate much longer sensing fibers than demonstrated previously [27]. It was also found in this work that strong spectral self-narrowing takes place when the laser operates above threshold, and the system shifts from OTDR sensing to a Φ-OTDR mode of operation. The narrow linewidth of the laser regime is uncharacteristic of conventional random lasers, which are often associated with broadband emission and lack of speckle and self-interference [39]. Here, the laser output is phase-sensitive in the addressed section, and its use as a distributed vibration sensor is demonstrated. The experimental results show good signal-to-noise ratio. The sensor can measure the frequency and amplitude of perturbations along 63-m of the sensing fiber with a spatial resolution of 1.37-m. Based on these specifications, the proposed sensor should be able to quantify and track multiple small objects moving along the fiber.

Funding. Conselho Nacional de Desenvolvimento Científico e Tecnológico (306332/2019-1, 140701/2019-2); Office of Naval Research Global (N62909-20-1-2033); INCT Fotônica (465.763/2014-6); Fundação Carlos Chagas Filho de Amparo à Pesquisa do Estado do Rio de Janeiro (E26/201.200/2021).

Acknowledgments. M. M. Correia thanks Center for Telecommunications Studies (CETUC) for making the resources available to carry out the research project; W. Margulis thanks the Research Institutes of Sweden RISE for the early stages of this work.

Disclosures. The authors declare no conflicts of interest.

Data availability. Data underlying the results presented in this paper are not publicly available at this time but may be obtained from the authors upon reasonable request.

References

1. S. V. Shatalin, V. N. Treschikov, and A. J. Rogers, "Interferometric optical time-domain reflectometry for distributed optical-fiber sensing," Appl. Opt. **37**(24), 5600–5604 (1998).
2. R. Juškaitis, A. M. Mamedov, V. T. Potapov, and S. V. Shatalin, "Interferometry with Rayleigh backscattering in a single-mode optical fiber," Opt. Lett. **19**(3), 225–227 (1994).
3. V. V. Spirin, "Transmission-reflection analysis for localization of temporally successive multipoint perturbations in a distributed fiber-optic loss sensor based on Rayleigh backscattering," Appl. Opt. **42**(7), 1175–1181 (2003).
4. L. Thévenaz, "Review and Progress in Distributed Fiber Sensing," in *Optical Fiber Sensors (OFS) 2006, OSA Technical Digest* (Optica Publishing Group, 2006), paper ThC1.
5. M. Barnoski, M. Rourke, S. Jensen, and R. Melville, "Optical time domain reflectometer," Appl. Opt. **16**(9), 2375–2379 (1977).
6. Y. Koyamada, M. Imahama, K. Kubota, and K. Hogari, "Fiber-Optic Distributed Strain and Temperature Sensing With Very High Measurand Resolution Over Long Range Using Coherent OTDR," J. Lightwave Technol. **27**(9), 1142–1146 (2009).
7. Y. Lu, T. Zhu, L. Chen, and X. Bao, "Distributed Vibration Sensor Based on Coherent Detection of Phase-OTDR," J. Lightwave Technol. **28**(22), 3243–3249 (2010).
8. J. C. Juarez, E. W. Maier, K. N. Choi, and H. F. Taylor, "Distributed Fiber-Optic Intrusion Sensor System," J. Lightwave Technol. **23**(6), 2081–2087 (2005).

Optics EXPRESS

9. J. C. Juarez and H. F. Taylor, "Polarization discrimination in a phase-sensitive optical time-domain reflectometer intrusion-sensor system," Opt. Lett. **30**(24), 3284–3286 (2005).
10. E. F. Williams, M. R. Fernández-Ruiz, R. Magalhaes, R. Vanthillo, Z. Zhan, M. González-Herráez, and H. F. Martins, "Distributed sensing of microseisms and teleseisms with submarine dark fibers," Nat. Commun. **10**(1), 5778 (2019).
11. H. F. Martins, M. R. Fernández-Ruiz, L. Costa, E. Williams, Z. Zhan, S. Martin-Lopez, and M. Gonzalez-Herraez, "Monitoring of remote seismic events in metropolitan area fibers using distributed acoustic sensing (DAS) and spatiotemporal signal processing," in *Optical Fiber Communication Conference (OFC) 2019, OSA Technical Digest* (Optica Publishing Group, 2019), paper M2J.1.
12. T. Liu, H. Li, F. Ai, J. Wang, C. Fan, Y. Luo, Z. Yan, D. Liu, and Q. Sun, "Ultra-high Resolution Distributed Strain Sensing based on Phase-OTDR," in *Optical Fiber Communication Conference (OFC) 2019, OSA Technical Digest* (Optica Publishing Group, 2019), paper Th2A.16.
13. Z. Romain, X. Liu, Y. Wang, J. Zhang, Y. Wang, and B. Jin, ", "Recent Progress in the Performance Enhancement of Phase-Sensitive OTDR Vibration Sensing Systems"," Sensors **19**(7), 1709 (2019).
14. X. Fan, G. Yang, S. Wang, Q. Liu, and Z. He, "Distributed Fiber-Optic Vibration Sensing Based on Phase Extraction From Optical Reflectometry," J. Lightwave Technol. **35**(16), 3281–3288 (2017).
15. Z. Qin, T. Zhu, L. Chen, and X. Bao, "High Sensitivity Distributed Vibration Sensor Based on Polarization-Maintaining Configurations of Phase-OTDR," IEEE Photonics Technol. Lett. **23**(15), 1091–1093 (2011).
16. Y. Muanenda, C. J. Oton, S. Faralli, T. Nannipieri, A. Signorini, and F. D. Pasquale, "Hybrid distributed acoustic and temperature sensor using a commercial off-the-shelf DFB laser and direct detection," Opt. Lett. **41**(3), 587–590 (2016).
17. Z. He and Q. Liu, "Optical Fiber Distributed Acoustic Sensors: A Review," J. Lightwave Technol. **39**(12), 3671–3686 (2021).
18. J. Tejedor, H. F. Martins, D. Piote, J. Macias-Guarasa, J. Pastor-Graells, S. Martin-Lopez, P. C. Guillén, F. De Smet, W. Postvoll, and M. González-Herráez, "Toward Prevention of Pipeline Integrity Threats Using a Smart Fiber-Optic Surveillance System," J. Lightwave Technol. **34**(19), 4445–4453 (2016).
19. M. Soriano-Amat, H. F. Martins, V. Durán, L. Costa, S. Martin-Lopez, M. Gonzalez-Herraez, and M. R. Fernández-Ruiz, "Time-expanded phase-sensitive optical time-domain reflectometry," Light: Sci. Appl. **10**(1), 51 (2021).
20. P. Tovar, G. Temporão, and J. P. von der Weid, "Longitudinal mode dynamics in SOA-based random feedback fiber lasers," Opt. Express **27**(21), 31001–31012 (2019).
21. T. Zhu, X. Bao, and L. Chen, "A Single Longitudinal-Mode Tunable Fiber Ring Laser Based on Stimulated Rayleigh Scattering in a Nonuniform Optical Fiber," J. Lightwave Technol. **29**(12), 1802–1807 (2011).
22. G. Yin, B. Saxena, and X. Bao, "Tunable Er-doped fiber ring laser with single longitudinal mode operation based on Rayleigh backscattering in single mode fiber," Opt. Express **19**(27), 25981–25989 (2011).
23. S. K. Turitsyn, S. A. Babin, A. E. El-Taher, P. Harper, D. V. Churkin, S. I. Kablukov, J. D. Ania-Castañón, V. Karalekas, and E. V. Podivilov, "Random distributed feedback fibre laser," Nat. Photonics **4**(4), 231–235 (2010).
24. S. A. Babin, A. E. El-Taher, P. Harper, E. V. Podivilov, and S. K. Turitsyn, "Tunable random fiber laser," Phys. Rev. A **84**(2), 021805 (2011).
25. M. Pang, X. Bao, L. Chen, Z. Qin, Y. Lu, and P. Lu, "Frequency stabilized coherent Brillouin random fiber laser: theory and experiments," Opt. Express **21**(22), 27155–27168 (2013).
26. L. Zhang, Y. Xu, S. Gao, B. Saxena, L. Chen, and X. Bao, "Multi-wavelength Coherent Brillouin Random Fiber Laser with High Optical Signal-to-Noise Ratio," in *Conference on Lasers and Electro-Optics (CLEO) 2017, OSA Technical Digest (online)* (Optica Publishing Group, 2017), paper SM2L.6.
27. W. Margulis, A. Das, J. P. von der Weid, and A. S. L. Gomes, "Hybrid electronically addressable random fiber laser," Opt. Express **28**(16), 23388–23396 (2020).
28. C. J. S. de Matos, L. D. S. Menezes, A. M. Brito-Silva, M. A. M. Gamez, A. S. L. Gomes, and C. B. de Araújo, "Random fiber laser," Phys. Rev. Lett. **99**(15), 153903 (2007).
29. C. Hong, S. Gao, M. Zhang, J. Zhang, L. Qiao, T. Wang, F. Gao, X. Hu, S. Li, and Y. Zhu, "Advances in Random Fiber Lasers and Their Sensing Application," Sensors **20**(21), 6122 (2020).
30. I. R. R. González, B. C. Lima, P. I. R. Pincheira, A. A. Brum, A. M. S. Macêdo, G. L. Vasconcelos, L. de S. Menezes, E. P. Raposo, A. S. L. Gomes, and R. Kashyap, "Turbulence hierarchy in a random fibre laser," Nat. Commun. **8**(1), 15731 (2017).
31. P. Lu, S. J. Mihailov, Y. Xu, and X. Bao, "Development of femtosecond random gratings for fiber laser and sensor applications," Proc. SPIE **11739**, 12 (2021).
32. Y. Han, T. V. A. Tran, S. Kim, and S. B. Lee, "Multiwavelength Raman-fiber-laser-based long-distance remote sensor for simultaneous measurement of strain and temperature," Opt. Lett. **30**(11), 1282–1284 (2005).
33. J. B. Murray, A. Cerjan, and B. Redding, "Distributed Brillouin fiber laser sensor," Optica **9**(1), 80–87 (2022).
34. S. Stepanov, "Dynamic population gratings in rare-earth-doped optical fibres," J. Phys. D: Appl. Phys. **41**(22), 224002 (2008).
35. S. J. Frisken, "Transient Bragg reflection gratings in erbium-doped fiber amplifiers," Opt. Lett. **17**(24), 1776–1778 (1992).
36. B. Fischer, J. L. Zyskind, J. W. Sulhoff, and D. J. DiGiovanni, "Nonlinear wave mixing and induced gratings in erbium-doped fiber amplifiers," Opt. Lett. **18**(24), 2108–2110 (1993).

Optics EXPRESS

37. K. Xu, "Silicon electro-optic micro-modulator fabricated in standard CMOS technology as components for all silicon monolithic integrated optoelectronic systems," J. Micromech. Microeng. **31**(5), 054001 (2021).
38. B. M. Haas and T. E. Murphy, "A Simple, Linearized, Phase-Modulated Analog Optical Transmission System," IEEE Photonics Technol. Lett. **19**(10), 729–731 (2007).
39. A. S. L. Gomes, A. L. Moura, C. B. de Araújo, and E. P. Raposo, "Recent advances and applications of random lasers and random fiber lasers," Prog. Quantum Electron. **78**, 100343 (2021).

Annex F

The paper “A mode-locked random fibre laser generating transform-limited optical pulses” was submitted in the Nature Communications in 2023.

A mode-locked random laser generating transform-limited optical pulses

Jean von der Weid (vdweid@puc-rio.br)
Pontifical Catholic University of Rio de Janeiro

Marlon Correia (marlon@opto.cetuc.puc-rio.br)
Pontifical Catholic University of Rio de Janeiro

Pedro Tovar (ptovarbr@uottawa.ca)
University of Ottawa

Anderson Gomes (anderson@df.ufpe.br)
Federal University of Pernambuco

Wa r Margulis (walter.margulis@fiberactivity.com)
R al Institute of Technology

Art e

Ke ords:

DO ttps://doi.org/

Additional Declarations: There is **NO** Competing Interest.

A mode-locked random fibre laser generating transform-limited optical pulses

Jean Pierre von der Weid[1], Marlon M. Correia[1], Pedro Tovar[2], Anderson S. L. Gomes[3] and Walter Margulis[1,4]

[1]*Center for Telecommunication Studies, Pontifical Catholic University of Rio de Janeiro, Rio de Janeiro, 22451-900, RJ, Brazil*
[2]*Department of Physics, University of Ottawa, 25 Templeton Street, Ottawa, ON K1N 6N5, Canada*
[3]*Departamento de Física, Universidade Federal de Pernambuco, Recife, 50670-901, PE, Brazil*
[4]*Department of Applied Physics, Royal Institute of Technology, Roslagstullsbacken 21, 106 91 Stockholm, Sweden*

Correspondence: Jean Pierre von der Weid (vdweid@puc-rio.br)

Abstract

Ever since the mid-1960's, locking the phases of modes enabled the generation of laser pulses of duration limited only by the uncertainty principle, opening the field of ultrafast science. In contrast to conventional lasers, random lasers usually lack at least a mirror and generally emit broadband low-coherence light. They have, nevertheless, cavity modes that distinguish them from amplifiers and superluminescent light sources. Mode spacing in random lasers is ill-defined because optical feedback comes from scattering centres at random positions. Although progress has been made towards locking spatial and longitudinal modes in random lasers, the literature lacks reports on transform-limited pulse generation despite the many decades of the field. Here the generation of sub-nanosecond transform-limited pulses from a mode-locked random fibre laser is described. Exceedingly weak (<-73 dB) Rayleigh backscattering from decimetre-long sections of telecom fibre serves as laser feedback, providing narrow spectral selectivity to the Fourier limit. This unique laser is adjustable in pulse duration (0.34-20 ns), repetition rate (0.714-1.05 MHz) and can be temperature tuned. The high spectral-efficiency pulses are applied in distributed temperature sensing with 9.0 cm and 3.3×10^{-3} K resolution, exemplifying how the results can drive advances in the fields of spectroscopy, telecommunications, and sensing.

Introduction

Laser light differs from spontaneous emission owing to the existence of cavity modes with well-defined and equally spaced frequencies. A mode-locked laser can generate transform-limited pulses when all modes are perfectly phase-locked to each other through a coupling mechanism such as periodic phase or amplitude modulation [1-4]. Random lasers [5,6,7] are based on a stochastic distribution of scattering centres that help form an effective cavity with laser modes, even when a laser mirror is lacking [8,9,10]. The random mode-spacing makes it difficult to lock the phases of the modes to each other [11-17]. Mode-locking random lasers where the gain and scattering coexist spatially, as in dyes [6] or semiconductor powders [18], is even more challenging. For this reason, few random laser reports exist on locking the spatial modes [11-16] and the longitudinal modal distribution [17], and none to the Fourier transform limit.

The generation of transform-limited pulses in random lasers can be attempted in a simplified system. In random single-mode fibre lasers [19], the complexity is reduced to one spatial dimension. Furthermore, it is possible to use lumped amplifiers to separate the section providing gain from the section with randomly distributed scatterers [20,21,22]. Random feedback from a telecom fibre lies at the

heart of the mode-locked transform-limited pulse generation discussed here. The mean backscattered power guided back in standard single-mode fibres amounts to a fraction ~-72 dB/m of the forward propagating power. The extremely faint Rayleigh backscattering in a short section of fibre (3 cm – 2 m) arbitrarily selected within a much longer fibre spool (10's m – 100's m) serves as laser feedback. The chosen backscattering section of fibre is much shorter than the entire laser cavity. Periodically gated optical amplification allows synchronizing the arrival of the backscattered light from the distributed mirror to the opening of the gain window. Light scattered either too early or too late (from points lying before or after the chosen "addressed" section) does not experience periodic amplification and dies off. Provided the amplification in a roundtrip compensates for the incurred loss, the laser reaches threshold. The duration of the optical pulse defines the length of the distributed laser mirror.

Similar to all other fibre segments, this section has an unknown and random distribution of scattering centres. However, the coherent sum of all backscattered optical fields from this segment at a given wavelength has a fixed (albeit unpredictable) value if external conditions such as temperature and strain are constant. The integrated phase value of the extended random mirror depends critically on the wavelength (optical frequency) of the input beam [23]. While some wavelengths experience mainly destructive interference, others add constructively to a peak in reflectivity, as commonly observed in phase optical time-domain reflectometry (ϕ-OTDR) [24,25]. Therefore, the chosen backscattering section of passive fibre behaves at its entrance as a time-constant faint coloured mirror reflecting various spectral peaks, like those obtained by printing low reflectivity random Bragg gratings [20]. The Rayleigh scattered light guided back from the extended random mirror repetitively feeds the laser cavity with a constant phase signal at the dominant wavelength, and spectrally filters laser emission. With periodic amplification, the highest of the reflected spectral peaks dominates, imprinting its central wavelength and bandwidth on the laser pulse formed. This backscattered signal can be reproduced after a phase-shift equal to an integral number of 2π radians accumulated along a roundtrip, and the modes of the laser cavity can be locked.

Synchronous mode-locking [26] is achieved with repetitive amplification of the circulating signal, where the pulse duration is largely determined by the time-gated amplification and by the sharply filtered feedback [27]. The pulses generated by the laser are found to be exactly or nearly transform-limited in a range of pulse durations (~0.34 ns – 20 ns) and cavity lengths (190 – 285 m). When choosing the laser pulse duration, one also automatically chooses the length of the spectral filter and its bandwidth, thus maintaining the time-bandwidth limit. Remarkably, a few centimetres of highly transparent single-mode telecom fibre can be used as a mirror in a laser cavity, one with narrow linewidth peaks that guarantee transform-limited pulse generation.

Results

Theory and simulations

Rayleigh scattering in optical fibres is generated by random fluctuations of the refractive index at the nanoscopic scale, but the interference of Rayleigh scattered coherent light and the backscattered intensity are governed by random fluctuations of the mean refractive index on a much larger scale. Backscattering of coherent light can be modelled as the sum of the contributions from every portion of the fibre in which the phase of each contribution is randomized [23]. This allows evaluating the reflectivity of the distributed random mirror embodied by a chosen section of the backscattering fibre. The intensity spectrum of the backscattered light at the input point is frequency-dependent and fluctuations can be described as:

$$I(k) \propto \left|\sum_{i=1}^{N} \exp(j\bar{n}_i kd)\right|^2 = < I > + \sum_{i \neq p} \exp(j[\bar{n}_i - \bar{n}_p]kd) \quad (1)$$

where the fibre section is considered as a series of *N* segments of mean length *d* and mean refractive index $\bar{n}_i$ with random variations from segment to segment. The second term of (1) is a double sum over all pairs of segments *i* and *p* and describe the fluctuations due to the interference between the optical field from all segments. The result is an intensity spectrum with strong frequency dependence, with fluctuations that can reach ~10 dB above the mean value in kilometre-long fibres [23], coming from constructive interference of the backscattered fields. As mentioned above, although very faint, this backscattered light can trigger laser action in a random fibre laser, provided there is sufficient gain in the roundtrip. Previously, kilometre lengths were used with Raman [28] and Brillouin [29] amplification to build random fibre lasers. Scattering in long fibre lengths was also used in combination with lumped amplification such as in SOA- or EDFA-based random lasers [10, 30].

The backscattered intensity spectrum calculated using Eq. (1) for typical standard single-mode fibres and *d* ~5 mm is shown in Fig. 1 (a) within a 10-GHz range of optical frequencies, for illustrative fibre sections lengths of 0.5, 1 and 2 m. In the full 100 GHz used in the simulations, peaks as high as 9 dB above the mean were found. All spectra present randomly spaced relatively strong peaks, whose spectral width is also random and sharpens as the length is increased. Fig. 1 (b) shows the distribution of peak widths (FWHM) of Rayleigh scattered light calculated in a 100-GHz spectral range. As expected, the mean width is inversely proportional to the length of the scattering fibre, and the longer the fibre section, the sharper the peak width distribution. Remarkably, the most likely spectral width reflected (e.g., 50 MHz or 0.4 pm linewidth) is that of a very weak FBG of the same length (e.g., 2 m long). A simple approach to understanding this feature is to consider the backscattering fibre section as consisting of a long fibre Bragg grating with a very small index depth and a random period over its length. The longer the grating, the sharper the reflection peaks [31].

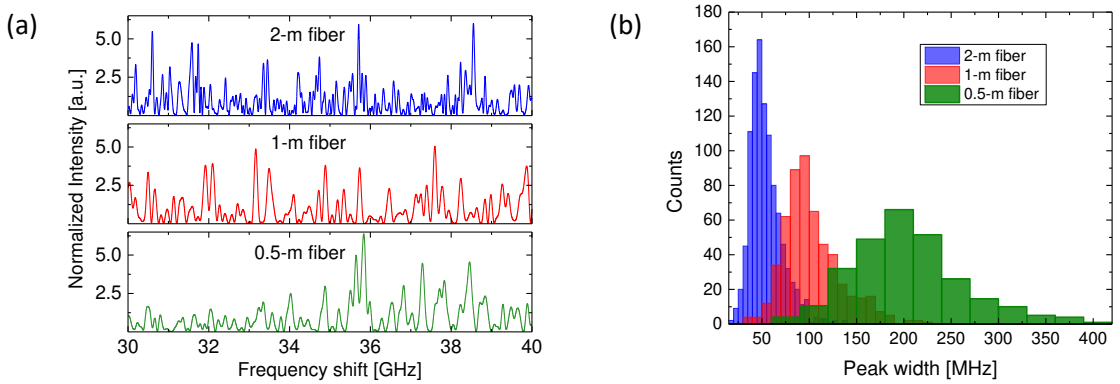

Fig. 1.(a) Typical simulated random backscattering spectrum in a 10 GHz range. Reflection peaks are formed, narrower and more frequent for longer fibre sections (e.g., 2 m). (b) Distribution of simulated peak widths for three lengths of backscattering fibre section calculated over a 100 GHz span. The most likely spectral width of the distributed random mirror (e.g., 50 MHz) predicted by Eq. (1) equals the width of a very weak FBG of same length (2 m).

Consider now a long lumped-gain laser cavity (e.g., 200 m) in which one of the mirrors is replaced by a short backscattering fibre section (e.g., 1 m). Of course, the enormous loss of this cavity must be compensated by a huge gain, so that the laser can reach threshold. This concept is displayed in Fig. 2, where a gated SOA generates a pulsed gain and a pumped EDF provides bidirectional CW gain. The lumped-gain configuration eliminates the need to consider all backscattered light but the one from the addressed section. Consider that a broad ASE pulse is launched by the SOA and reaches the addressed section after amplification in the EDF. The faint and randomly colored backscattered signal coming from this section is guided back to the SOA, arriving at the very moment when another current pulse opens the

gain window. When the EDF gain is sufficient, so that the spectral density at a given coherence spike of the backscattered pulse exceeds the spontaneous emission density, then this wavelength dominates the stimulated emission, depleting the gain at other wavelengths. The spectral width of the coherence spike defines the lasing linewidth. Any of these peaks accommodates hundreds of equally spaced cavity modes that could be phase-locked.

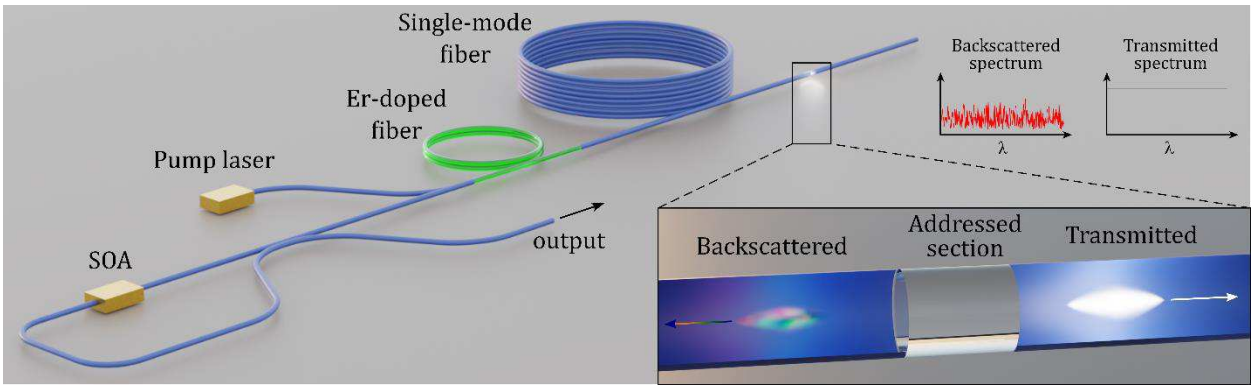

Fig. 2. Schematic diagram of the mode-locked random fibre laser near but below threshold. The distributed random mirror is arbitrarily chosen as a short section of the single-mode telecom fibre. See text and supplementary material for further experimental details.

Laser measurements

Experiments were performed with a fibre laser cavity in a sigma configuration, comprising a fibre loop and an open-ended fibre patch. The loop consisted of a gated semiconductor optical amplifier (SOA) and a length of fibre used as a delay (125 m), both connected to the two fibres of a 50% fused coupler, as schematically shown in Fig. 2. In some experiments when more gain was needed, an additional commercial erbium-doped fibre amplifier (EDFA) and an adjustable spectral filter were added to the loop to increase the gain and reduce the amplified spontaneous emission, respectively. The open-ended fibre section was also connected to the coupler and included a 27-m long EDFA without isolators, providing optical gain in both directions, and a passive single-mode fibre (SMF) spool that backscattered light into the loop. In most experiments, dispersion shifted fibre was employed, but a standard Corning SMF-28 telecom fibre was also used with the inclusion of the extra amplifier that provided enough gain for laser action. The fourth leg of the coupler was used as a laser output port. The EDFA(s) provided CW gain. The SOA was gated with nanosecond current pulses from a tuneable generator and prevented light transmission while unpumped (~-60 dB). The repetition rate of the electrical pulses was adjusted in the interval 714 kHz – 1.047 MHz. As mentioned above, this allowed matching the nanosecond gain window to the arrival at the SOA of light from the chosen short section within the spool of telecom fibre (~3 cm – 2 m). The length of the distributed random mirror was selected by choosing the duration of the electrical pulse applied to the SOA (e.g., ~1 m for 10 ns pulses). The laser output was characterized in time with an amplified 26-GHz photodiode and a 3.5-GHz oscilloscope, and spectrally with a 20-MHz frequency (0.16 pm wavelength) resolution optical spectrum analyser (OSA).

Fig. 3 presents the laser average output power as a function of the EDFA pump power when the system is driven at 820 kHz with square current pulses with widths 5, 10 and 20 ns. The corresponding optical pulse durations were 3.6, 8.6 and 18.7 ns, respectively. A distinct random laser threshold is observed in all cases [32,33] with a clear sharp laser line emerging from the broadband ASE when the threshold is reached, as shown in the inset. The higher feedback provided by longer, distributed random

reflectors reduces the pump power needed for lasing as more power is backscattered. Considering the sum of point losses and the cavity roundtrip gain (see complementary material), the average Rayleigh scattering capture coefficient of the fibre is insufficient to sustain laser oscillation. Indeed, a coherent reflectivity spike ~10 dB above the average is needed for the laser to reach threshold, in agreement with the model above [23].

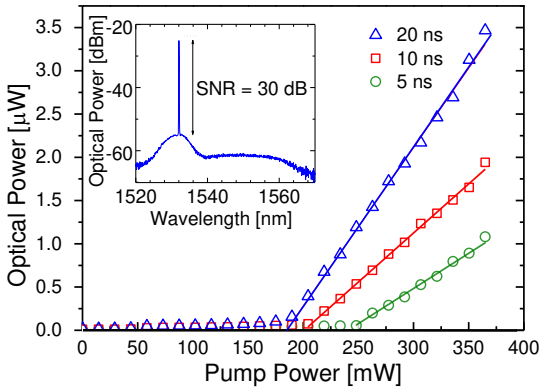

Fig. 3. Distinct random laser threshold for three current pulse durations. The threshold EDF pump power decreases for longer pulses. The inset shows the optical spectrum for 20-ns pulses at full pump power.

Fig. 4 (a) presents the experimental optical spectra of laser emission as a function of frequency shift around 1532 nm wavelength when the gated amplifier is driven with top-hat current pulses of duration 5, 10 and 20 ns. The traces displayed show an average of 50 measurements. A solid line is also displayed, indicating the best $sinc^2$ fit for the three data sets. Good agreement (R2~0.99) is observed between the experimental data and the model predictions shown in Fig. 1. The measured bandwidths (227 MHz, 125 MHz and 65 MHz, respectively) are approximately inversely proportional to the pulse duration, that is, to the length of the fibre section providing feedback to the random laser. Considering the case of 125 MHz bandwidth pulses at a repetition rate of 0.82 MHz, ~152 modes are phase-locked in the 3-dB optical bandwidth. The averaging used here prevents a more quantitative comparison between the measured pulses and the Fourier limit. For example, the time-bandwidth product in this case is 17% higher than the 0.89 value expected for square pulses [34]. The laser linewidths are the same as expected for the backscattering reflectivity peak, which is consistent with the fact that the laser linewidth is defined by the spectral width of the coherence spike. In fact, given the extremely low feedback of the backscattering section, almost all photons leave the cavity at every roundtrip, being filtered just once. It is worth mentioning that laser action is maintained from shot to shot by the few coherent photons backscattered from the preceding pulse. Coherence in this random laser comes from the constructive interference at the backscattering section, rather than from constructive interference at each cavity roundtrip. Cavity modes are automatically phase locked by the periodic pulsed gain.

Fig. 4 (b-e) shows time-domain (traces (b) and (d)) and spectral-domain (traces (c) and (e)) measurements for electrical pulses of duration 10 ns (top, (b) and (c)) and 2 ns (bottom, (d) and (e)). The time and spectral measurements shown were taken in single sweep mode and near synchronism. The optical pulses are shorter than the electrical ones (8.6 ns and 340 ps FWHM, respectively) and are fitted in (b) to a square pulse shape and in (d) to a Gaussian, both illustrated by a red solid line. The red solid lines in Figs. 4 (c) and (e) are the corresponding Fourier transform curves, with $Sinc^2$ and Gaussian shapes, respectively, with no width adjustment. When the pulse shapes were closer to Gaussian (e.g., Fig. 4(d)) than top-hat (e.g., Fig. 4(b)), the time-bandwidth product reduced from ~0.89 to ~0.44, as expected [34]. The good agreement of the Fourier-transform curves in red and the experimental traces in black in Figs. 4 (c) and 4 (e) demonstrate that the present mode-locked random laser can generate transform-limited

pulses using the Rayleigh backscattering from a section of telecom fibre as short as 3.4 cm as cavity feedback (c.f. Fig 4 (e)). Even shorter pulses should be possible, but experiments here were electronics-limited.

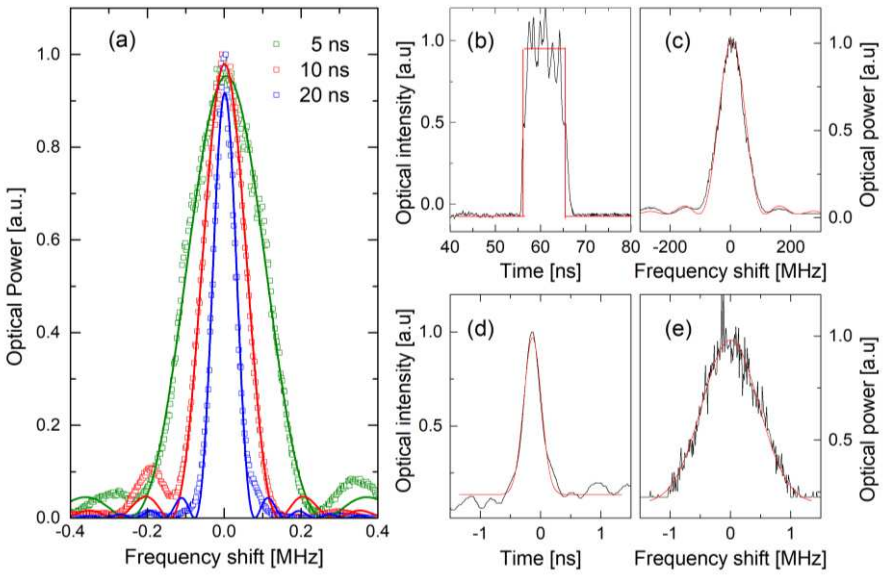

Fig. 4.(a) Laser spectral bandwidth measured with an optical spectrum analyser (50x average) for square current pulse durations 5 ns (green), 10 ns (red) and 20 ns (blue). The FWHM spectral widths fitted to Sinc² functions are 227, 125 and 65 MHz, respectively, close to those expected for transform-limited pulses. (b) Temporal and (c) spectral features of 8.6 ns FWHM laser pulse. (d) Temporal and (e) spectral characteristics of a ps Gaussian pulse. Both pulses are transform-limited, as shown with the Sinc² and Gaussian Fourier transform pairs of curves (red solid lines). All frequency shifts are measured around 1532 nm wavelength.

More extensive investigations were conducted for various pulse durations. While longer current pulses lead more often to pulsing at two frequencies separated by hundreds of MHz that beat in the time domain, the pulses remain transform-limited. This double-pulsing behaviour has been described in other rare-earth laser systems that lack a saturable absorber [35,36]. Single-pulse generation was more readily obtained for current pulses ≤3 ns.

Application

Distributed temperature sensing is an important application area of optical fibres in industrial settings, to optimise production processes and minimise maintenance and repair costs. Although one Kelvin temperature sensitivity and metre-long spatial resolution suffice in many cases, such as in oil-well facilities, in other applications, such as monitoring water seepage through temperature variation in dams and dikes to prevent accidents, much better performance parameters are advantageous [37]. Typically, distributed temperature sensors (DTS) make use of the relative intensities of Stokes and anti-Stokes signals from Raman scattering in fibres, monitored via optical time domain reflectometry [38,39]. Wavelength-dependent loss due to fibre bending or ageing is a problem that single-wavelength monitoring systems do not have. Besides, the poor signal-to-noise ratio in Raman DTS is a limitation not usually encountered when measuring the output wavelength of a laser. The configurable random laser here, which allows for in-situ selection of the length and bandwidth of the transform-limited probe pulses, can be exploited in distributed temperature sensing, as an example of an application area. From Eq. (1), it is clear that the frequency spectrum shifts as the mean refractive index of the considered fibre section varies with temperature. Given the sharpness of the lasing peak, even a tiny spectral shift can be detected precisely.

As proof of principle, the open-ended telecom fibre was unwound from the spool, and a section ~1 m close to the end was immersed in water in an enclosed polystyrene box. The water temperature was initially raised, and the cooling process was monitored using a thermocouple-based thermometer and the laser wavelength. The repetition rate of the laser was tuned to 728.2 kHz so that optical feedback was provided from the section of fibre immersed in water. In order to avoid edge effects and to maximise temperature uniformity in the immersed fibre, the pulse duration was limited to 900 ps (i.e., the laser feedback came from a central 9.0 cm long fibre section). An optical spectrum analyser was used to monitor the frequency (wavelength) shift, similar to monitoring the spectrum of simple intra-cavity FBG systems [40,41]. Fig. 5 illustrates the temperature evolution as a function of frequency shift, measured with ~4-MHz resolution. The frequency dependence on temperature in this small range is linear and approximately 1.19 GHz/K, similar to that found for FBG's. However, different from FBG's that only offer point sensing, distributed measurement here is accomplished by scanning the repetition rate of the laser. In addition, the mode-locked random laser also exhibits advantages over distributed sensing techniques such as Φ-OTDR, since frequency shifts are directly measured (no post-processing), have a high signal-to-noise ratio and are robust to power fluctuations. Moreover, the spectral width of the laser line is much smaller than those of typical Bragg gratings used for local temperature measurements, so that the spectral shift can be better determined. (See Supplementary Information for details).

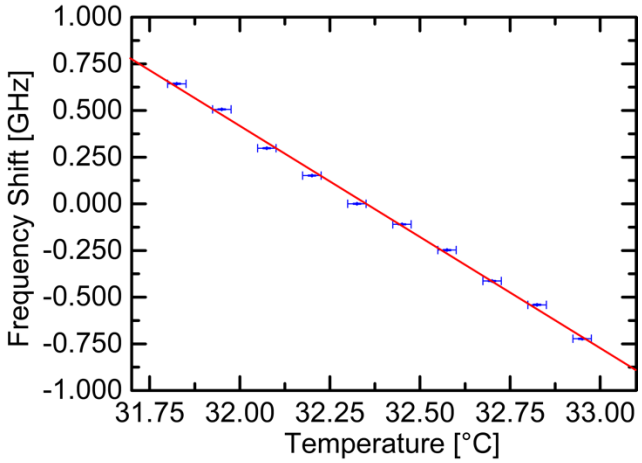

Fig. 5. Temperature sensing using Rayleigh scattering in single-mode telecom fibre. Transform-limited pulse generation makes the laser system highly spectrally efficient. Here, 9.0 cm resolution and 0.0033 K precision are demonstrated.

The robustness of the experimental set-up was verified by re-starting a measurement campaign a few days later and controlling that the peak position depends only on the sample temperature. Note that the laser cavity was protected in the laboratory but not temperature-stabilised. The spectral measurements depend almost entirely on the temperature of the particular fibre section being addressed. Other temperature-induced fluctuations affect the cavity modes but to a large extent do not alter the spectrum of the random mirror. A temperature variation of 1 K, over the full 200-m fibre circuit, would change the optical path of the cavity by a mere ~1 mm, well below the spatial resolution of the system. The spectral analysis of the backscattered light, however, can easily detect a variation two orders of magnitude smaller.

Discussion

A unique mode-locked random fibre laser, generating transform-limited optical pulses was demonstrated. The extremely weak Rayleigh backscattering of a short piece of telecom fibre is used as cavity feedback, leading to linewidth filtering to the Fourier limit of the laser pulses. With such weak

feedback, the cavity is extremely lossy and therefore with extremely low Q-value. Consequently, a gain of the order of 100 dB is required to compensate for the loss. These loss and gain values are amongst the most extreme ever reported for a laser. An estimate of the number of photons in a 340-ps pulse backscattered in the telecom fibre gives $\sim 10^2$ photons. It is likely that shorter pulses, well into the picosecond regime could be generated and exploited here. This means that lasing could start with an even smaller number of photons and the system could be useful to explore more fundamental questions, such as manifestations of the quantum behaviour of the laser source and how the optical pulse evolves from white light to the coherent regime and Fourier limit. Pulses of duration under 0.3 ns were not generated for limitations in the electronics available. The nanosecond regime does, nevertheless, find important applications [42,43], as exemplified above for distributed sensing. The high-resolution measurements made possible with the transform limited pulses here can be useful for instance in early warning of water seepage in dams. The good temperature sensitivity should allow for the use of the fibre even in a rugged cable, as necessary for field installations. One strength of the work described here is the possibility of using short sections of installed standard telecom fibre for distributed sensing. In some cases, it may be advantageous to deploy a fibre with enhanced Rayleigh scattering, as obtained for instance by exposure to UV radiation. Up to 20 dB increase in backscattering has been demonstrated [44]. This and other means [45, 46] could alleviate the need for an additional amplifier in the laser cavity. Furthermore, the physics of Rayleigh backscattering of coherent light is not restricted to single-mode fibres, and could also be applied to other scattering media. Given the sensitivity of the system to extremely low levels of backscattered light, its concept can conceivably be applied to distributed sensing of dilute scattering particles in free space, as a lasing-LIDAR with transform-limited resolution.

References

1. DeMaria, A. J., Stetser, D. A., Glenn, W. H. et al. Ultrashort Light Pulses. *Science* 156, 1557-1568 (1967).
2. Shank, C. V. & Ippen, E. P. Subpicosecond kilowatt pulses from a modelocked cw dye laser. *Appl. Phys. Lett*. 24, 373–375 (1974).
3. Keller, U. Recent developments in compact ultrafast lasers. *Nature* 424, 831–838 (2003).
4. Rafailov, E., Cataluna, M. & Sibbett, W. Mode-locked quantum-dot lasers. *Nature Photon* 1, 395–401 (2007).
5. Letokhov, V. S. Quantum statistics of multi-mode radiation from an ensemble of atoms. Sov. Phys. JETP 26, 1246–1251 (1968).
6. Lawandy, N. M., Balachandran, R. M., Gomes, A. S. L. & Sauvain, E. Laser action in strongly scattering media. Nature 368, 436–438 (1994).
7. Gomes, A. S. L., Moura, A. L., Araújo, C. B. et al. Recent advances and applications of random lasers and random fiber lasers. Prog. Quantum Electron. 78, 100343 (2021).
8. Van der Molen, K. L., Tjerkstra, R. W., Mosk, A. P et al. Spatial Extent of Random Laser Modes. *Phys. Rev. Lett.* 98, 143901 (2007).
9. Andreasen, A. A. J., Asatryan, L. C. B. et al. Modes of random lasers. *Advances in Optics and Photonics* 3, 88–127 (2011).
10. Tovar, P., Temporão, G. & von der Weid, J. P. Longitudinal mode dynamics in SOA-based random feedback fiber lasers. Optics Express 27(21), 31001-31012 (2019).
11. Kalt, H. Towards mode-locking. Nature Photon 5, 573–574 (2011).
12. Leonetti, M., Conti, C. & Lopez, C. The mode-locking transition of random lasers. *Nature Photon* 5, 615–617 (2011).
13. Antenucci, F., Lerario, G., Fernandéz, B. S. et al. Demonstration of Self-Starting Nonlinear Mode Locking in Random Lasers. Phys. Rev. Lett. 126, 173901 (2021).
14. Trivedi, M., Saxena, D., Ng, W.K. et al. Self-organized lasers from reconfigurable colloidal assemblies. Nat. Phys. 18, 939–944 (2022).
15. Mujumdar, S., Türck, V., Torre, R. & Wiersma D. S. Chaotic behavior of a random laser with static disorder. *Phys. Rev. A* 76, 033807 (2007).
16. Leonetti, M., Conti, C. & López, C. Dynamics of phase-locking random lasers. *Phys. Rev. A* 88, 043834 (2013).
17. Hu, B., Cui, H., Zhang, Y. L. et al. Mode locking of a coherent random fiber laser with selectable repetition rates. Optics Express 28, 36380 (2020)
18. Cao, H., Xu, J.Y., Ling, Y. et al. Random lasers with coherent feedback. IEEE J. Selected Topics in Quantum Electronics 9, 111-119 (2003).
19. De Matos, C. J. S., Menezes, L. D. S., Brito-Silva, A. M. et al, Random fiber laser. *Phys. Rev. Lett.* 99, 153903–153907 (2007).
20. I. R. R. González, B. C. Lima, P. I. R. Pincheira et al. Turbulence hierarchy in a random fibre laser. Nat. Commun. 8(1), 15731 (2017).
21. Margulis, W., Das, A., von der Weid, J. P. et al. Hybrid electronically addressable random fiber laser. Opt. Express 28(16), 23388–23396 (2020).
22. Skvortsov, M. I., Wolf, A. A., Dostovalov, A. V. et al. Narrow-Linewidth Er-Doped Fiber Lasers With Random Distributed Feedback Provided By Artificial Rayleigh Scattering. Journal of Lightwave Technology 40, 1829-1835 (2022).
23. Tovar, P., Lima, B. C. & von der Weid, J. P. Modelling Intensity Fluctuations of Rayleigh Backscattered Coherent Light in Single-Mode Fibers. Journal of Lightwave Technology 40, 4765 (2022).
24. Soriano-Amat, M., Martins, H. F., Durán, V. et al. Time-expanded phase-sensitive optical time-domain reflectometry. Light: Science & Applications 10, 51 (2021).

25. Rao, Y., Wang, Z., Wu, H. et al. Recent Advances in Phase-Sensitive Optical Time Domain Reflectometry (Φ-OTDR). Photonic Sensors 11(1), 1–30 (2021).
26. Nyushkov, B. N., Kobtsev, S. M., Komarov, A. K., et al. SOA fiber laser mode-locked by gain modulation. J. Optical Society of America B 35, 2582-2587 (2018).
27. Cutler, C. C. The regenerative pulse generator. Proceedings I. R. E. 43, 140 (1955).
28. Turitsyn, S. K., Babin, S. A., El-Taher, A. E. et al. Random distributed feedback fibre laser. Nature Photonics 4, 231–235 (2010).
29. Pang, M., Bao, X. & Chen, L. Observation of narrow linewidth spikes in the coherent Brillouin random fiber laser. Opt. Letters 38, 1866 (2013).
30. Zhang, W. L., Li, S. W., Ma, R et al. Random Distributed Feedback Fiber Laser Based on Combination of Er-Doped Fiber and Single-Mode Fiber. IEEE J. Selected Topics in Quantum Electronics 21, 0900406 (2015).
31. Kashyap, R. Fibre Bragg gratings. Ac. Press 1st ed, 155 (1999).
32. Samuel, D. W., Namdas, E. B. & Graham, A. T. How to recognize lasing. Nature Photonics 3, 547 (2009).
33. Sapienza, R. Determining random lasing action. Nat Rev Phys 1, 690–695 (2019).
34. Sala, K., Kenney-Wallace, G. & Hall, G. CW Autocorrelation measurements of picosecond laser pulses. IEEE Journal of Quantum Electronics 16, 990-996 (1980).
35. Kryukov, P. G. & Letokhov, V. S. Fluctuation mechanism of ultrashort pulse generation by laser with saturable absorber. IEEE J. Quantum Electronics QE-8, 766 (1972).
36. Geoffrey, H. C. N. Theory of Passive Mode-Locking in Giant Pulse Lasers. Proceedings of the IEEE 67(3), 380 (1979).
37. Dang, L.Y., Huang, L.G., Shi, L.L. et al. Ultra-high spectral purity laser derived from weak external distributed perturbation. Opto-Electron Adv 6, 210149 (2023).
38. Henault, J-M., Moreau, G. & Blairon, S. Truly distributed optical fiber sensors for structural health monitoring: from the telecommunication optical fiber drawling tower to water leakage detection in dikes and concrete structure strain monitoring. Advances in Civil Engineering 930796 (2010).
39. Li, J. & Zhang, M. Physics and applications of Raman distributed optical fiber sensing. Light: Science & Applications 11, 128 (2022).
40. Madrigal, J., Fraile-Peláez, F. J., Zheng, D., et al. Characterization of a FBG sensor interrogation system based on a mode-locked laser scheme, Optics Express 25, 24650-24657 (2017).
41. Margulis, W., Lindberg, R., Laurell, F. et al. Intracavity interrogation of an array of fiber Bragg gratings. Optics Express 29, 111-118 (2021).
42. Kelleher, E. J. R., Travers, J. C., Sun, Z. et al. Nanosecond-pulse fiber lasers mode-locked with nanotubes. Applied Physics Letters 95, 111108 (2009).
43. Kues, M., Reimer, C., Wetzel, B. et al. Passively mode-locked laser with an ultra-narrow spectral width. Nature Photon 11, 159–162 (2017).
44. Loranger, S. Gagné, M. Lambin-Lezzi, V. et al. Rayleigh scatter-based order of magnitude increase in distributed temperature and strain sensing by simple UV exposure of optical fibre. Scientific Reports 5, 11177 (2015).
45. Fuertes, V., Grégoire, N., Labranche, P. et al. Engineering nanoparticle features to tune Rayleigh scattering in nanoparticles-doped optical fibers. *Sci Rep* **11**, 9116 (2021).
46. Redding, B., Murray, M. J., Donko, A., et al. Low-noise distributed acoustic sensing using enhanced backscattering fiber with ultra-low-loss point reflectors, Optics Express 28, 14638-14647 (2020).

Supplementary information

Laser set-up

The fibre laser cavity used in this work consisted of a loop and an open-ended section (cf. Fig. 2 and in more detail in Fig. SI 1). Gated amplification was provided inside the loop by driving with current pulses a semiconductor optical amplifier, Thorlabs SOA 1013SXS. A 125 m delay fibre was also included in the loop to increase the round-trip time of the cavity to the ~1 μs range. In some experiments, particularly with very short-duration pulses, a commercial erbium-doped fibre amplifier (EDFA Thorlabs 100S) was also inserted in the loop. It amplified the weak backscattered signal from the distributed mirror by up to ~36 dB before the SOA. When the extra EDFA was included, an adjustable spectral filter (Alnair-Labs-CVF-300CL) was also used to reduce the amplified spontaneous emission, and limit the feedback signal to the neighbourhood (<20 GHz) of the wavelength of interest. The 3 dB fused fibre coupler connected the loop to the open-ended fibre section of the cavity. A large fraction of the amplification needed for the laser to go above threshold (54.5 dB) was provided by a 27 m long Corning erbium-doped fibre (1550C3) without isolators, working in both directions. Gain was provided to the EDF by a 365 mW CW-pumped diode laser at 976 nm wavelength. An open-ended 63-m long spool of single-mode fibre completed the laser cavity. The output of the laser was monitored with a 26 GHz amplified photodiode model UPD-15-IR2-FC and a 3.5 GHz 40 GSamples/s Tektronix DPO7354 oscilloscope. The spectrum of the laser output was measured with an Apex AP2050A optical spectrum analyser with an optical frequency resolution as narrow as 20 MHz (0.16 pm wavelength). The current pulses for the SOA were provided by an Avtech pulse generator (AVM-2) delivering up to 300 milliamperes with a rise time <1ns and durations up to 20 ns. The trigger for the pulse generator came from a two-channel Keysight arbitrary function generator Model 33500B which allowed for pulse frequency tuning to the millihertz resolution. The short section of fibre providing for Rayleigh backscattering was chosen in position and in length along the fibre spool by adjusting the repetition rate and the duration of the electrical pulses driving the SOA. The single-mode fibre end was angle-cleaved and bent sharply to prevent backscattering from the termination. Lasing was observed along the entire spool length, but the pulse amplitude and stability varied because of the random feedback.

When measuring temperature, a section of the single-mode fibre was attached to the bottom of a polystyrene box containing approximately 3 litres of water. Two 4.5 digits thermometers and one thermocouple were also attached to its bottom inner surface. The voltage from the type k (Chromel-Alumel) thermocouple was monitored with a microvoltmeter HP 34401A. A preliminary calibration of the thermocouple gave a linear 40 μV/K voltage dependence in the limited temperature range studied, simulating a possible dam monitoring temperature range. The resolution of the microvoltmeter and the uniformity of the temperature of the water bath were the main limiting factors in the determination of the temperature displayed in Fig. 5. Increased accuracy of the measurement would require calibration of the temperature against a fixed and known value such as the fusion point of ice. Such a procedure was not carried out in this proof-of-concept experiment.

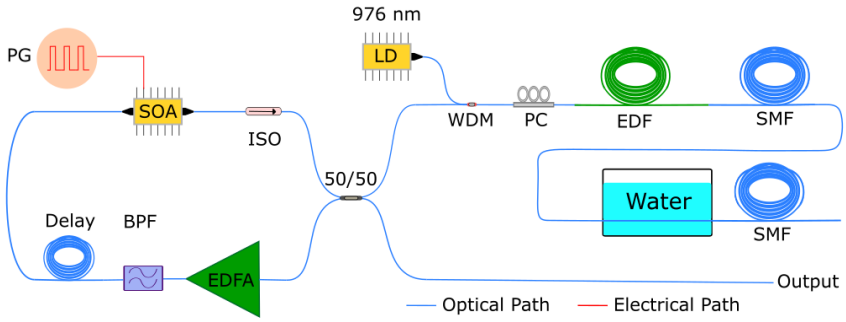

Fig. SI 1. Schematic diagram of distributed temperature sensing using Rayleigh scattering in single-mode telecom fibre. Transform-limited pulse generation makes the laser system highly spectrally efficient. Here, 9.0 cm resolution and 3.3×10^{-3}K precision were demonstrated.

Gain measurements, threshold

The loss of individual components and connectors and the gain provided by the amplifiers were evaluated to better understand the gain dynamics and the limits of operation of the laser. In its simplest configuration of Fig. 2, dispersion shifted (DS) fibre was used. The total loss from all components splices and connections was 11 dB, including the 6-dB double pass over the coupler, whereas the maximum roundtrip-gain was found to be 69 dB, with 54.5 dB coming from the double-pass in the pumped EDF and 14.5 dB from the single-pass at the SOA. Naturally, the highest loss of the cavity was at the distributed back reflector, which amounts to the mean value of ~ -72 dB/m for a typical single-mode fibre and -69 dB/m for DS fibre. With 10-ns pulses in the DS fibre, the laser reached threshold near the maximum gain, meaning that a coherent reflectivity spike ~11 dB was available within the ~250 GHz (~2 nm) spectral region of maximum gain of the pumped EDF. Laser pulses in a standard fibre or shorter laser pulses in the DS fibre could only be observed by increasing the maximum gain, which was obtained by adding a commercial EDFA into the loop and a band pass filter to limit the ASE input on the SOA as displayed in Fig. SI 1. This configuration provided a maximum gain of 105 dB, which was comfortable to generate lasing pulses with durations down to ~0.3 ns, electronics limited. Furthermore, reducing the available spectral width to a flat-top 20 GHz band allowed for better stability of the laser.

Electrical vs optical pulses

The optical pulses generated by the SOA are shorter than the current pulses used for driving it, as shown in Fig. SI 3, for 10-ns (left) and 3-ns (right) bias. The optical pulses measured have duration 8.6 and 1.6-ns FWHM, respectively. The exact relative timing between the electrical and optical pulses is unknown. The figure shows that the response of the SOA in an open cavity (no optical feedback) and the signal-to-noise ratio is relatively poor because of the low sensitivity and high noise level of the ultrafast photodiode. Fig. SI 2 illustrates how sub-nanosecond optical pulses can be formed for current pulses <2 ns, and also that the shape of the optical pulse generated for the shortest durations deviates significantly from a top-hat function.

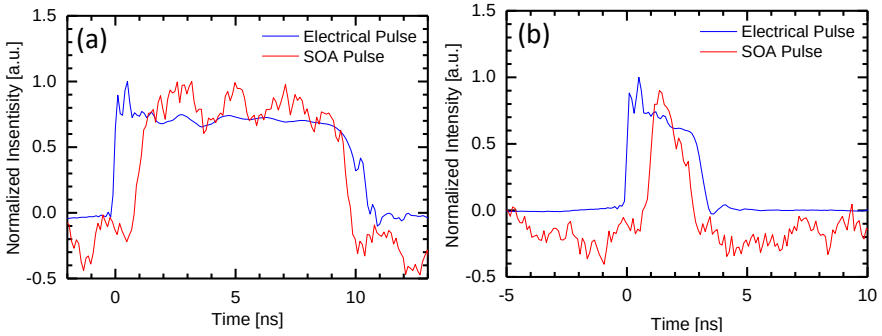

Fig. SI 2. Oscilloscope traces of current pulses applied to the SOA (blue traces) and correspondent optical signals (red traces) with the optical cavity opened. (a) 10.ns current pulse; (b) 3-ns current pulse.

Temperature measurements

In the proof-of-concept application discussed here, the temperature of the water tank was initially raised to ~40°C and the liquid stirred. Subsequently, the polystyrene lid was closed, and the system's temperature left to gradually reduce. The cooling process took several hours. The spectral acquisition and data recording took a fraction of a minute between measured points. The range of temperatures measured was chosen to be a representative temperature at a realistic warm dam location, to allow for the temperature to be in quasi-equilibrium, and to allow for data recording before the electronics instrumentation for temperature measurements showed any variation. The error bar in the temperature measurements is ±0.0125 K. Higher precision would have been possible with better instrumentation (e.g., a nanovoltmeter to read the voltage of the immersed thermocouple).

Fig. SI 3 exemplifies two spectra measured of 900-ps laser pulses with the optical feedback provided by the backscattering fibre section immersed in the water tank. The blue and red traces show spectra at a temperature difference of 0.13 ^{o}C. It is clear that the entire spectrum shifts with temperature, but this shift is better quantified by determining the centre position of the laser line using a Gaussian fit, considering the 70% upper part of the signal to minimise the influence of noise. The error in the determination of the peak frequency was the standard error provided by the Levenberg-Marquardt fitting algorithm and is clearly more precise than the simple determination of the maximum, which was much more affected by the noise. The spectral peak of the two data sets can be determined with a precision ~3 MHz, corresponding to a temperature 2.5 mK. The sensitivity of the technique was evaluated by considering the quality of the least squares fit over 24 independent measurements. The average R2-value was 0.975±0.015 while the standard error in the position of the laser line was 3.2 MHz ±750 kHz, so that the overall sensitivity of a typical spectral position in this case should be ~4 MHz or 3.3 mK in this 9 cm fibre section. Indeed, a longer fibre section used to determine the average temperature would provide sharper spectral lines whose frequency could be determined with even better precision, but the spatial resolution would be compromised accordingly. This distributed temperature measurement is Fourier Transform limited: $\Delta z \times \Delta T = 3 \times 10^{-4}$ m.K.

It is worth stressing that the accuracy of the measurements is significantly poorer, since the two thermometers employed for absolute measurements were not calibrated against a good temperature reference. Nevertheless, in field-applications, it is often the temperature deviation from the expected value, from for example neighbouring points, daily and seasonal variations, etc., that is most useful.

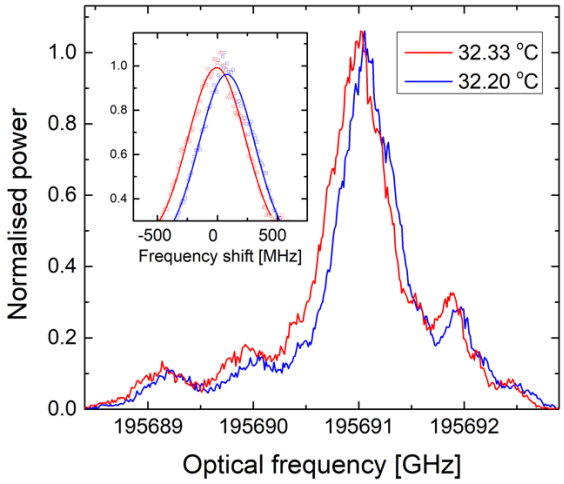

Fig. SI 3. Spectra of 900-ps optical pulses measured at close temperatures The inset displays the Gaussian fit to the 70% upper part of the spectrum, used in the determination of the central frequency.

Acknowledgments

The authors thank J. Murray and B. Redding (NRL, Washington DC) for useful discussions. Funding from CNPq (403233/2017-8, 306332/2019-1, 140701/2019-2), FAPERJ (E-26/201.200/2021), National Institute of Photonics - INCT de Fotônica (465.763/2014-6), Office of Naval Research Global (N62909-20-1-2033), K. A. Wallenberg Foundation and Swedish Research Council are gratefully acknowledged.